OPTICAL AND FUNCTIONAL IMAGING IN LUNG CANCER

Kornelis Harm van der Leest

OPTICAL AND FUNCTIONAL IMAGING IN LUNG CANCER

OPTICAL AND FUNCTIONAL IMAGING IN LUNG CANCER

Optische en functionele beeldvorming in longkanker

Proefschrift

ter verkrijging van de graad van doctor aan de
Erasmus Universiteit Rotterdam
op gezag van de
rector magnificus

Prof.dr. H.G. Schmidt

en volgens besluit van het College voor Promoties

De openbare verdediging zal plaatsvinden op
Vrijdag 28 mei 2010 om 9.30 uur

door

Kornelis Harm van der Leest

geboren te Brunssum

ERASMUS UNIVERSITEIT ROTTERDAM

PROMOTIECOMMISSIE

Promotor	**Prof.dr. H.C. Hoogsteden**
Overige leden	**Prof.dr. H.J.C.M. Sterenborg**
	Prof.dr. B.N. Lambrecht
	Prof.dr. K.G. Tournoy
Copromotor	**Dr. J.G.J.V. Aerts**

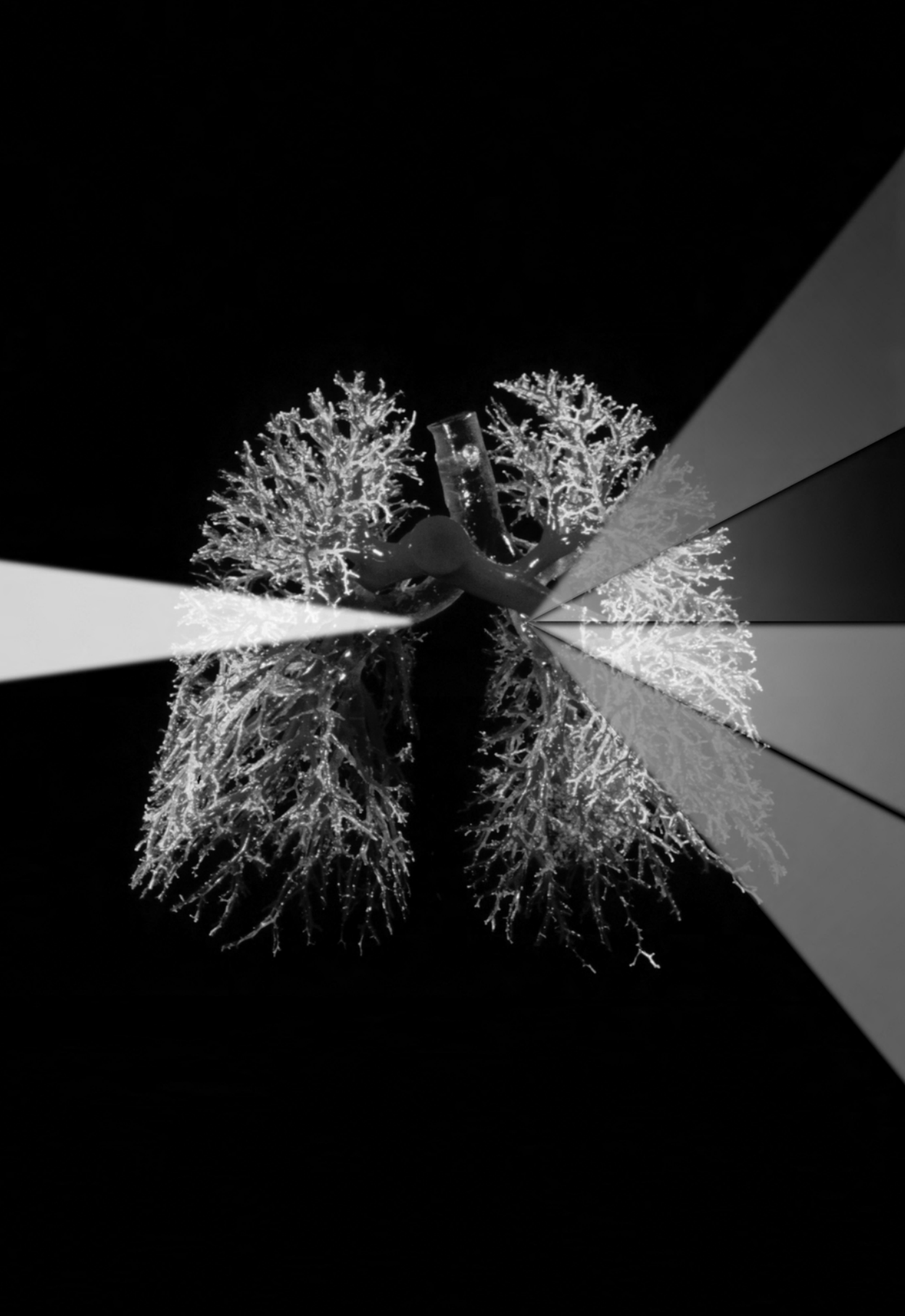*"It is better to light a candle than to curse the darkness"*

Chinese wijsheid

voor mijn ouders

Index

Chapter 1

General introduction

and aim of the thesis

adapted from

Biomedical Applications of Light Scattering

A. Wax

V. Backman

Chapter 11: Fiberoptic Probe Designs

Differential Pathlength Spectroscopy

H.J.C.M. Sterenborg[1]

C. van der Leest[2,3]

S.C. Kanick[1]

J.G.J.V. Aerts[2,3]

A. Amelink[1]

1 Center for Optical Diagnostics and Therapy, Department of Radiation Oncology, Erasmus MC, Rotterdam, The Netherlands

2 Department of Pulmonary Diseases, Erasmus MC, Rotterdam, The Netherlands

3 Department of Pulmonary Diseases, Amphia Hospital, Breda, The Netherlands

General Introduction

1. Epidemiology
Lung cancer is the second most common cancer in men and women, and is the leading cause of cancer related death. In industrialized countries the mortality rate of lung cancer is higher than the mortality rate of breast, colorectal and prostate cancer combined [1]. When lung cancer is diagnosed at an early stage patients are considered to have the best overall survival rate [2]. Unfortunately, only a minority of patients is currently diagnosed at a curable stage of disease. The lack of specific symptoms at an early stage of the disease, the rapid growth of tumor cells and the metastatic behavior of lung tumors are the main reasons for a diagnosis at an advanced stage.
Non-small-cell lung cancer (NSCLC) can be divided into three major histological subtypes: squamouscell carcinoma, adenocarcinoma, and large-cell carcinoma [3]. Eighty-five percent of the lung cancer patients are diagnosed with NSCLC, and 75% of the patients are diagnosed with an incurable stage IIIB or IV disease [4, 5]. Fifteen percent of the lung cancer patients have small-cell-lung cancer (SCLC) and the 5-year survival for them is even lower than for NSCLC [6].
Whereas originally smoking is at the root of all types of lung cancer, the incidence of lung cancer in never smokers increases [7]. Smoking is most strongly linked with SCLC and squamous-cell carcinoma [8, 9], although after the introduction of filter cigarets an increased incidence of adenocarcinomas was observed [10]. This resulted in a change in ratio of adenocarcinomas-squamous cell carcinomas towards adenocarcinomas [8, 11]. In some countries squamous cell carcinoma is still the most common histological type of lung cancer in male patients, e.g. France (41%) and United Kingdom (40%). In other countries adenocarcinoma is the most common type e.g. USA and Canada [12]. In patients without a smoking history adenocarcinoma is most common [13-16].
Despite new insights and improved medical treatments, lung cancer remains the type of cancer with the highest mortality. Additional studies are needed to improve detection of lung cancer in an early (pre)malignant stage to improve survival. Improved pretreatment staging of lung cancer is necessary to prevent under- or over treatment. Furthermore a better understanding of tumor behavior improves treatment modalities.
In this introduction the histological subtypes of lung cancer, the microenvironment of lung cancer and systemic treatment modalities are described. Furthermore several imaging techniques to analyze the microenvironment of lung cancer tissue are discussed.

2. Histological subtype classification.
2.1. Introduction
Historically, the distinction between NSCLC and SCLC determined the choice of treatment and prognosis [17, 18]. Since the development of new treatment options it has become more important to distinguish the histological subtypes of NSCLC, such as adeno-, squamous cell- and undifferentiated carcinoma [19-24].
According to the World Health Organization (WHO) classification, the diagnosis of lung cancer is based on the morphological evaluation of histological sections [3]. The classification of the histological subtypes of lung cancer is largely based on standard hematoxylin and eosin section [3].

2.2. Adenocarcinoma

Morphologically, adenocarcinomas show variable glandular structures. Tumor cells may be arranged in gland-like aggregates or papillary structures, have vacuolated cytoplasm, and feature nuclei with prominent nucleoli [3]. Adenocarcinomas of the lung often show differentiation toward type II (Clara cells) [25]. Thyroid transcription factor 1 (TTF1) plays an important role in production of surfactant [26]. This factor is expressed in 75% of pulmonary adenocarcinomas [26]. Other markers related to pulmonary adenocarcinomas are Cytokeratin (CK)7 and CK20 [26]. Adeno-carcinomas are mainly located in the peripheral lung parenchyma, but other locations are possible such as in central bronchial tissue or they may occur in combination with lung fibrosis [3]. Approximately 35% of all adenocarcinomas are diagnosed as stage IV disease [3].

2.3. Squamous cell carcinoma

Squamous cell carcinomas are characterized by variable keratinizing tumor cells and the presence of intercellular bridges [25]. These tumors are macroscopic grey or white and can be large in size and cavitate. Squamous cell carcinoma is characterized by a high level expression of keratin genes [26]. Especially keratin genes 5,6,13,14,16,17 and 19 are prominent among the expression markers [3, 26]. Also over expression of p53 related gene p63 is characterized for squamous cell carcinoma [3]. TTF-1 is mainly negative (90%) in squamous cell carcinomas [26].
Prognosis of squamous cell carcinoma is in general better than adenocarcinomas[3]. It metastasizes less frequently than other lung cancers [27]. Loco regional recurrence is more common in squamous cell carcinomas than in other lung tumors [27]. The mortality rate in patients with resected T2aN0M0 squamous cell carcinomas is better compared to adenocarcinomas with the same staging [28].

2.4. Adenosquamous carcinoma

Adenosquamous carcinoma has components of both adenocarcinoma and squamous cell carcinoma with each comprising at least 10% of the tumor [29]. The frequency of this type of tumor is 0.4-4% of all lung carcinomas [3, 29]. Diagnosis of this type of cancer is difficult. Squamous cell carcinomas with alveolar or acinar structures can easily be mistaken for glandular differentiation. Also easily misinterpreted is an adenocarcinoma with squamous metaplasia on the attached bronchiolar structures. Adenosquamous carcinoma is more aggressive than the regular adenocarcinoma or squamous cell carcinoma [29, 30]. Etiology of the tumor is still unclear. Some suggest that the two cell components (squamous and adeno) arise from the same clone or genetically related cellular clones [31].

2.5. Large cell carcinoma

Large cell carcinomas are by definition poorly differentiated tumors and account for approximately 9% of all lung carcinomas [3]. It is a diagnosis of exclusion, made after ruling out the presence of a component of squamous cell carcinoma, adenocarcinoma or SCLC [3]. Whether large cell carcinoma itself is a separate type of lung cancer or a poorly differentiated type of squamous cell- or adenocarcinoma is unknown. Histological presentation consists of nests with large polygonal cells with vesicular nuclei, prominent nucleoli and a moderate amount of cytoplasm [3]. No specific immunohistochemical markers are present for large cell carcinomas.

2.6. Large cell carcinomas with neuroendocrine differentiation

Large cell carcinomas with neuroendocrine differentiation (LCNEC) account for about 3% of all types of lung cancer [32, 33]. Microscopically the cells are large with abundant cytoplasm. Nucleoli are frequent and prominent, facilitating the distinction with SCLC [3]. Confirmation of neuroendocrine differentiation can be obtained by immunohistochemical markers such as chromogranin, synaptophysin and CD56 [34]. Differentiation of LCNEC from other types of NSCLC is important because this type of tumor resembles the biological behavior of a SCLC [34] and is associated with a higher recurrence rate [35].

2.7. Small cell lung cancer

SCLC is an epithelial tumor consisting of small cells with scant cytoplasm, ill-defined cell borders, finely granular nuclear chromatin, and absent or not clearly visible nucleoli [25]. The cells are round, oval, and spindle-shape and nuclear molding is prominent [25]. Necroses and a high mitotic count are typical for SCLC [3]. Around 60% of the SCLC tumors is positive for CD56 and chromogranin [36]. Also 90% is positive for TTF-1 [3, 26]. Negative prognostic parameters include extensive staging, low performance score, elevated serum LDH, low plasma sodium and albumin [37-39].

Although the precise cell of origin is not known for SCLC, it is likely to be a pluripotent bronchial precursor cell that can differentiate into each of the major histological subtypes of lung cancer [3].

SCLC appears as hilar or perihilar masses often with mediastinal lymphadenopathy. Superior Vena Cava obstruction is seen in 10% of the patients at diagnosis [40].

Due to widespread dissemination at diagnosis, it was common to divide SCLC in limited and extended disease. Limited was defined as restricted to one hemi thorax with regional lymph node metastases [41]. The included lymph nodes are hilar and mediastinal ipsilateral and contralateral as well as ipsilateral and contralateral supraclavicular lymph nodes [2]. In addition, ipsilateral pleural effusion (independent of cytology) was limited disease [2]. All patients with sites of disease beyond the definition of limited disease, equivalent to stage IV, were defined as extended disease [2]. Within the 7th edition of the TNM classification of lung tumors, it is recommended to use the TNM classification for all SCLC cases [42, 43].

2.8. Carcinoid tumor

Carcinoid tumors are characterized by neuroendocrine differentiation growth patterns [3]. Histologically tumor cells have a uniform cytological feature. Carcinoid tumors are classified as typical and atypical carcinoids [44]. Typical carcinoid is a tumor with less than 2 mitosis per 2 mm^2 and the absence of necrosis. Atypical carcinoid has 2-10 mitosis per 2 mm^2 and/or foci of necrosis [44]. Although this tumor is indolent, it is classified as a malignancy because it can invade and metastasize [45]. Diagnosis can be confirmed by histology or cytology obtained during bronchoscopy, but a large piece of well-preserved tumor is needed to differentiate between typical and atypical carcinoid [45]. Pulmonary carcinoids are derived from neuroendocrine cells which exist in normal airways. These neuroendocrine cells are numerous in fetal lungs and become less common in adult lungs. Histopathologically, the most common carcinoid patterns are organic and trabecular, in which the tumor cells are respectively arranged in nests or cords[3].

2.9. Conclusion
Although awareness of different histological subtypes in lung cancer existed, the distinction was limited to NSCLC and SCLC. This was due to limitation of treatment options. Nowadays differences in tumor location, growth rate, and metastasis behavior have been observed within the group of NSCLC. The consequence is more recognition of certain treatment modalities, and changes in prognosis between the histological subtypes. Microscopical differences between the histological subtypes are a major challenge for pathologists. The positive predictive value for SCLC is high (94%) [46] but this does not account for large cell carcinomas (23%). This is probably because the specific features for adenocarcinomas and squamous cell carcinomas are missing [46]. Sample size is an important factor in achieving the correct diagnosis [46]. The increased numbers of cytology specimen obtained by endoscopic ultrasound fine needle aspiration (EUS-FNA) and endobronchial ultrasound (EBUS) will make it more difficult for the pathologist.

3. Metabolic microenvironment of lung cancer
3.1. Introduction
A solid tumor must be seen as a poorly organized "organoid" [47]. Its function is maintained by interaction between neoplastic and host cells. This interaction constitutes the tumor metabolic microenvironment [47]. The metabolic microenvironment defined by Vaupel *et al* includes tumor perfusion, tumor oxygenation, pH distribution and metabolic bioenergetic status [48]. The concept of tumor metabolic microenvironment is beyond the scope of this introduction. The introduction will be restricted to the three main features of metabolic microenvironment: hypoxia, angiogenesis and glycolysis.

3.2. Hypoxia
Hypoxia is defined as a state of reduced O_2 availability or decreased O_2 partial pressure below critical thresholds, restricting or even abolishing the function of organs, tissues, or cells [49]. It has been reported as a key factor in the aggressiveness of solid cancer tumors [49-51]. Evidence exists that hypoxia is an early step in carcinogenesis [52-54].
Tumor hypoxia is the result of imbalance between oxygen consumption and oxygen supply [55]. Several mechanisms are responsible for hypoxia [56]. First, hypoxia can be caused by inadequate blood flow in the tumor tissue [56]. Inadequate vascular network and impaired blood vessels result in an absence of flow regulation or stasis. Second, hypoxia can be caused by increased diffusion distance [48, 56]. By tumor expansion without increasing microvessel network the distance between the oxygen providing vessel and the cell becomes too large. Third, anemia can cause a reduced oxygen supply to tumors [56, 57].
Hypoxia can induce apoptotic cell death in normal and malignant cells [58], but malignant cells are able to adapt to low hypoxia levels by changing their gene expression pattern. Hypoxia-inducible factor 1 (HIF1) is one of the best known and studied transcription factors for hypoxia [49]. This transcription factor consists of a HIF-1a and HIF-1b subunit. HIF-1a reflects HIF1 activity due to rapid expression in hypoxic conditions [59], HIF 1b is hypoxia independent [60]. In the absence of oxygen the prolyl hydroxylase domains that use oxygen in the hydroxylation reaction are inactive [60]. HIF "escapes" hydroxylation and reaches a higher steady state level. HIF1a when stabilized rapidly translocates to the nucleus and binds its partner

HIF1b [60]. Together they bind to target genes through a recognition DNA sequence, 5′-RCGTG-3′, referred to as a hypoxia response element [60]. So, in the absence of oxygen where the prolyl hydroxylase domain is inactive, HIF modulates the expression of genes involved in functions such as metabolism, invasion/metastasis and apoptosis/survival [60]. HIF1a expression also induces the transcription of vascular endothelial growth factor-A (VEGF-A) genes by binding HIF to the VEGF-A-promoter [60]. The product of this gene stimulates neoangiogenesis and re-establishes oxygen and nutritional homeostasis [61]. In several studies HIF1-a expression is associated with poor prognosis in early stage of lung cancer [59, 62, 63]. Tumor hypoxia has a heterogeneous distribution and has been related with invasive growth and metastasis [64, 65]. HIF1a is able to induce expression of certain epithelial-mesenchymal transition regulators [62]. Epithelial-mesenchymal transition is considered as one of the major molecule mechanisms inducing metastasis [62, 66]. Due to diminished oxygen radicals, tumor hypoxia is related to increasing resistance to radiation therapy [67]. A decrease in efficiency of certain cytotoxic drugs in hypoxic tumor tissue is also reported, although this effect is probably an effect of impaired vascularization of the tissue [68].

3.3. Angiogenesis

Oxygenation of tumors is facilitated by the creation of new blood vessels. In response to hypoxemia, tumors secrete angiogenic cytokines inducing the formation of microvessels from the surrounding host vasculature [69]. Many studies have investigated the role of tumor vessels in context of architecture, constituents, genetic abnormalities and angiogenic signaling [70-72].

Vascular endothelial growth factor (VEGF) is one of the most important angiogenetic cytokines [73]. VEGF is the most potent known angiogenic factor with specific mitogenic activity on endothelial cells [74]. High serum VEGF levels or high expression of tumor tissue VEGF are associated with poor prognosis and survival in different histological subtypes of lung cancer [75-78].

Some studies suggest that neoangiogenesis is already present in pre-invasive and early invasive bronchial lesions [79-81]. This indicates that angiogenesis is a relatively early event during lung cancer pathogenesis [79-81].

Neoangiogenesis is based on sprouting from existing blood vessels. The newly formed vessels are leaky and tortuous. The endothelial cell lining of these vessels has abnormal morphology and the basement membrane is irregular [82]. Treatment with angiogenesis inhibitor agents showed an improved survival benefit in a number of malignant tumors [83].

3.4. Glycolysis

Glycolysis is a set of multiple reactions which eventually convert one glucose molecule into two molecules pyruvate [84]. Glycolysis is a source of energy that does not require oxygen and can take place under aerobic or anaerobic conditions and is often associated with tumors [85]. Hypoxic environment causes activation of multiple genes in tumor cells involved in glycolysis, cell proliferation, cell survival, angiogenesis, invasion and metastasis, which affect glucose metabolism and other associated cellular processes [86, 87].

Malignant cells exhibit an increased glycolytic flux caused by an over expression of glucose transporters GLUT-1 [88]. Also enzymes that are involved in the glycolytic pathway like lactate dehydrogenase (LDH) are elevated [89].

Upregulated HIF-1 plays an important role in the expression of glucose transporters and glycolytic enzymes [50]. The end product of glycolysis is pyruvate and, in the presence of LDH [89], it catalyzes the quantitative formation of lactate. Lactate in primary tumors may provide a useful metabolic classification for tumors, which can serve as a prognostic parameter [90], but data are limited for well-founded treatment decision.

4. Treatment of lung cancer
4.1. Introduction
Tumor resection is still the first choice of treatment in stage I and II NSCLC disease. For patients diagnosed with SCLC or advanced NSCLC, systemic treatment (with or without radiotherapy) is the first choice of treatment [91]. Systemic treatment can be divided into a cellular treatment and an environmental treatment response.

4.2. Cellular treatment
Standard systemic treatment in patients with NSCLC or SCLC is a platinum based combination chemotherapy regime [91]. Platinum-based chemotherapy agents (cisplatin, carboplatin) act by cross-linking subunits of DNA. These agents work during any part of cell cycle by impairing DNA synthesis, transcription, and function [92]. The damaged DNA elicits DNA repair mechanisms, but when repair is impossible apoptosis is induced. Platinum-based chemotherapy agents are combined nowadays with one of the following chemotherapeutic for a combination regime.
Gemcitabine is a nucleotide analog which replaces one of the nucleic acids during DNA replication [93]. Hereby, the process arrests tumor growth, because newly attached nucleotides are blocked. This process results in apoptosis of the cell.
Paclitaxel and docetaxel, both antimitotic chemotherapeutics interfere with the normal function of microtubulin. Microtubules are responsible for the position of chromosomes during their replication and subsequently separation of two new cells [94]. The result of these chemotherapeutics is inhibition of mitosis. Furthermore, paclitaxel and docetaxel induce programmed cell death by binding to an inhibitor of apoptosis Bcl2, thereby arresting its function [95].
Vinorelbine is a semisynthetic vinca alkaloid which also influences microtubule function [96].
Etoposide inhibits the enzyme topoisomerase II [97]. Topoisomerase II is essential for separation of two new cells at the end of replication. Separation failure leads to cell death.
An additional first line treatment in advanced NSCLC is pemetrexed. Observations showed that this multitarget anti-folate pemetrexed in combination with Cisplatin was superior to gemcitabin/cisplatin in patients with a non-squamous cell carcinoma [19]. Pemetrexed is a potent inhibitor of thymidylate synthase and other folate-dependent enzymes, including dihydrofolate reductase and glycinamide ribonucleotide formyl transferase [21]. By inhibiting these enzymes pemetrexed prevents the formation of DNA and RNA which are essential in growth and survival of normal and cancer cells.
A second novel therapy of first line treatment is epidermal growth factor receptor (EGFR) tyrosine kinase inhibitors (TKIs). EGFR is over expressed in lung cancer which leads to an inappropriate activation of the anti-apoptotic RAS signaling cascade [98]. This leads eventually to uncontrolled cell proliferation. Mutation in the

EGFR tyrosine kinase domain is responsible for activation of anti-apoptotic pathways [99]. EGFR mutations are present in approximately 10% of the western patients with NSCLC. The population with a EGFR mutation, treated with EGFR-TKIs, has shown response rate of 65-82% [98].

4.3. Microenvironment treatment
Nowadays systemic treatment options which influence the microenvironment have been developed. Best known is bevacizumab: an angiogenesis inhibitor, which is a humanized monoclonal antibody [24]. Bevacizumab blocks VEGF-A thereby preventing the growth of new blood vessels. The American Society of Clinical Oncology (ASCO) [22] guidelines recommend the addition of bevacizumab to carboplatin/paclitaxel in first line cytotoxic therapy, except for patients with squamous cell carcinoma, or patients with exclusion criteria prescribed in the registration trial [100].
A number of other agents working on tumor vasculature are under development. One of these is ASA404, a tumor vascular disrupting agent which induces apoptosis of tumor vascular endothelial cells and cytokine production, leading to tumor vascular collapse [101, 102]. ASA404 has been studied in a phase II study in patients with advanced NSCLC. The median extension of survival was 5 months compared to chemotherapy alone [101, 102]. A phase III study has finished accrual recently.
An early study with a hypoxic cytotoxin tirapazamine has shown promising results in patients with NSCLC [103]. Tirapazamine is an aromatic heterocycle di-*N*-oxide, which is activated to a toxic radical only at very low levels of oxygen [104]. A phase III study (CATAPULT I) showed a benefit of the combination cisplatin and tirapazamine over cisplatin alone [105]. Unfortunately the next study (CATAPULT II) showed no benefit of cisplatin and tirapazamine over cisplatin and etoposide [104].

5. Methods of analyzing in vivo tumor microenvironment
5.1. Imaging introduction
Imaging techniques are expanding ever since the development of X-ray and bronchoscopy. Nowadays, a numerous amount of techniques have been developed to provide information about (pre)malignant lung lesions. The conventional techniques have been incorporated in the standard work-up of lung cancer detection and staging procedure. More recently a functional imaging technique, Positron Emission Tomography (PET), has been incorporated in the standard work-up of lung cancer. By imaging metabolic activity, information on metastatic spread of the tumor can be obtained. A combination of these imaging techniques is able to inform us about the localization of the primary tumor and the possibility of lymph or distance metastasis. Recent data showed that PET scanning may also be of prognostic value [106-108]. Unfortunately, the standard imaging techniques, such as X-ray and CT scan, are unable to inform us about the microenvironment of the tumor. Therefore functional imaging techniques and optical techniques have to be used.

5.2. Imaging techniques that provide information about hypoxia in lung cancer
5.2.1. Direct measurement of hypoxia
The present "gold standard" in hypoxia measurements is intratumor polarographic measurement of O2 partial pressures using microsensor techniques that adhere to the systematic random sampling principle [109-111]. The polarographic electrode is

not flexible and therefore mainly usable in tumors that are easy to reach like head and neck tumors, skin tumors and mamma carcinomas. Only one study with an Eppendorf polarographic electrode for per-operative hypoxia measurements has been performed in stage I and II lung cancer [112]. This study showed that the median tumor pO2 ranged from 0.7 to 46 mmHg and was lower than normal lung tissue [112].

5.2.2. Reflectance spectroscopy
5.2.2.1. Introduction

Light absorption and reflection of tissue is wavelength dependent, and by analyzing these absorption and reflection data, information about tissue can be obtained. Light absorption in tissue is predominantly by oxy and deoxyhemoglobin. Light scattering is caused by various cellular compounds like nuclei, nucleoli and mitochondria and extracellular compounds like collagen and elastin [113, 114]. Reflectance spectroscopy is useful in analyzing malignant tissue [115]. Absorption and reflectance spectra are susceptible to microenvironmental changes and changes in absorption and reflectance spectra have been observed between normal and malignant bronchial tissue [115, 116]. The development of flexible fibers makes delivery of light for absorption and reflection analyses of tissue by a scope technique possible. With these flexible fibers spectroscopic analyses could be performed in lung tissue during bronchoscopy. To analyze only the submucosa of bronchial epithelium, differential path length (DPS) spectroscopy was created [117].

DPS technique consists of two flexible fibers (figure 1): one delivery-collecting (dc) fiber and a collecting (c) fiber. Light travels through the dc fiber and brings light to the investigated bronchial tissue. Reflected light is collected by both the dc and the c fiber. Reflected light of the dc and the c fiber is then analyzed by a spectrometer. Re-emitted light collected by the dc fiber contains superficial and deeper reflected light, whereas only deeper reflected light is collected by the c fiber. The subtraction of the two spectra data forms the DPS spectra, which contains only superficial tissue reflection.

DPS spectra such as in figures 2 and 3 look very similar to the general picture seen in reflection- and elastic scattering spectroscopy: a slight overall decrease in signal when going from the blue to the near infrared wavelengths indicating Mie scattering and several characteristic absorption bands from blood [118]. To translate the spectra accurately in terms of biologically relevant parameters it is necessary to model the shape of these DPS-spectra and fit these models to the measured spectra. To do so, it is possible to analyze what exactly is going on right in front of the dc-fiber. However, the part that can be modeled analytically (the diffuse part of the light) has been subtracted away. What remains to form the DPS-spectrum is that part of the photon distribution for which no analytical models exist. Since Monte-Carlo methods do not allow inverse calculations, the only remaining option here is empirical modeling. The development of our mathematical model to describe the DPS spectra was based on careful analysis of Monte Carlo simulations, phantom experiments and a little trial and error. The basic equation with which we analyze DPS spectra is:

$$DPS(\lambda) = \mu_S(\lambda) e^{\left(-\tau \mu_a(\lambda)\right)}$$

eq.1.

where $\mu_s(\lambda)$ stands for the scattering coefficient, $\mu_a(\lambda)$ for the absorption coefficient and τ for the pathlength. Absorption and scattering are wavelength dependent functions and in principle the pathlength τ is as well. The pathlength can be considered constant.

5.2.2.2. DPS-Measurements in vivo
Main features
A typical DPS spectrum measured in vivo is shown in figure 2. Clearly visible are the blood absorption dips on a background of Mie Scattering. A fit was made using eq 1 on these curves using Mie scattering and blood absorption:

$$\mu_s(\lambda) = a\left(\frac{\lambda}{\lambda_0}\right)^b$$

$$\mu_a(\lambda) = \rho\left(S_tO_2\,\mu_a^{oxyHemo}(\lambda) + (1 - S_tO_2)\mu_a^{Hemo}(\lambda)\right)$$

eq.2.

where a and b are Mie scattering parameters, λ_0 = 800 nm, ρ the blood volume fraction and S_tO_2 the oxygen saturation of the blood. The resulting curve shown in figure 2 shows that the model roughly fits the data from 450 nm up. In this fit we intentionally ignored the lower wavelengths, because the violet absorption band would have seriously worsened the fit.

Technical improvements to the setup expanding the wavelength range to 350 nm yielded an excellent view on the Soret absorption band of hemoglobin but also indicated an issue requiring improvement: The Soret absorption band of blood around 415 nm appeared to be systematically overestimated by the model. This has to do with a phenomenon called pigment packaging. In this wavelength range the absorption of hemoglobin in blood vessels is so high that it partly shields itself from the incoming light. The intensity of this effect and hence the correction factor depends on the "packing diameter"; i.e. the diameter of the areas of high concentration. In this case it refers to the diameter of the blood vessels. A correction for this phenomenon has been derived and introduced the effective absorption coefficient μ_a'[119] where R stands for the radius of the blood vessel.

$$\mu_a'(\lambda) = \frac{\left(1 - e^{(-2R\mu_a(\lambda))}\right)}{2R}$$

eq.3.

This correction assumes packing of the absorber in cylinder shaped vessels. A slightly different correction can be derived for different packing shape[120]. Our cylinder approach may become problematic if we go from cylindrical micro vessel to the smallest capillary where single red blood cells pass from time to time. Not only do the red blood cells have complicated non cylindrical shapes, they also change shape continuously while passing through the smallest capillaries. Hence, for simplicity, and because it seems to fit well we use the cylindrical correction

factor even for diameter values that suggest single red blood cells rather than a well filled cylindrical vessel. This is important to keep in mind when interpreting the values of this parameter.

The packing effect is not limited to hemoglobin, but affects all absorbers present in the blood vessel. Any other vascular absorber can be added to the absorption of hemoglobin and oxyhemoglobin before the packing correction is performed. Any absorber that is homogeneously distributed over the tissue can be added after the packing correction:

$$\mu_a^{\cdot}(\lambda) = \rho \left[\frac{\left(1 - e^{\left(-2R\left(S_t O_2 \mu_a^{oxyHemo}(\lambda) + (1 - S_t O_2)\mu_a^{Hemo}(\lambda)\right) + \mu_a^{other}(\lambda)\right)}\right)}{2R} \right] + \mu_a^{hom}(\lambda)$$

eq.4.

where μ_a^{other} stands for the other vascular absorbers and μ_a^{hom} for an additional homogeneously distributed absorber. The resulting fit and the residue spectrum for a typical measurement are shown in figure 3. Judging from the values of χ^2 we have a much better fit here (significantly better at $p<0.05$ F-test) when looking at the entire wavelength range. As expected the improvements are limited to the <450 nm band.

5.2.3. 18F-fluoromisonidazol and Positron Emission Tomography

Hypoxia imaging by PET is possible. This has been introduced by a class of probes called hypoxic markers [121]. These hypoxic markers seem to be able to bind to hypoxic cells. Several hypoxic markers have been investigated [85, 121]. Most widely used and investigated is tracer 18F-fluoromisonidazol (18F-FMISO), it contains 2-nitroimidazoles which have maximum binding to hypoxic cells [122, 123].18F-FMISO enters cells by passive diffusion. In cells with reduced tissue oxygen partial pressure it is reduced by nitroreductase enzymes to become trapped [124]. When oxygen is abundant in normally oxygenated cells, the parent compound is quickly regenerated by re-oxidation and metabolites do not accumulate [124]. However, in hypoxic cells, the low oxygen partial pressure prevents re-oxidation of 18F-FMISO metabolites, resulting in tracer accumulation in hypoxic cells. Because 18F-FMISO only accumulates in hypoxic cells with functional nitroreductase enzymes, 18F-FMISO only accumulates in viable cells but not in dead necrotic cells [124].

Comparisons between direct hypoxic measurement by the Eppendorf polarographic electrode and 18F-FMISO have been performed [125, 126]. Difference in accuracy was observed between different type of tumors. Measurement between head and neck tumors measured by the Eppendorf polarographic electrode and 18F-FMISO had the highest correlation [125]. Due to the difficulty of measurement of lung tumors by the Eppendorf polarographic electrode, no data are present. 18F-FMISO has been studied to predict treatment response and survival in patients with NSCLC [124, 127, 128].

5.3. Imaging techniques that provide information about vascular patterns
5.3.1. Narrow Band Imaging
The Narrow Band Imaging (NBI) technique is based upon a light source with sequential red-green-blue (RGB) illumination [129]. The NBI system has special RGB filters of which the band-pass ranges have been narrowed from the standard 400-700nm (B 400-500nm, G 500-600nm and R 600-700nm) to 400-590nm (B1 400-430nm, B2 420-470nm and G 560-590nm) [129]. Also, the relative contribution of blue light (B1) has been increased. With this choice of filters NBI enables enhanced visualization of the mucosal morphology. Blue light allows optimal superficial imaging due to its small penetration depth [129, 130]. Blue light is also a main chromophore of haemoglobin in bronchial tissue. Haemoglobin has a maximum absorption wavelength near 415 nm. Because Narrow band imaging-Blue 1 (NBI-B1) covers the absorption wavelength for haemoglobin, a more accurate detection of the superficial vessel structures can be obtained [131]. The biological hypothesis is that the microvascular patterns of (pre)malignant lesions are different from that of normal bronchial mucosa [79, 80, 132]. Clinically, microvessels, vascular networks and dotted vessels were observed with NBI, and histological biopsies of areas with dotted vessels showed premalignant lesions and angiogenetic squamous dysplasia (ASD) [130].

5.3.2. DCE-MRI and DCE-CT
Dynamic contrast-enhanced magnetic resonance imaging (DCE-MRI) can be used to evaluate tissue vascularization [133]. By using an injection with paramagnetic contrast agent, like gadolinium, increase signal intensity of blood on T1-weighted images can be seen [133]. All tissues with an adequate blood supply will enhance, but malignant areas, with abnormal microvessels and increased permeability, tend to have increased signal intensity [133]. Quantitative related data of tissue perfusion and microvessel permeability can be obtained by calculating the concentration of gadolinium in the region of interest. The relation between the changes of signal intensity is non-linear and therefore not easy to define [134]. Limited results have been achieved in lung malignancies. Motions by the heart and lungs, and a low signal to noise ration due to the small amount of lung tissue, makes it difficult to obtain adequate images. An alternative modality is dynamic contrast-enhanced computer tomography (DCE-CT) also known as perfusion CT. The relation between contrast concentration iodine and enhancement is straightforward with CT, making it easier to use [134].

5.3.3. Sonography of mediastinal lymph nodes
Sonography is not a regular tool in the detection of lung cancer. It is mostly used in easy reachable malignancies like head and neck tumors. The introduction of echo Doppler provides more information about the vascularization of a tumor [135-137]. By using the sonographic option of the EUS-FNA and EBUS, it is possible to obtain vascular information of mediastinal lymph nodes. Previous studies showed that lymph node metastases had systematic effects on the vascular patterns within the node [136, 138]. Aberrant vessels, displacement of vessels, and avascular areas in the center of the node were observed, indicating a compromised vascular network within the center of the node [136, 138].

5.4. Imaging technique that provide information about the glycolysis
5.4.1. Positron Emission Tomography
Positron emission tomography (PET) is a non invasive imaging technique which is able to provide physiological information of the body [139]. Positron-editing radionuclide (tracer) can be introduced into the body on a biological active molecule. Pairs of gamma rays that are emitted indirectly by the tracer can be detected by a PET scan. [18F]Fluorodeoxyglucose (18F-FDG) is the most commonly used tracer in clinical oncology. This tracer is a glucose analog that is taken up by glucose-using cells [140]. Once 18F-FDG has entered a cell it is phosphorylated by hexokinase to deoxyglucose 6-phosphate [140]. The next step in the glycolysis, the production of deoxyfructosis 6-phosphate, is not possible because the oxygen atom, which is replaced by F-18 to generate 18F-FDG, is required for the next step in glucose metabolism in all cells [140]. Therefore no further reactions occur in 18F-FDG and 18F-FDG is trapped in the cell [140]. This results in intense radiolabeling of tissues with high glucose uptake, such as the brain, the liver and most cancers [128, 141]. A high uptake of 18F-FDG reflects an increased glucose metabolism[141].
Computed tomography (CT) used to be the standard imaging technique for the analysis of lung cancer. Over the past decade 18F-FDG-PET has proved to be a valuable imaging technique in the standard work-up of NSCLC [142]. The additional information gained was detection of lesions initially not seen on CT-scan [143]. Moreover, in tumor staging of patients with NSCLC, analysis of integrated PET/CT images was superior to that of CT images alone, PET images alone, and PET and CT images viewed side by side [144-146].
The concentration of 18F-FDG in a cell can be quantified by a standard uptake value (SUV). This can be calculated as shown by equation 5 [147].

$$ SUV = \frac{ACvoi\,(kBq/ml)}{FDGdose\,(MBq)/BW\,(kg)}. $$

eq. 5.

In this equation the SUV is dependent on the Average activity Concentration in the specific volume of interest (ACvoi), Dose of 18F-FDG (FDGdose) and Body weight (BW). SUV is a simplified quantitative measurement which can be seen as a metabolism parameter. SUVmax, the maximum of 18F-FDG concentration, showed to be a prognostic and predictive marker in patients with stage I or II NSCLC [107, 108, 148]. Physiology as well as technical factors can affect the SUV outcome [147]. Many of these factors have only a relatively small effect; however an accumulation of these factors can lead to substantial differences [147]. Technical factors include: incorrect synchronization of clocks of PET/CT camera and dose calibrator, paravenous administration of 18F-FDG, and residual activity in administration system [147]. Some physiological factors are: blood glucose level of the patient [149], patient comfort [147], and inflammation [150].
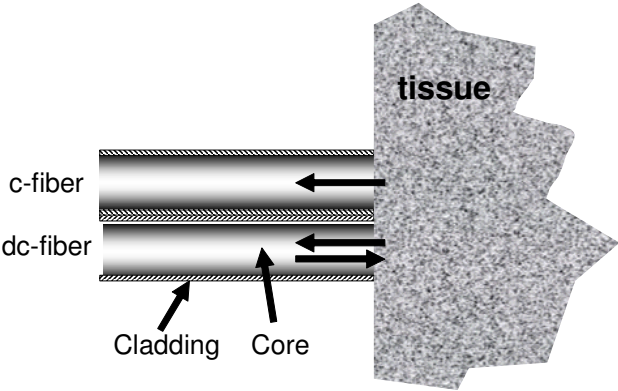
Figure 1: basic DPS geometry: two optical fibers tightly together in contact with the tissue. One delivering light (d), and both collecting light (c)
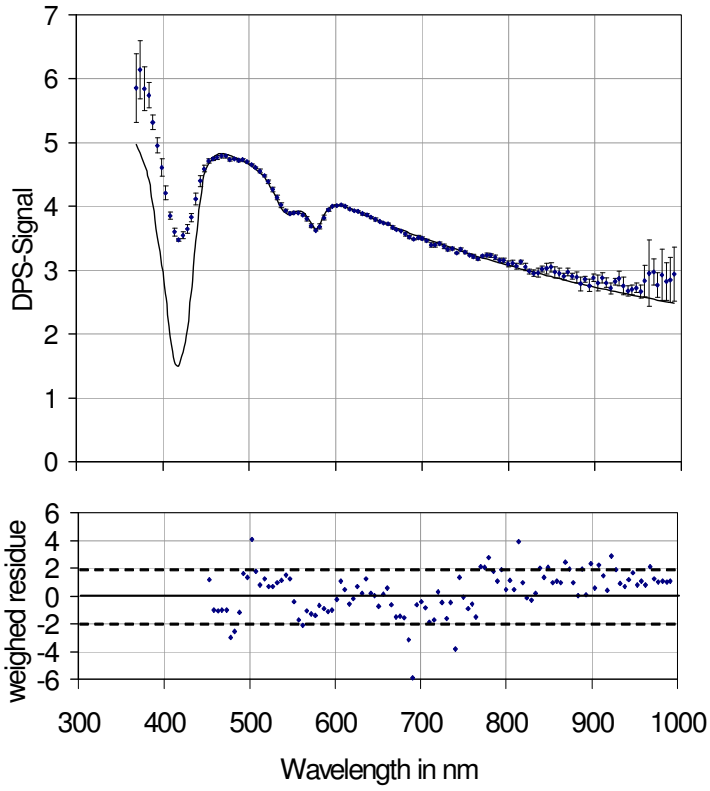
Figure 2. Typical DPS spectrum measured endoscopically on normal bronchial mucosa with fit of the model of equation 2 and noise weighed residues
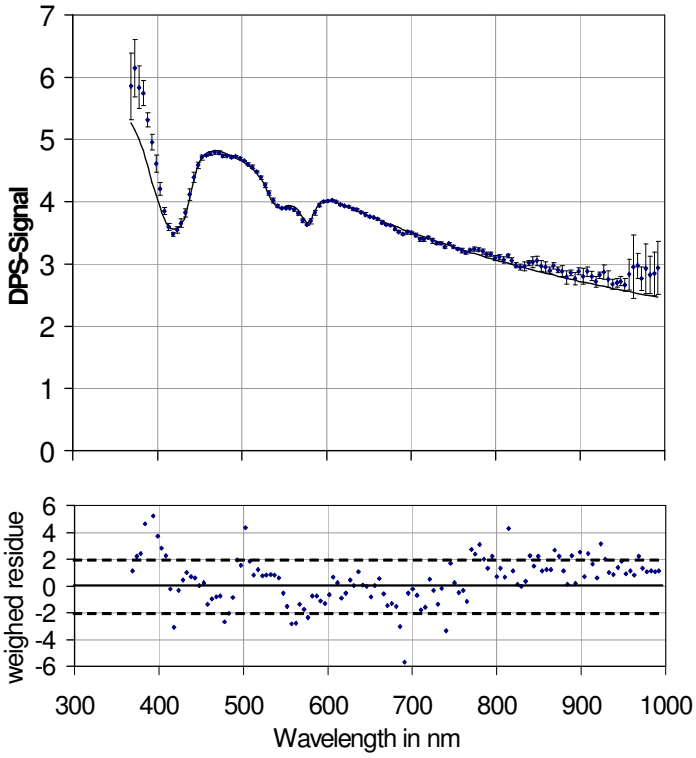
Figure 3. Typical DPS spectrum measured endoscopically on normal bronchial mucosa with fit of the model of equation 4 and noise weighed residues

Aim of the thesis

The aim of this thesis was to investigate optical and functional imaging in patients with lung cancer. In this thesis reflectance spectroscopy and Positron Emission Tomography were studied. The use of reflectance spectroscopy in the analysis of patients diagnosed with endobronchial tumors was studied in the first place. For this study a fiberoptic instrument was used which can be utilized for DPS measurements during bronchoscopy. To obtain reflectance spectroscopic measurements in mediastinal lymph nodes a single fiber optical probe which could be used for reflectance spectroscopy measurements during EUS-FNA was constructed. Furthermore the use of PET scanning in patients diagnosed with SCLC was studied.

In **chapter 2** the available optical techniques for detection of premalignant lesions in the central airways were described and the techniques were divided into different categories. We set out the technical aspects of the imaging and point measurement techniques. Furthermore the underlying biological mechanisms resulting in the optical contrast for each technique, and the clinical use of these novel optical techniques were discussed. Reflectance spectroscopy seemed to be a promising technique for imaging and physiological studies; further research with this technique was performed.

In **chapter 3** the microvascular data obtained by DPS was compared to the expression of a hypoxia related protein: HIF1a. HIF1a is a well-known and often used protein in tumor hypoxia related studies. A significant correlation between a low microvascular saturation measured by DPS and an elevated expression of HIF1a was observed, concluding that hypoxia related data can be studied by DPS.

As hypoxia is related to aggressiveness of malignant diseases, in **chapter 4**, the relation between the peripheral microvascular saturation measured by DPS in the different types of lung cancer was reported. No differences were found between NSCLC and SCLC, but differences between the four subtypes were found instead. Peripheral microvascular saturation of adenocarcinomas and squamous cell carcinomas was higher compared to large cell carcinomas and SCLC. Observed differences suggested a poor vascular pattern in poor differentiated tumors. No survival variation between the microvascular saturation data was seen.

Whether the reflectance spectroscopy technique could be useful in other diagnostic techniques was unknown and the possibilities were explored in **chapter 5.** An original optical instrument was developed for the analysis of lymph node optical properties. A single fiber probe was constructed to guide through an EUS-FNA needle to obtain reflectance spectra in mediastinal lymph nodes during EUS-FNA procedure.

In **chapter 6** the feasibility of reflectance spectroscopy in lymph nodes during EUS-FNA procedure was described. The procedure without complications was performed in 10 patients. Differences in spectra were observed between normal and malignant lymph nodes. Decreased blood volume fraction and microvascular saturation were seen in malignant lymph nodes.

In the future optical imaging techniques will probably become more important in detection and staging of (pre)malignancies. Because optical imaging techniques can provide information about the microenvironment of a malignancy, optical imaging techniques might have predictive and prognostic value. Functional imaging, especially PET scanning, can be implemented in this respect. Perhaps a combination of these two modalities works additively. To study the value of

functional imaging, research was conducted with PET scanning in patients diagnosed with SCLC.

In **chapter 7** the value of PET scanning in detection of metastatic soft tissue lesions in patients diagnosed with SCLC was investigated, since this modality is not a standard procedure in the work-up of SCLC patients yet. PET scanning was responsible for change of stage in 7.9% of the 63 patients. We concluded that PET scanning has an additive value in the staging work-up of patients diagnosed with SCLC.

In **chapter 8** the value of SUVmax in 75 patients with SCLC was examined and the conclusion was that the SUVmax value of the primary tumor was lower in patients diagnosed with LD compared to ED. Furthermore, the SUVmax value showed to be a predictive factor in the PFS and OS in patients with ED. In this patient group high SUVmax was correlated with a better PFS and OS compared to patients with a low SUVmax value. These results were not observed in LD patients.

References

1. Jemal A, Siegel R, Ward E, Murray T, Xu J, Thun MJ. Cancer statistics, 2007. CA Cancer J Clin 2007;57:43-66.
2. Mountain CF. Revisions in the International System for Staging Lung Cancer. Chest 1997;111:1710-7.
3. W.D Travis EB, H.K. Muller-Hermelink, C.C Harris. Pathology and genetics of Tumours of the Lung, Pleura, Thymus and Heart; 2004: 9-124.
4. Janssen-Heijnen ML, Coebergh JW. The changing epidemiology of lung cancer in Europe. Lung Cancer 2003;41:245-58.
5. Serke M, Schonfeld N. [Diagnosis and staging of lung cancer]. Dtsch Med Wochenschr 2007;132:1165-9.
6. Dowell JE. Small cell lung cancer: are we making progress? Am J Med Sic 2010;339:68-76.
7. Subramanian J, Govindan R. Lung cancer in never smokers: a review. J Clin Oncol 2007;25:561-70.
8. Stellman SD, Muscat JE, Hoffmann D, Wynder EL. Impact of filter cigarette smoking on lung cancer histology. Prev Med 1997;26:451-6.
9. Satoh H, Yamashita YT, Ishikawa H, Kamma H, Ohtsuka M, Sekizawa K. Smoking and smoking-related lung cancer in female patients. Anticancer Res 1999;19:5627-30.
10. B'Chir F, Laouani A, Ksibi S, Arnaud MJ, Saguem S. Cigarette filter and the incidence of lung adenocarcinoma among Tunisian population. Lung Cancer 2007;57:26-33.
11. Stellman SD, Muscat JE, Thompson S, Hoffmann D, Wynder EL. Risk of squamous cell carcinoma and adenocarcinoma of the lung in relation to lifetime filter cigarette smoking. Cancer 1997;80:382-8.
12. Youlden DR, Cramb SM, Baade PD. The International Epidemiology of Lung Cancer: geographical distribution and secular trends. J Thorac Oncol 2008;3:819-31.
13. Sun S, Schiller JH, Gazdar AF. Lung cancer in never smokers--a different disease. Nat Rev Cancer 2007;7:778-90.
14. Spira A, Beane J, Shah V, et al. Effects of cigarette smoke on the human airway epithelial cell transcriptome. Proc Natl Acad Sci U S A 2004;101:10143-8.
15. Mao L, Lee JS, Kurie JM, et al. Clonal genetic alterations in the lungs of current and former smokers. J Natl Cancer Inst 1997;89:857-62.
16. Sato M, Shames DS, Gazdar AF, Minna JD. A translational view of the molecular pathogenesis of lung cancer. J Thorac Oncol 2007;2:327-43.
17. Hirsch FR, Spreafico A, Novello S, Wood MD, Simms L, Papotti M. The prognostic and predictive role of histology in advanced non-small cell lung cancer: a literature review. J Thorac Oncol 2008;3:1468-81.
18. Selvaggi G, Scagliotti GV. Histologic subtype in NSCLC: does it matter? Oncology (Williston Park) 2009;23:1133-40.
19. Scagliotti GV, Parikh P, von Pawel J, et al. Phase III study comparing cisplatin plus gemcitabine with cisplatin plus pemetrexed in chemotherapy-naive patients with advanced-stage non-small-cell lung cancer. J Clin Oncol 2008;26:3543-51.
20. Tiseo M, Bartolotti M, Gelsomino F, Ardizzoni A. First-line treatment in advanced non-small-cell lung cancer: the emerging role of the histologic subtype. Expert Rev Anticancer Ther 2009;9:425-35.
21. Kubota K, Niho S, Enatsu S, et al. Efficacy differences of pemetrexed by histology in pretreated patients with stage IIIB/IV non-small cell lung cancer: review of results from an open-label randomized phase II study. J Thorac Oncol 2009;4:1530-6.
22. Azzoli CG, Baker S, Jr., Temin S, et al. American Society of Clinical Oncology Clinical Practice Guideline update on chemotherapy for stage IV non-small-cell lung cancer. J Clin Oncol 2009;27:6251-66.
23. Ciardiello F, Tortora G. EGFR antagonists in cancer treatment. N Engl J Med 2008;358:1160-74.
24. Gridelli C, Maione P, Rossi A, De Marinis F. The role of bevacizumab in the treatment of non-small cell lung cancer: current indications and future developments. Oncologist 2007;12:1183-93.
25. Brambilla E, Travis WD, Colby TV, Corrin B, Shimosato Y. The new World Health Organization classification of lung tumours. Eur Respir J 2001;18:1059-68.

26. Jagirdar J. Application of immunohistochemistry to the diagnosis of primary and metastatic carcinoma to the lung. Arch Pathol Lab Med 2008;132:384-96.
27. Newlin HE, Iyengar M, Morris CG, Olivier K. Unresectable squamous cell carcinoma of the lung: an outcomes study. Int J Radiat Oncol Biol Phys 2009;74:370-6.
28. Ost D, Goldberg J, Rolnitzky L, Rom WN. Survival after surgery in stage IA and IB non-small cell lung cancer. Am J Respir Crit Care Med 2008;177:516-23.
29. Gawrychowski J, Brulinski K, Malinowski E, Papla B. Prognosis and survival after radical resection of primary adenosquamous lung carcinoma. Eur J Cardiothorac Surg 2005;27:686-92.
30. Nakagawa K, Yasumitu T, Fukuhara K, Shiono H, Kikui M. Poor prognosis after lung resection for patients with adenosquamous carcinoma of the lung. Ann Thorac Surg 2003;75:1740-4.
31. Kanazawa H, Ebina M, Ino-Oka N, et al. Transition from squamous cell carcinoma to adenocarcinoma in adenosquamous carcinoma of the lung. Am J Pathol 2000;156:1289-98.
32. Jiang SX, Kameya T, Shoji M, Dobashi Y, Shinada J, Yoshimura H. Large cell neuroendocrine carcinoma of the lung: a histologic and immunohistochemical study of 22 cases. Am J Surg Pathol 1998;22:526-37.
33. Takei H, Asamura H, Maeshima A, et al. Large cell neuroendocrine carcinoma of the lung: a clinicopathologic study of eighty-seven cases. J Thorac Cardiovasc Surg 2002;124:285-92.
34. Iyoda A, Hiroshima K, Nakatani Y, Fujisawa T. Pulmonary large cell neuroendocrine carcinoma: its place in the spectrum of pulmonary carcinoma. Ann Thorac Surg 2007;84:702-7.
35. Lemire JM, Archer DC. 1,25-dihydroxyvitamin D3 prevents the in vivo induction of murine experimental autoimmune encephalomyelitis. J Clin Invest 1991;87:1103-7.
36. Buys TP, Aviel-Ronen S, Waddell TK, Lam WL, Tsao MS. Defining genomic alteration boundaries for a combined small cell and non-small cell lung carcinoma. J Thorac Oncol 2009;4:227-39.
37. Tas F, Aydiner A, Demir C, Topuz E. Serum lactate dehydrogenase levels at presentation predict outcome of patients with limited-stage small-cell lung cancer. Am J Clin Oncol 2001;24:376-8.
38. Hansen O, Sorensen P, Hansen KH. The occurrence of hyponatremia in SCLC and the influence on prognosis A retrospective study of 453 patients treated in a single institution in a 10-year period. Lung Cancer 2010;68:111-4.
39. Brueckl WM, Herbst L, Lechler A, et al. Predictive and prognostic factors in small cell lung carcinoma (SCLC)--analysis from routine clinical practice. Anticancer Res 2006;26:4825-32.
40. Rowell NP, Gleeson FV. Steroids, radiotherapy, chemotherapy and stents for superior vena caval obstruction in carcinoma of the bronchus: a systematic review. Clin Oncol (R Coll Radiol) 2002;14:338-51.
41. Zelen M. Keynote address on biostatistics and data retrieval. Cancer Chemother Rep 3 1973;4:31-42.
42. Shepherd FA, Crowley J, Van Houtte P, et al. The International Association for the Study of Lung Cancer lung cancer staging project: proposals regarding the clinical staging of small cell lung cancer in the forthcoming (seventh) edition of the tumor, node, metastasis classification for lung cancer. J Thorac Oncol 2007;2:1067-77.
43. Vallieres E, Shepherd FA, Crowley J, et al. The IASLC Lung Cancer Staging Project: proposals regarding the relevance of TNM in the pathologic staging of small cell lung cancer in the forthcoming (seventh) edition of the TNM classification for lung cancer. J Thorac Oncol 2009;4:1049-59.
44. Travis WD, Rush W, Flieder DB, et al. Survival analysis of 200 pulmonary neuroendocrine tumors with clarification of criteria for atypical carcinoid and its separation from typical carcinoid. Am J Surg Pathol 1998;22:934-44.
45. Detterbeck FC. Management of carcinoid tumors. Ann Thorac Surg;89:998-1005.
46. Field RW, Smith BJ, Platz CE, et al. Lung cancer histologic type in the surveillance, epidemiology, and end results registry versus independent review. J Natl Cancer Inst 2004;96:1105-7.
47. Baronzio G, Hager E. Hyperthermia in Cancer Treatment: A Primer. New york: Landes Bioscience; 2006: 1-366.

48. Vaupel P, Kallinowski F, Okunieff P. Blood flow, oxygen and nutrient supply, and metabolic microenvironment of human tumors: a review. Cancer Res 1989;49:6449-65.
49. Hockel M, Vaupel P. Tumor hypoxia: definitions and current clinical, biologic, and molecular aspects. J Natl Cancer Inst 2001;93:266-76.
50. Harris AL. Hypoxia--a key regulatory factor in tumour growth. Nat Rev Cancer 2002;2:38-47.
51. Zander R, Vaupel P. Proposal for using a standardized terminology on oxygen transport to tissue. Adv Exp Med Biol 1985;191:965-70.
52. Polosukhin VV, Lawson WE, Milstone AP, et al. Association of progressive structural changes in the bronchial epithelium with subepithelial fibrous remodeling: a potential role for hypoxia. Virchows Arch 2007;451:793-803.
53. Griffiths EA, Pritchard SA, McGrath SM, et al. Increasing expression of hypoxia-inducible proteins in the Barrett's metaplasia-dysplasia-adenocarcinoma sequence. Br J Cancer 2007;96:1377-83.
54. Griffiths EA, Pritchard SA, Valentine HR, et al. Hypoxia-inducible factor-1alpha expression in the gastric carcinogenesis sequence and its prognostic role in gastric and gastro-oesophageal adenocarcinomas. Br J Cancer 2007;96:95-103.
55. Higginbotham GE, Huber JT, Wallentine MV, Johnston NP, Andrus D. Influence of protein percentage and degradability on performance of lactating cows during moderate temperature. J Dairy Sci 1989;72:1818-23.
56. Vaupel P, Harrison L. Tumor hypoxia: causative factors, compensatory mechanisms, and cellular response. Oncologist 2004;9 Suppl 5:4-9.
57. Vaupel P, Kelleher DK, Hockel M. Oxygen status of malignant tumors: pathogenesis of hypoxia and significance for tumor therapy. Semin Oncol 2001;28:29-35.
58. Riva C, Chauvin C, Pison C, Leverve X. Cellular physiology and molecular events in hypoxia-induced apoptosis. Anticancer Res 1998;18:4729-36.
59. Enatsu S, Iwasaki A, Shirakusa T, et al. Expression of hypoxia-inducible factor-1 alpha and its prognostic significance in small-sized adenocarcinomas of the lung. Eur J Cardiothorac Surg 2006;29:891-5.
60. Brahimi-Horn C, Pouyssegur J. The role of the hypoxia-inducible factor in tumor metabolism growth and invasion. Bull Cancer 2006;93:E73-80.
61. Carmeliet P. Angiogenesis in health and disease. Nat Med 2003;9:653-60.
62. Hung JJ, Yang MH, Hsu HS, Hsu WH, Liu JS, Wu KJ. Prognostic significance of hypoxia-inducible factor-1alpha, TWIST1 and Snail expression in resectable non-small cell lung cancer. Thorax 2009;64:1082-9.
63. Kim SJ, Rabbani ZN, Dewhirst MW, et al. Expression of HIF-1alpha, CA IX, VEGF, and MMP-9 in surgically resected non-small cell lung cancer. Lung Cancer 2005;49:325-35.
64. Gort EH, Groot AJ, van der Wall E, van Diest PJ, Vooijs MA. Hypoxic regulation of metastasis via hypoxia-inducible factors. Curr Mol Med 2008;8:60-7.
65. Frieboes HB, Zheng X, Sun CH, Tromberg B, Gatenby R, Cristini V. An integrated computational/experimental model of tumor invasion. Cancer Res 2006;66:1597-604.
66. Thiery JP. Epithelial-mesenchymal transitions in tumour progression. Nat Rev Cancer 2002;2:442-54.
67. Gray LH, Conger AD, Ebert M, Hornsey S, Scott OC. The concentration of oxygen dissolved in tissues at the time of irradiation as a factor in radiotherapy. Br J Radiol 1953;26:638-48.
68. Teicher BA, Holden SA, al-Achi A, Herman TS. Classification of antineoplastic treatments by their differential toxicity toward putative oxygenated and hypoxic tumor subpopulations in vivo in the FSaIIC murine fibrosarcoma. Cancer Res 1990;50:3339-44.
69. Ciardiello F. Epidermal growth factor receptor inhibitors in cancer treatment. Future Oncol 2005;1:221-34.
70. McDonald DM, Choyke PL. Imaging of angiogenesis: from microscope to clinic. Nat Med 2003;9:713-25.
71. Dvorak HF, Nagy JA, Feng D, Brown LF, Dvorak AM. Vascular permeability factor/vascular endothelial growth factor and the significance of microvascular hyperpermeability in angiogenesis. Curr Top Microbiol Immunol 1999;237:97-132.
72. Hida K, Hida Y, Amin DN, et al. Tumor-associated endothelial cells with cytogenetic abnormalities. Cancer Res 2004;64:8249-55.
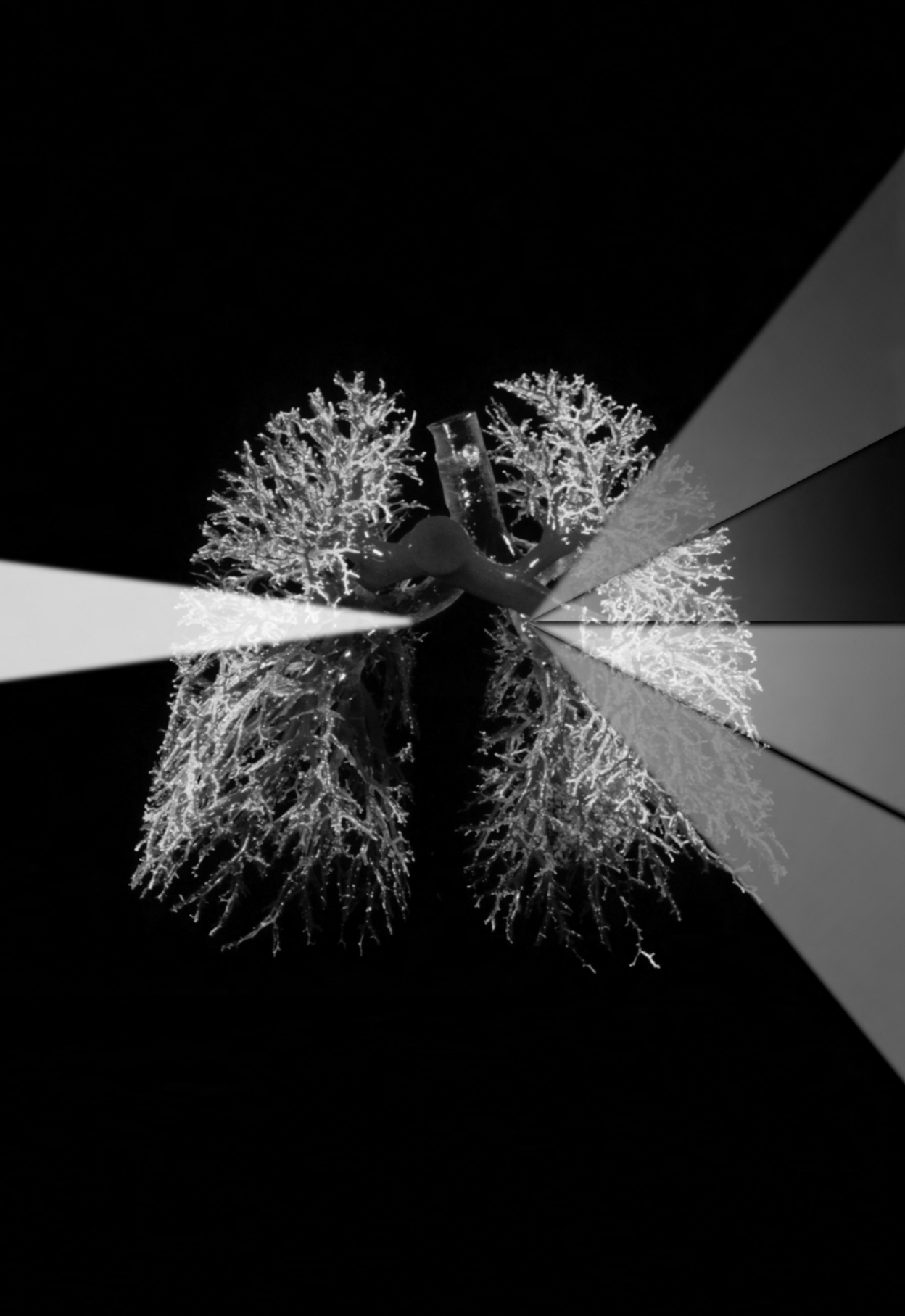73. Goudar RK, Vlahovic G. Hypoxia, angiogenesis, and lung cancer. Curr Oncol Rep 2008;10:277-82.

74.   Bharti A, Ma PC, Salgia R. Biomarker discovery in lung cancer--promises and challenges of clinical proteomics. Mass Spectrom Rev 2007;26:451-66.
75.   Fontanini G, Vignati S, Boldrini L, et al. Vascular endothelial growth factor is associated with neovascularization and influences progression of non-small cell lung carcinoma. Clin Cancer Res 1997;3:861-5.
76.   Volm M, Koomagi R, Mattern J. Prognostic value of vascular endothelial growth factor and its receptor Flt-1 in squamous cell lung cancer. Int J Cancer 1997;74:64-8.
77.   Imoto H, Osaki T, Taga S, Ohgami A, Ichiyoshi Y, Yasumoto K. Vascular endothelial growth factor expression in non-small-cell lung cancer: prognostic significance in squamous cell carcinoma. J Thorac Cardiovasc Surg 1998;115:1007-14.
78.   Salven P, Ruotsalainen T, Mattson K, Joensuu H. High pre-treatment serum level of vascular endothelial growth factor (VEGF) is associated with poor outcome in small-cell lung cancer. Int J Cancer 1998;79:144-6.
79.   Keith RL, Miller YE, Gemmill RM, et al. Angiogenic squamous dysplasia in bronchi of individuals at high risk for lung cancer. Clin Cancer Res 2000;6:1616-25.
80.   Fisseler-Eckhoff A, Rothstein D, Muller KM. Neovascularization in hyperplastic, metaplastic and potentially preneoplastic lesions of the bronchial mucosa. Virchows Arch 1996;429:95-100.
81.   Fontanini G, Calcinai A, Boldrini L, et al. Modulation of neoangiogenesis in bronchial preneoplastic lesions. Oncol Rep 1999;6:813-7.
82.   Jain RK. Normalization of tumor vasculature: an emerging concept in antiangiogenic therapy. Science 2005;307:58-62.
83.   Lyseng-Williamson KA, Robinson DM. Spotlight on bevacizumab in advanced colorectal cancer, breast cancer, and non-small cell lung cancer. BioDrugs 2006;20:193-5.
84.   Pauwels EK, Sturm EJ, Bombardieri E, Cleton FJ, Stokkel MP. Positron-emission tomography with [18F]fluorodeoxyglucose. Part I. Biochemical uptake mechanism and its implication for clinical studies. J Cancer Res Clin Oncol 2000;126:549-59.
85.   Krohn KA, Link JM, Mason RP. Molecular imaging of hypoxia. J Nucl Med 2008;49 Suppl 2:129S-48S.
86.   Bertout JA, Patel SA, Simon MC. The impact of O2 availability on human cancer. Nat Rev Cancer 2008;8:967-75.
87.   Denko NC. Hypoxia, HIF1 and glucose metabolism in the solid tumour. Nat Rev Cancer 2008;8:705-13.
88.   Zips D, Adam M, Flentje M, et al. Impact of hypoxia and the metabolic microenvironment on radiotherapy of solid tumors. Introduction of a multi-institutional research project. Strahlenther Onkol 2004;180:609-15.
89.   Shim H, Dolde C, Lewis BC, et al. c-Myc transactivation of LDH-A: implications for tumor metabolism and growth. Proc Natl Acad Sci U S A 1997;94:6658-63.
90.   Walenta S, Schroeder T, Mueller-Klieser W. Lactate in solid malignant tumors: potential basis of a metabolic classification in clinical oncology. Curr Med Chem 2004;11:2195-204.
91.   Pfister DG, Johnson DH, Azzoli CG, et al. American Society of Clinical Oncology treatment of unresectable non-small-cell lung cancer guideline: update 2003. J Clin Oncol 2004;22:330-53.
92.   Reed E. Platinum-DNA adduct, nucleotide excision repair and platinum based anti-cancer chemotherapy. Cancer Treat Rev 1998;24:331-44.
93.   Burkes RL, Shepherd FA. Gemcitabine in the treatment of non-small-cell lung cancer. Ann Oncol 1995;6 Suppl 3:S57-60.
94.   Kumar N. Taxol-induced polymerization of purified tubulin. Mechanism of action. J Biol Chem 1981;256:10435-41.
95.   Srivastava RK, Mi QS, Hardwick JM, Longo DL. Deletion of the loop region of Bcl-2 completely blocks paclitaxel-induced apoptosis. Proc Natl Acad Sci U S A 1999;96:3775-80.
96.   Lobert S, Vulevic B, Correia JJ. Interaction of vinca alkaloids with tubulin: a comparison of vinblastine, vincristine, and vinorelbine. Biochemistry 1996;35:6806-14.
97.   Hande KR. Etoposide: four decades of development of a topoisomerase II inhibitor. Eur J Cancer 1998;34:1514-21.
98.   Riely GJ. Second-generation epidermal growth factor receptor tyrosine kinase inhibitors in non-small cell lung cancer. J Thorac Oncol 2008;3:S146-9.
99.   Sordella R, Bell DW, Haber DA, Settleman J. Gefitinib-sensitizing EGFR mutations in lung cancer activate anti-apoptotic pathways. Science 2004;305:1163-7.

100. Sandler A, Gray R, Perry MC, et al. Paclitaxel-carboplatin alone or with bevacizumab for non-small-cell lung cancer. N Engl J Med 2006;355:2542-50.
101. McKeage MJ, Reck M, Jameson MB, et al. Phase II study of ASA404 (vadimezan, 5,6-dimethylxanthenone-4-acetic acid/DMXAA) 1800mg/m(2) combined with carboplatin and paclitaxel in previously untreated advanced non-small cell lung cancer. Lung Cancer 2009;65:192-7.
102. McKeage MJ, Von Pawel J, Reck M, et al. Randomised phase II study of ASA404 combined with carboplatin and paclitaxel in previously untreated advanced non-small cell lung cancer. Br J Cancer 2008;99:2006-12.
103. Weitman S, Mangold G, Marty J, et al. Evidence of enhanced in vivo activity using tirapazamine with paclitaxel and paraplatin regimens against the MV-522 human lung cancer xenograft. Cancer Chemother Pharmacol 1999;43:402-8.
104. Reddy SB, Williamson SK. Tirapazamine: a novel agent targeting hypoxic tumor cells. Expert Opin Investig Drugs 2009;18:77-87.
105. von Pawel J, von Roemeling R, Gatzemeier U, et al. Tirapazamine plus cisplatin versus cisplatin in advanced non-small-cell lung cancer: A report of the international CATAPULT I study group. Cisplatin and Tirapazamine in Subjects with Advanced Previously Untreated Non-Small-Cell Lung Tumors. J Clin Oncol 2000;18:1351-9.
106. Berghmans T, Dusart M, Paesmans M, et al. Primary tumor standardized uptake value (SUVmax) measured on fluorodeoxyglucose positron emission tomography (FDG-PET) is of prognostic value for survival in non-small cell lung cancer (NSCLC): a systematic review and meta-analysis (MA) by the European Lung Cancer Working Party for the IASLC Lung Cancer Staging Project. J Thorac Oncol 2008;3:6-12.
107. Chen JC, Huang TW, Cheng YL, et al. Prognostic value of 18-FDG uptake in early stage NSCLC. Thorac Cardiovasc Surg 2009;57:413-6.
108. Um SW, Kim H, Koh WJ, et al. Prognostic value of 18F-FDG uptake on positron emission tomography in patients with pathologic stage I non-small cell lung cancer. J Thorac Oncol 2009;4:1331-6.
109. Kallinowski F, Zander R, Hoeckel M, Vaupel P. Tumor tissue oxygenation as evaluated by computerized-pO2-histography. Int J Radiat Oncol Biol Phys 1990;19:953-61.
110. Hockel M, Schlenger K, Knoop C, Vaupel P. Oxygenation of carcinomas of the uterine cervix: evaluation by computerized O2 tension measurements. Cancer Res 1991;51:6098-102.
111. Collingridge DR, Young WK, Vojnovic B, et al. Measurement of tumor oxygenation: a comparison between polarographic needle electrodes and a time-resolved luminescence-based optical sensor. Radiat Res 1997;147:329-34.
112. Le QT, Chen E, Salim A, et al. An evaluation of tumor oxygenation and gene expression in patients with early stage non-small cell lung cancers. Clin Cancer Res 2006;12:1507-14.
113. Bartlett M, Huang G, Larcom L, Jiang H. Measurement of particle size distribution in mammalian cells in vitro by use of polarized light spectroscopy. Appl Opt 2004;43:1296-307.
114. Beauvoit B, Chance B. Time-resolved spectroscopy of mitochondria, cells and tissues under normal and pathological conditions. Mol Cell Biochem 1998;184:445-55.
115. Bard MP, Amelink A, Hegt VN, et al. Measurement of hypoxia-related parameters in bronchial mucosa by use of optical spectroscopy. Am J Respir Crit Care Med 2005;171:1178-84.
116. Bard MP, Amelink A, Skurichina M, et al. Optical spectroscopy for the classification of malignant lesions of the bronchial tree. Chest 2006;129:995-1001.
117. Amelink A, Sterenborg HJ, Bard MP, Burgers SA. In vivo measurement of the local optical properties of tissue by use of differential path-length spectroscopy. Opt Lett 2004;29:1087-9.
118. Mourant JR, Bigio IJ, Boyer J, Conn RL, Johnson T, Shimada T. Spectroscopic diagnosis of bladder cancer with elastic light scattering. Lasers Surg Med 1995;17:350-7.
119. van Veen RL, Verkruysse W, Sterenborg HJ. Diffuse-reflectance spectroscopy from 500 to 1060 nm by correction for inhomogeneously distributed absorbers. Opt Lett 2002;27:246-8.
120. Finlay JC, Foster TH. Hemoglobin oxygen saturations in phantoms and in vivo from measurements of steady-state diffuse reflectance at a single, short source-detector separation. Med Phys 2004;31:1949-59.
121. Ash KO, Holmer M, Johnson CS. Bilirubin-protein interactions monitored by difference spectroscopy. Clin Chem 1978;24:1491-6.

122. Amelink A, Robinson DJ, Sterenborg HJ. Confidence intervals on fit parameters derived from optical reflectance spectroscopy measurements. J Biomed Opt 2008;13:054044.
123. Krause BJ, Beck R, Souvatzoglou M, Piert M. PET and PET/CT studies of tumor tissue oxygenation. Q J Nucl Med Mol Imaging 2006;50:28-43.
124. Vikram DS, Zweier JL, Kuppusamy P. Methods for noninvasive imaging of tissue hypoxia. Antioxid Redox Signal 2007;9:1745-56.
125. Dunphy MP, Lewis JS. Radiopharmaceuticals in preclinical and clinical development for monitoring of therapy with PET. J Nucl Med 2009;50 Suppl 1:106S-21S.
126. Lee ST, Scott AM. Hypoxia positron emission tomography imaging with 18f-fluoromisonidazole. Semin Nucl Med 2007;37:451-61.
127. Gagel B, Reinartz P, Dimartino E, et al. pO(2) Polarography versus positron emission tomography ([(18)F] fluoromisonidazole, [(18)F]-2-fluoro-2'-deoxyglucose). An appraisal of radiotherapeutically relevant hypoxia. Strahlenther Onkol 2004;180:616-22.
128. Bentzen L, Keiding S, Nordsmark M, et al. Tumour oxygenation assessed by 18F-fluoromisonidazole PET and polarographic needle electrodes in human soft tissue tumours. Radiother Oncol 2003;67:339-44.
129. Cherk MH, Foo SS, Poon AM, et al. Lack of correlation of hypoxic cell fraction and angiogenesis with glucose metabolic rate in non-small cell lung cancer assessed by 18F-Fluoromisonidazole and 18F-FDG PET. J Nucl Med 2006;47:1921-6.
130. Shankar LK, Sullivan DC. Functional imaging in lung cancer. J Clin Oncol 2005;23:3203-11.
131. Vincent BD, Fraig M, Silvestri GA. A pilot study of narrow-band imaging compared to white light bronchoscopy for evaluation of normal airways and premalignant and malignant airways disease. Chest 2007;131:1794-9.
132. Shibuya K, Hoshino H, Chiyo M, et al. High magnification bronchovideoscopy combined with narrow band imaging could detect capillary loops of angiogenic squamous dysplasia in heavy smokers at high risk for lung cancer. Thorax 2003;58:989-95.
133. Amelink A, Kaspers OP, Sterenborg HJ, van der Wal JE, Roodenburg JL, Witjes MJ. Non-invasive measurement of the morphology and physiology of oral mucosa by use of optical spectroscopy. Oral Oncol 2008;44:65-71.
134. Herth FJ, Eberhardt R, Anantham D, Gompelmann D, Zakaria MW, Ernst A. Narrow-band imaging bronchoscopy increases the specificity of bronchoscopic early lung cancer detection. J Thorac Oncol 2009;4:1060-5.
135. Zahra MA, Hollingsworth KG, Sala E, Lomas DJ, Tan LT. Dynamic contrast-enhanced MRI as a predictor of tumour response to radiotherapy. Lancet Oncol 2007;8:63-74.
136. Marcus CD, Ladam-Marcus V, Cucu C, Bouche O, Lucas L, Hoeffel C. Imaging techniques to evaluate the response to treatment in oncology: current standards and perspectives. Crit Rev Oncol Hematol 2009;72:217-38.
137. Wu CH, Chang YL, Hsu WC, Ko JY, Sheen TS, Hsieh FJ. Usefulness of Doppler spectral analysis and power Doppler sonography in the differentiation of cervical lymphadenopathies. AJR Am J Roentgenol 1998;171:503-9.
138. Chikui T, Yuasa K, Maemura S, Kanda S. Change of angiostructure and hemodynamics in lymph node metastases in rabbits. Oral Surg Oral Med Oral Pathol Oral Radiol Endod 2002;93:350-7.
139. Tschammler A, Ott G, Schang T, Seelbach-Goebel B, Schwager K, Hahn D. Lymphadenopathy: differentiation of benign from malignant disease--color Doppler US assessment of intranodal angioarchitecture. Radiology 1998;208:117-23.
140. Ahuja AT, Ying M. Sonographic evaluation of cervical lymph nodes. AJR Am J Roentgenol 2005;184:1691-9.
141. Sachs S, Bilfinger TV. The impact of positron emission tomography on clinical decision making in a university-based multidisciplinary lung cancer practice. Chest 2005;128:698-703.
142. Erasmus JJ, McAdams HP, Patz EF, Jr., Goodman PC, Coleman RE. Thoracic FDG PET: state of the art. Radiographics 1998;18:5-20.
143. Bading JR, Shields AF. Imaging of cell proliferation: status and prospects. J Nucl Med 2008;49 Suppl 2:64S-80S.
144. Toloza EM, Harpole L, McCrory DC. Noninvasive staging of non-small cell lung cancer: a review of the current evidence. Chest 2003;123:137S-46S.

145. De Wever W, Stroobants S, Coolen J, Verschakelen JA. Integrated PET/CT in the staging of nonsmall cell lung cancer: technical aspects and clinical integration. Eur Respir J 2009;33:201-12.
146. Devaraj A, Cook GJ, Hansell DM. PET/CT in non-small cell lung cancer staging-promises and problems. Clin Radiol 2007;62:97-108.
147. Kligerman S, Digumarthy S. Staging of non-small cell lung cancer using integrated PET/CT. AJR Am J Roentgenol 2009;193:1203-11.
148. Schoder H, Erdi YE, Larson SM, Yeung HW. PET/CT: a new imaging technology in nuclear medicine. Eur J Nucl Med Mol Imaging 2003;30:1419-37.
149. Boellaard R. Standards for PET image acquisition and quantitative data analysis. J Nucl Med 2009;50 Suppl 1:11S-20S.
150. Dooms C, van Baardwijk A, Verbeken E, et al. Association between 18F-fluoro-2-deoxy-D-glucose uptake values and tumor vitality: prognostic value of positron emission tomography in early-stage non-small cell lung cancer. J Thorac Oncol 2009;4:822-8.
151. Hoekstra CJ, Hoekstra OS, Stroobants SG, et al. Methods to monitor response to chemotherapy in non-small cell lung cancer with 18F-FDG PET. J Nucl Med 2002;43:1304-9.
152. Gorospe L, Raman S, Echeveste J, Avril N, Herrero Y, Herna Ndez S. Whole-body PET/CT: spectrum of physiological variants, artifacts and interpretative pitfalls in cancer patients. Nucl Med Commun 2005;26:671-87.

Chapter 2

Optical detection of preneoplastic lesions of the central airways

A Review

C. van der Leest[1,2]

A. Amelink[3]

R.J. van Klaveren[1]

H.C. Hoogsteden[1]

H.J.C.M. Sterenborg[3]

J.G.J.V. Aerts[1,2]

1 Department of Pulmonary Diseases, Erasmus MC, Rotterdam, The Netherlands

2 Department of Pulmonary Diseases, Amphia Hospital, Breda, The Netherlands

3 Center for Optical Diagnostics and Therapy, Department of Radiation Oncology, Erasmus MC, Rotterdam, The Netherlands

Abstract
Current routine diagnosis of premalignant lesions of the central airways is hampered due to a limited sensitivity (white light bronchoscopy) and resolution (Computer tomography (CT), Positron Emission Tomography (PET)) of currently used techniques. To improve the detection of these subtle mucosal abnormalities, novel bronchoscopic optical imaging techniques have been developed over the past decade. In this review we highlight the technological developments in the field of endoscopic imaging, and describe their advantages and disadvantages in clinical use.

1. Introduction

Lung cancer is the second most common cancer in men and women, and the leading cause of cancer related death. In industrialized countries, the mortality rate of lung cancer is higher than of breast, colorectal and prostate cancer combined (1). Lung cancer is divided in small cell lung cancer (SCLC) and non small cell lung cancer (NSCLC). NSCLC is subdivided in 3 different major histological classes: squamous cell carcinoma (SCC), adenocarcinoma and undifferentiated large cell carcinoma(2). Fifty years ago Auerbach *et al* discovered that preinvasive lesions of different grades of severity were associated with lung tumors of squamous cell histology. This observation lead to the hypothesis that SCC arises from these preinvasive changes (3). It was shown that SCC develops sequentially: from normal to metaplasia, dysplasia, carcinoma in situ (CIS) and eventually invasive carcinoma (4). Early detection of preinvasive lesions is important because local treatment can preclude patients from getting invasive cancer. Local treatment have been developed and include photo dynamic therapy (PDT)(5-7), electrocautery(8), brachytherapy(9) and cryotherapy(10). Treatment with PDT has extensively been investigated. PDT showed in 99 patients with stage 0 and 56 patients with stage IA disease a complete response of 86%. Especially success response was seen in lesions smaller than 1 cm (complete response 95%) (11).

Since the epithelial changes associated with premalignancy are very subtle, no current routine imaging technique is sensitive enough to detect these lesions. Non-optical imaging techniques such as ultrasound, Magnetic resonance imaging (MRI), Computer tomography (CT), Positron Emission Tomography (PET) do not have a sufficient spatial resolution to detect the subtle mucosal abnormalities. Currently, premalignant lesions are only detected by bronchoscopy.

Unfortunately, the sensitivity and specificity for the detection of premalignant lesions is low using standard white light bronchoscopy (12). Therefore, novel endoscopic imaging techniques have been developed over the past decade to increase its sensitivity. Furthermore, optical point (spectroscopic) techniques have been developed to increase the specificity of the imaging modalities. In this review we describe the technical aspects of these imaging and point measurement techniques, discuss the underlying biological mechanisms resulting in the optical contrast for each technique, and discuss the clinical use of these novel optical techniques.

2. Biological changes

2.1. Morphology

SCC is mainly located in the central bronchial tree of the lung. This has been associated with cigarette smoke exposure and the higher concentration of carcinogens in the more central airways. The lesions are mainly located on the bifurcation segment bronchi but no predominant place within these central airways is present. Comparable to the development of malignant lesions in other organs like oesophageal cancer by chronic inflammation due to bile acid irritation and cervical cancer by chronic Human Pappilomavirus (HPV) inflammation (13), lung cancer development seems to be driven by chronic irritation mostly due to smoking(14, 15) but also HPV inflammation(16). As result of chronic irritation/stimulation cells may differentiate towards a phenotype better adapted to the prevailing environment, and squamous metaplasia occurs (17).

It is believed that SCC develops according a stepwise process which can be observed with histological biopsies (4). Hyperplasia and metaplasia are thought to be reactive lesions, with goblet cell hyperplasia and basal cell hyperplasia. Dysplasia is considered as a true preneoplastic lesion and may vary in degree, from mild to moderate and severe. Mild dysplastic lesions are characterized by minimal architectural and cytological disturbance. Moderate dysplasia exhibits more cytological irregularity, which is even more pronounced in severe dysplasia. In severe dysplasia it is accompanied by cellular polymorphism. In a subset of dysplastic changes, angiogenetic squamous dysplasia (ASD), the basal membrane thickens and there is vascular growth in the subepithelial tissues that results in papillary protrusions (18, 19). The observed cellular changes include modifications in the volume, form, and orientation of the nuclei, an increase in nucleus chromatin content, variations in the nucleus-cytoplasm ratio, and changes in the intra-cytosolic content (20). Also major architectural changes occur, such as a disorganized fibered network microstructure (21), and reticular basement membrane thickening (22), inducing a thickening of the epithelial layer.

2.2. Physiology

In several types of solid cancers, hypoxia has been reported as a key factor in the aggressiveness of a tumor (2, 23). Heterogeneous distribution of oxygen and nutrients within the tumor has been related to invasive growth (24). Some evidence exists that hypoxia is an early step in carcinogenesis (22, 25, 26), but for early lung cancer this has not been investigated. We did observe hypoxia in later stages of endobronchial cancer, but this cannot be extrapolated to premalignant disease (27).

Oxygenation of solid tumors is facilitated by the creation of new blood vessels (neoangiogenesis). In response to hypoxia, tumours secrete angiogenic cytokines, such as vascular endothelial growth factor (VEGF), inducing the formation of microvessels from the surrounding host vasculature (28). Some studies suggest that neoangiogenesis is present in preinvasive and early invasive bronchial lesions, indicating that angiogenesis is an early event in lung cancer carcinogenesis (18, 29, 30). Fisseler-Eckhoff *et al* found an increasing vessel count in the bronchial mucosa when progressing from inflammation to hyperplasia, metaplasia, moderate dysplasia, severe dysplasia and carcinoma *in situ* (29). Angiogenetic squamous dysplasia (ASD) was identified in dysplastic bronchial epithelium (18, 19) as well. Whether or not ASD is an indicator of progression to invasive carcinoma is undetermined (31). Furthermore, whether an increase in vascularisation is related to progression of a lesion to malignancy and whether it is driven by hypoxia remains to be elucidated.

Recently, Meert *et al* did not find significant differences in microvessel count between different stages of premalignant bronchus carcinoma. However, they did find an elevated expression of neoangiogenetic proteins in premalignant lesions (32). Furthermore, the use of vessel density to characterize premalignant lesions is limited because other biological factors such as infections, or chronic obstructive pulmonary disease, may increase the vessel density as well. In conclusion, the vasculature appears to be altered in premalignant disease but data are not uniform and no differentiation between changes in vessel density due to premalignant disease or due to other biological causes can be made.

2.3. Biochemistry
Hypothetically, the cellular metabolic activity is elevated in premalignant lesions, leading to intracellular changes in the concentration of nicotinamide adenine dinucleotide (NADH) and/or nicotinamide adenine phosphor dinucleotide (NADPH), which are both fluorescent molecules. In cancerous bronchial cells, a decreased fluorescence intensity of NADH and NADPH has been reported (33, 34). Of note, these studies were performed in vitro, and translating these results to an in vivo environment is difficult, as discussed in section 3.

3. Detection of premalignant lesions: wide-field optical imaging
Based on the possible biological mechanisms involved in early carcinogenesis, different techniques have been developed to detect premalignant lesions with higher sensitivity and specificity than white light bronchoscopy. Detection of premalignant lesions is usually performed in a wide-field imaging mode due to the large size of the bronchial tissue area that has to be investigated. In the following section we will discuss the technical aspects of the imaging techniques, relate the technology to the biological aspects of lung carcinogenesis, and discuss the clinical use of the techniques.

3.1. Autofluorescence imaging
Autofluorescence bronchoscopy is the most widely used and investigated technique in the detection of premalignant bronchus lesions. Several autofluorescence devices are available. The LIFE (Lung Imaging Fluorescence Endoscopy) is the first and best known autofluorescence bronchoscope (35-44). first published by Lam *et al.* (12). Other devices such as the D-light autofluorescence (45-47) , Pentax-SAFE 1000 (48) and its successor the Pentax 3000 (11, 49, 50) are similar in its use.
Autofluorescence imaging uses the natural fluorescence properties of the tissue itself, i.e. no exogenous contrast agents have been applied. When a natural fluorophore is excited to a higher electronic state by absorption of a photon of an appropriate wavelength, the fluorophore may return to its ground electronic state by emission of a photon of a higher wavelength (fluorescence). When the bronchial surface is illuminated with blue light (wavelengths ranging from 400-450 nm), the fluorescent light of a higher wavelength (>450 nm, i.e. green and red) can be visualised using long pass filters that block the excitation light but transmit the higher wavelength fluorescent light. Since autofluorescence imaging is performed in a wide-field non-contact imaging mode, the detected fluorescent photons originate from various depths of tissue. The detected fluorescence consists of contributions from fluorophores that are involved in cellular metabolic processes such as nicotinamide adenine dinucleotide (NADH) and flavins (FAD) or are associated with their structural matrix (keratin, elastin and collagen). In a wide-field imaging mode, it is expected that the latter fluorophores are the dominant contributors to the signal. Furthermore, spectral distortion of the measured fluorescence arises due to the scattering properties of tissue and absorption of both the excitation light and emitted fluorescence by tissue chromophores (specifically, hemoglobin). As a consequence, the optical contrast between premalignant and normal bronchial tissue using autofluorescence imaging is based on a combination of the three different biological mechanisms (biochemistry, physiology and morphology). First, the local concentrations of

natural fluorophores involved in cellular metabolism such as NADH may change in premalignant tissues (51). However, since the dominant source of detected fluorescence is the structural matrix, this is not very likely to yield large contrasts. Second, an increased blood supply in the adjacent lamina propria is likely to play a key role in the reduction of autofluorescence in premalignant tissues, and thus in the generation of the autofluorescence contrast in bronchial tissues (52). However, since other biological factors such as infections, or chronic obstructive pulmonary disease, may increase the blood supply as well, this contrast is not likely to be very specific. Third, epithelial thickening will cause less excitation light to reach the structural matrix, thereby also reducing the detected fluorescence. Based on these biological mechanisms, premalignant tissue is expected to show reduced autofluorescence, but this effect will not be very specific.

These considerations are generally confirmed in clinical studies. Autofluorescence bronchoscopy was shown to increase the sensitivity for detection of premalignant bronchial lesions, but is hampered by a low specificity (35-44, 46, 47). Difficulties exist in distinguishing benign epithelial chances such as bronchitis and inflammation from precancerous lesions. Studies have demonstrated about two third of the lesions to be false positive results after correlation with pathology (38, 53, 54).

A number of modified versions of autofluorescence imaging have been introduced, which rely on the same principles of autofluorescence imaging but introduce additional filter sets to enhance the specificity of the images to the mucosal blood supply. The autofluorescence imaging bronchovideoscope system (AFI, Olympus) displays a composite image integrating autofluorescence with filtered reflected green and red light; the reflected green light is sensitive to mucosal blood due to the high absorption of green light by blood, whereas the reflected red light is basically unaffected by the presence of blood (55). In a study including 32 patients sensitivity of detecting dysplasia by AFI was 96.7%, specificity was 83.3 % (55). An other study, including 31 patients, sensitivity of detecting severe dysplasia or worse with AFI was 94.7% and the specificity was 71.1% (56).

The Onco-LIFE device contains a white light and a fluorescence mode. In fluorescence mode, the device uses blue light (395-455nm) and small amount of red light (675-720nm) from a filtered mercury lamp arc lamp for illumination. The camera captured and combines the fluorescence green light and the reflected red light and displays it on a normal color video monitor. The green fluorescence light will change in places with bronchial pathology; the red reflected light is not affected by tissue pathology. Illuminated normal bronchial epithelium by blue light, fluoresces in green. When blue light is illuminated on abnormal bronchial epithelium it transforms through different grades of dysplasia into a progressive decrease in green fluorescence due to increased epithelial thickness and vascularization making these abnormal areas appear red. Red light is less absorbed by hemoglobin and therefore less influenced by changes in vascularity associated with inflammation (57). The red reflected light can therefore be a reference for different light intensities from changes in angle and distance of the bronchoscope to the bronchial surface. Combining the reflected and fluorescence images enhances the contrast of normal, premalignant and malignant bronchial tissue (57). It is possible to analyse the Red/Green (R/G) ratio in the central portion of the displayed image providing quantitative data. Combining the data of two medical centers, 738 individuals underwent a bronchoscopy with the Onco-LIFE device. The corresponding R/G ratio increased when the premalignant

lesions became more malignant. Validated data showed that R/G ratio of 0.54 had a 85% sensitivity and a 80% specificity for the detection of high grade and moderate dysplasia (58). The concept of color fluorescence ratio is not device specific, and can be integrated into any reflectance fluorescence imaging system. Lee *et al* introduced real time dual video and autofluorescence bronchoscopic imaging (59), allowing to display both video and autofluorescence bronchoscopic images of the target simultaneously. This hypothetically makes it easier to identify benign lesions such as bronchitis, although the biological mechanism behind this hypothesis is not clear. Dual band imaging has been studied in only one study, reporting a sensitivity and specificity in detection of preneoplastic lesions 0.86 and 0.94, respectively (59). However, sample size in that study was relatively small; secondly, it was not a comparative study where individual imaging modalities (video and AF bronchoscopy) were assessed independently before dual imaging.

The recently introduced color fluorescence endoscopic system, PDS-2000, uses a color intensified charge coupled device (ICCD) (60) instead of a regular CCD, but the advantages of such a device are not clear. In a clinical study, sensitivity and specificity were 89.2% and 52.6%, respectively, while for white light bronchoscopy these numbers 54.1% and 77.7%, respectively. No studies comparing color fluorescence bronchoscopy and autofluorescence bronchoscopy have been performed.

3.2. Narrrow band imaging

Shibuya *et al* developed narrow band imaging (NBI)(31). The NBI-system (Olympus Corp, Tokyo, Japan) is based upon a light source with sequential red-green-blue (RGB) illumination. White light from a Xenon lamp is passed through a rotary RGB filter that separates the white light into the colors red, green, and blue, which are used to sequentially illuminate the mucosa. The red, green, and blue reflected light is detected separately by a monochromatic charged coupled device (CCD) placed at the tip of the endoscope, and the three images are integrated into a single color image by the video processor (31). In addition to the conventional RGB filters for white light endoscopy, the narrow band imaging system has special RGB filters of which the band-pass ranges have been narrowed from the standard 400-700nm (B 400-500nm, G 500-600nm and R 600-700nm) to 400-590nm (B1 400-430nm, B2 420-470nm and G 560-590nm) (61). Also, the relative contribution of blue light (B1) has been increased. With this choice of filters, NBI enables enhanced visualization of the mucosal morphology because blue light allows for optimal superficial imaging due to its small penetration depth. Secondly, because Narrow Band Imaging filter B1 covers the absorption maximum for hemoglobin, a detailed image of the superficial vessel structures can be obtained. The NBI filter can be manually enabled and disabled during endoscopy making it easy to switch between the standard mode and the NBI-mode. The biological hypothesis driving the development of NBI is that the microvascular patterns of premalignant lesions are different than of normal bronchial mucosa (31).In contrast to autofluorescence imaging, which is predominantly sensitive to total mucosal blood volume, NBI is sensitive to microvascular patterns with high spatial resolution, making the image contrast complementary to autofluorescence imaging (62, 63). Clinically, microvessels, vascular networks and dotted vessels were observed with NBI, and histological biopsies of areas with dotted vessels showed premalignant lesions and ASD (64). NBI detected five instances of dysplasia or cancer (23% of all

included patients) that were not detected with normal with light bronchoscopy (p< 0.005).

4. Improving the specificity of imaging: point (spectroscopic) techniques

Novel imaging modalities increase the sensitivity for detection of premalignant bronchial lesions, at the cost of a low specificity. Difficulties exist in distinguishing benign epithelial chances such as bronchitis and inflammation from precancerous lesions. To increase the specificity of the imaging modalities, additional optical methods have been developed to be used in conjunction with wide-field imaging. These techniques provide more detailed information about small tissue areas/volumes; information that may be used to classify a suspicious lesion as either premalignant or benign. Although all technologies discussed in the next section are point-techniques, they are categorized here as point-imaging or point-spectroscopic techniques.

Point Imaging
4.1. Fibered Confocal Fluorescence Microscopy

Fibered Confocal Fluorescence microscopy (FCFM) is a technique that can be used to image the microscopic structure of the bronchial wall (21). It is based on the principle of confocal microscopy, which provides a clear, in-focus image of a thin section within a biological sample by a flexible fiberoptic miniprobe.

The 1-mm diameter fiberoptic probe, which can be introduced into the working channel of a flexible bronchoscope, produces images from a layer of 0 to 50 µm in depth below the bronchial surface, with a lateral resolution of 5 µm, and a field-of-view up to 600 µm in diameter (21). This ultra high magnification system provides the endoscopist a cross-sectional image of the bronchial mucosa epithelium, resulting in images similar to histology during bronchoscopy (65, 66). Basement membrane and upper submucosa can be made visible with a nice quality. Thiberville *et al* tested FCFM in twenty-nine high risk patients for lung cancer underwent an autofluorescence bronchoscopy. A specific pattern of the bronchial wall microstructure could be observed in some precancerous conditions showing a disorganised fibered network. This was observed in one invasive cancer, three CIS, two mild and one moderate dysplastic and three metaplastic lesions (21). However, the absent of visualisation of epithelial cells, resulted in a difficulty of true differentiation of the premalignant bronchial lesions (65). By adding an exogenous nontoxic fluorophore agent, such as methylene blue, reproducibility imaging of the epithelial cells could be obtained (66). Future studies have to show whether FCFM with methylene blue is possible to differentiate between normal, premalignant and malignant bronchus lesions.

FCFM can be easily performed during a bronchoscopy under local anaesthesia. The miniprobe can be guided through the working channel of the bronchoscope. Interpretation of FCFM images of premalignant lesions relies on the fluorescence properties of the imaged tissue. Because the obtained images are similar to histology, the scopist must know the characteristics of premalignant histology to draw conclusions.

4.2. Optical coherence tomography

Optical coherence tomography (OCT) is an optical imaging modality that performs high-resolution, cross-sectional, subsurface tomographic imaging of the microstructure of tissues (67). It has been used to image subsurface tissue morphology in several other fields (68-75).The physical principle of OCT is similar to that of B-mode ultrasound imaging. Instead of using sound waves, near-IR light is passed into the tissue, and by detecting the reflected light as it interacts with tissue structures as a function of depth, a cross-sectional image is created through optical interferometry (76). In principle, OCT is capable of imaging the morphology of mucosal lesions. OCT is possible with an OCT probe with an outer diameter of 1.5mm and a depth focus of 3mm. It is possible to insert it in a working channel of a bronchoscope. For adequate subsurface tissue imaging, the OCT must be positioned closely to the airway wall. Images are real-time monitored.

Tsuboi *et al* suggested that *in situ* and invasive carcinoma can be distinguished from normal bronchial epithelium (77). Lam *et al* concluded that autofluorescence endoscopy–guided OCT imaging of bronchial lesions is technically feasible, and may be a promising nonbiopsy tool for *in vivo* imaging of preneoplastic bronchial lesions (78).

Interpretation of the OCT imaging is complex and experience is required. To analyze the images and to differentiate between inflammatory and premalignant lesions, it is necessary to know more about the histopathology images of premalignant lesions. It seems that differentiation between different premalignant stages can be quantified by measurement of the epithelial thickness (78). The epithelial thickness was significantly different between invasive cancer and CIS. Also the epithelial layer of mild, moderate and severe dysplasia lesions was significantly thicker than of metaplastic lesions.

The detection rate of premalignant lesions by OCT is probably related to the skills of the bronchoscopist and the individual imaging interpretation. Unfortunately the availability of OCT is limited due to the limitations of the current research results and the high costs of the equipment.

4.3. Endo-Cytoscopy System (ECS)

A recently introduced endoscopic microscopic technique is the Endo-Cytoscopy System (ECS) that enables microscopic imaging of the tracheobronchial tree (79). ECS is able to magnify up to x450 on a video monitor. By staining areas of interest with methylene blue, high magnification imaging was possible. Images corresponded with the light microscopy. With this technique in vivo discrimination between normal and dysplastic lesions is possible. A limitation of the technique is that contact with the bronchial tree is necessary, which may cause bleeding, hampering a clear view. Unfortunately, no clinical data are available at the moment.

Point spectroscopy
4.4. Autofluorescence spectroscopy

Autofluorescence spectroscopy (AFS) works similar to autofluorescence imaging, but instead of visualising the remitted fluorescence of a large tissue area using a CCD camera with only a few wavelength bands (mostly red and/or green), the remitted fluorescence of a small tissue area is coupled (usually with a fiber) into a spectrometer which resolves the fluorescence into a complete spectrum (80). However, AFS suffers from the same problems as autofluorescence imaging: it

cannot discriminate between premalignant and benign disease such as bronchitis and inflammation (80).

4.5. Reflectance spectroscopy

The absorption and scattering coefficients of tissue are wavelength-dependent and their value at each wavelength reflects the probability that a photon will be absorbed or scattered by the tissue. The absorption coefficient is given by the product of the extinction coefficient and the concentration of dominant tissue chromophores such as oxygenated hemoglobin (HbO_2) and deoxygenated hemoglobin (Hb), bilirubin, betacarotene, water, and lipids. The absorption coefficient is therefore also related to physiological parameters such as total hemoglobin concentration ($THb=HbO_2+Hb$) and blood oxygen saturation ($StO_2=HbO_2/THb$). Scattering in tissue originates from spatial heterogeneities of the optical refractive index that occur on size scales ranging from a few nanometers to a few millimeters. Since these refractive index fluctuations depend on the concentration and type of tissue constituents, the light scattering signature (both the light scattering amplitude and wavelength dependence) is sensitive to the microarchitecture of the tissue and can be used for tissue diagnosis. Differential path length spectroscopy (DPS) is a novel reflectance spectroscopic technique developed for the purpose of studying the superficial layer of the bronchial mucosa (27, 81-83). DPS utilizes a unique fiber-optic geometry to selectively sample photons that have propagated shallow depths into tissue, making it very suitable for the classification of superficial lesions such as preneoplasias. In DPS the path length is approximately equal to the fiber diameter, independent of absorption and scattering. This fiber geometry overcomes the classical limitation of unknown photon path length during diffuse reflectance measurements; this allows real-time quantitative information (THb, StO_2) to be extracted from DPS measurements. Using DPS we have measured a significant difference in THb and StO_2 between normal tissue and cancerous tissue. However, no significant differences in these parameters were found between normal and premalignant tissues (82), although the number of truly premalignant lesions (dysplasia, CIS) included in that study was very low.

Zeng *et al* used an integrated endoscopy system for simultaneous imaging and spectroscopy. This system is capable of obtaining white-light bronchoscopy, autofluorescence bronchoscopy and both reflectance and fluorescence spectroscopy without introducing optical fibers through the working channel (84). The advantage of this technique is the non-contact procedure. The integrated endoscopy system was tested in 63 patients and showed that the experimental system was able to provide identical spectra to those obtained by fiber-optic probes (85). Significant differences of reflectance and fluorescence spectra from malignant tissue compared to normal lung tissue were observed. Due to the limited numbers of premalignant lesions, no information of improving the sensitivity or specificity of detection of premalignant lesions could be presented.

Discussion

No single optical detection modality is sufficiently accurate to gain clinical acceptance as a screening tool for preneoplastic bronchial lesions. Except for autofluorescence bronchoscopy, limited patient data on these new techniques are available. Autofluorescence bronchoscopy has proven its value in the detection of

neoplastic lesions, but unfortunately the low specificity limits this technique to be used as a screenings tool.

Based on the currently available techniques a combination of a wide-field optical imaging technique and a point (imaging) technique might improve the detection rate. A wide field technique is used to locate several suspicious lesions, and a point imaging technique is subsequently used to differentiate between true positive or false positive lesions.

For the first purpose, autofluorescence bronchoscopy seems momentarily the best wide field optical technique since a large number of investigations has been proven that this technique is with a high sensitivity.

For the second purpose, OCT combined with DPS have the highest potential value. OCT provides a histological-like diagnosis on site based on endogenous contrast, which increases the specificity of the fluorescence bronchoscopy during bronchoscopy and it is the only non-contact point imaging techniques. The non-contact possibility prevents contact bleeding and therefore misinterpretations of investigated lesions. Furthermore, it is a technique where quantitative data of the epithelial thickness can help to draw conclusions about the seriousness of a premalignant lesion.

DPS informs about the superficial morphology and physiology of the bronchial tissue, and therefore provides information complementary to OCT images. The incorporation of these three techniques includes the three important conditions of detection of premalignant lesions. Firstly, a wide field technique for detection of suspicious lesions. Secondly, a point imaging technique to give more local information about the histology of the suspicious lesions, and thirdly, a spectroscopic technique which gives information about the physiology of the local tissue.

Conclusion

In conclusion, a combination of autofluorescence bronchoscopy with OCT and DPS seems for now the best technique to be used in future studies on premalignant lesions. In addition, none of the presented techniques, or a combination of techniques, can be advised to be used outside a research setting.

References

1   A. Jemal, R. Siegel, E. Ward, T. Murray, J. Xu and M. J. Thun. Cancer statistics, 2007. *CA Cancer J Clin 57*, 43-66 (2007).
2   E. B. William D Travis, H.Konrad Müller-Hermelink, Curtis C Harris. *Tumours of the Lung, Pleura, Thymus and Heart*. 9-124 (2004).
3   O. Auerbach, J. B. Forman, J. B. Gere, D. Y. Kassouny, G. E. Muehsam, T. G. Petrick, H. J. Smolin and A. P. Stout. Changes in the bronchial epithelium in relation to smoking and cancer of the lung; a report of progress. *N Engl J Med 256*, 97-104 (1957).
4   P. Nettesheim, R. A. Griesemer, D. H. Martin and J. E. Caton, Jr. Induction of preneoplastic and neoplastic lesions in grafted rat tracheas continuously exposed to benzo(a)pyrene. *Cancer Res 37*, 1272-1278 (1977).
5   R. Ono, S. Ikeda and K. Suemasu. Hematoporphyrin derivative photodynamic therapy in roentgenographically occult carcinoma of the tracheobronchial tree. *Cancer 69*, 1696-1701 (1992).
6   N. L. Chiaia, C. A. Bennett-Clarke and R. W. Rhoades. Effects of cortical and thalamic lesions upon primary afferent terminations, distributions of projection neurons, and the cytochrome oxidase pattern in the trigeminal brainstem complex. *J Comp Neurol 303*, 600-616 (1991).
7   E. S. Edell and D. A. Cortese. Bronchoscopic phototherapy with hematoporphyrin derivative for treatment of localized bronchogenic carcinoma: a 5-year experience. *Mayo Clin Proc 62*, 8-14 (1987).
8   T. J. van Boxem, B. J. Venmans, F. M. Schramel, J. C. van Mourik, R. P. Golding, P. E. Postmus and T. G. Sutedja. Radiographically occult lung cancer treated with fibreoptic bronchoscopic electrocautery: a pilot study of a simple and inexpensive technique. *Eur Respir J 11*, 169-172 (1998).
9   M. Perol, R. Caliandro, P. Pommier, C. Malet, X. Montbarbon, C. Carrie and J. M. Ardiet. Curative irradiation of limited endobronchial carcinomas with high-dose rate brachytherapy. Results of a pilot study. *Chest 111*, 1417-1423 (1997).
10   N. Deygas, M. Froudarakis, G. Ozenne and J. M. Vergnon. Cryotherapy in early superficial bronchogenic carcinoma. *Chest 120*, 26-31 (2001).
11   T. C. Kennedy, A. McWilliams, E. Edell, T. Sutedja, G. Downie, R. Yung, A. Gazdar and P. N. Mathur. Bronchial intraepithelial neoplasia/early central airways lung cancer: ACCP evidence-based clinical practice guidelines (2nd edition). *Chest 132*, 221S-233S (2007).
12   S. Lam, C. MacAulay, J. Hung, J. LeRiche, A. E. Profio and B. Palcic. Detection of dysplasia and carcinoma in situ with a lung imaging fluorescence endoscope device. *J Thorac Cardiovasc Surg 105*, 1035-1040 (1993).
13   R. R. Sital, J. G. Kusters, F. W. De Rooij, E. J. Kuipers and P. D. Siersema. Bile acids and Barrett's oesophagus: a sine qua non or coincidence? *Scand J Gastroenterol Suppl*, 11-17 (2006).
14   N. Gungor, A. Haegens, A. M. Knaapen, R. W. Godschalk, R. K. Chiu, E. F. Wouters and F. J. van Schooten. Lung inflammation is associated with reduced pulmonary nucleotide excision repair in vivo. *Mutagenesis 25*, 77-82 (2010).
15   J. L. Pauly, L. A. Smith, M. H. Rickert, A. Hutson and G. M. Paszkiewicz. Review: Is lung inflammation associated with microbes and microbial toxins in cigarette tobacco smoke? *Immunol Res 46*, 127-36 (2009).
16   K. J. Syrjanen. HPV infections and lung cancer. *J Clin Pathol 55*, 885-891 (2002).
17   K. M. Kerr. Pulmonary preinvasive neoplasia. *J Clin Pathol 54*, 257-271 (2001).
18   R. L. Keith, Y. E. Miller, R. M. Gemmill, H. A. Drabkin, E. C. Dempsey, T. C. Kennedy, S. Prindiville and W. A. Franklin. Angiogenic squamous dysplasia in bronchi of individuals at high risk for lung cancer. *Clin Cancer Res 6*, 1616-1625 (2000).
19   W. A. Franklin. Diagnosis of lung cancer: pathology of invasive and preinvasive neoplasia. *Chest 117*, 80S-89S (2000).
20   E. Brambilla, W. D. Travis, T. V. Colby, B. Corrin and Y. Shimosato. The new World Health Organization classification of lung tumours. *Eur Respir J 18*, 1059-1068 (2001).
21   L. Thiberville, S. Moreno-Swirc, T. Vercauteren, E. Peltier, C. Cave and G. Bourg Heckly. In vivo imaging of the bronchial wall microstructure using fibered confocal fluorescence microscopy. *Am J Respir Crit Care Med 175*, 22-31 (2007).
22   V. V. Polosukhin, W. E. Lawson, A. P. Milstone, S. M. Egunova, A. G. Kulipanov, S. G. Tchuvakin, P. P. Massion and T. S. Blackwell. Association of progressive structural changes in the bronchial epithelium with subepithelial fibrous remodeling: a potential role for hypoxia. *Virchows Arch 451*, 793-803 (2007).

23   M. Hockel and P. Vaupel. Tumor hypoxia: definitions and current clinical, biologic, and molecular aspects. *J Natl Cancer Inst 93*, 266-276 (2001).

24   H. B. Frieboes, X. Zheng, C. H. Sun, B. Tromberg, R. Gatenby and V. Cristini. An integrated computational/experimental model of tumor invasion. *Cancer Res 66*, 1597-1604 (2006).

25   E. A. Griffiths, S. A. Pritchard, S. M. McGrath, H. R. Valentine, P. M. Price, I. M. Welch and C. M. West. Increasing expression of hypoxia-inducible proteins in the Barrett's metaplasia-dysplasia-adenocarcinoma sequence. *Br J Cancer 96*, 1377-1383 (2007).

26   E. A. Griffiths, S. A. Pritchard, H. R. Valentine, N. Whitchelo, P. W. Bishop, M. P. Ebert, P. M. Price, I. M. Welch and C. M. West. Hypoxia-inducible factor-1alpha expression in the gastric carcinogenesis sequence and its prognostic role in gastric and gastro-oesophageal adenocarcinomas. *Br J Cancer 96*, 95-103 (2007).

27   M. P. Bard, A. Amelink, M. Skurichina, V. Noordhoek Hegt, R. P. Duin, H. J. Sterenborg, H. C. Hoogsteden and J. G. Aerts. Optical spectroscopy for the classification of malignant lesions of the bronchial tree. *Chest 129*, 995-1001 (2006).

28   F. Ciardiello. Epidermal growth factor receptor inhibitors in cancer treatment. *Future Oncol 1*, 221-234 (2005).

29   A. Fisseler-Eckhoff, D. Rothstein and K. M. Muller. Neovascularization in hyperplastic, metaplastic and potentially preneoplastic lesions of the bronchial mucosa. *Virchows Arch 429*, 95-100 (1996).

30   G. Fontanini, A. Calcinai, L. Boldrini, M. Lucchi, A. Mussi, C. A. Angeletti, C. Cagno, M. A. Tognetti and F. Basolo. Modulation of neoangiogenesis in bronchial preneoplastic lesions. *Oncol Rep 6*, 813-817 (1999).

31   K. Shibuya, H. Hoshino, M. Chiyo, A. Iyoda, S. Yoshida, Y. Sekine, T. Iizasa, Y. Saitoh, M. Baba, K. Hiroshima, H. Ohwada and T. Fujisawa. High magnification bronchovideoscopy combined with narrow band imaging could detect capillary loops of angiogenic squamous dysplasia in heavy smokers at high risk for lung cancer. *Thorax 58*, 989-995 (2003).

32   A. P. Meert, F. Feoli, B. Martin, V. Ninane and J. P. Sculier. Angiogenesis in preinvasive, early invasive bronchial lesions and micropapillomatosis and correlation with EGFR expression. *Histopathology 50*, 311-317 (2007).

33   J. D. Pitts, R. D. Sloboda, K. H. Dragnev, E. Dmitrovsky and M. A. Mycek. Autofluorescence characteristics of immortalized and carcinogen-transformed human bronchial epithelial cells. *J Biomed Opt 6*, 31-40 (2001).

34   G. A. Wagnieres, W. M. Star and B. C. Wilson. In vivo fluorescence spectroscopy and imaging for oncological applications. *Photochem Photobiol 68*, 603-632 (1998).

35   S. Lam, T. Kennedy, M. Unger, Y. E. Miller, D. Gelmont, V. Rusch, B. Gipe, D. Howard, J. C. LeRiche, A. Coldman and A. F. Gazdar. Localization of bronchial intraepithelial neoplastic lesions by fluorescence bronchoscopy. *Chest 113*, 696-702 (1998).

36   K. Shibuya, T. Fujisawa, H. Hoshino, M. Baba, Y. Saitoh, T. Iizasa, M. Suzuki, M. Otsuji, K. Hiroshima and H. Ohwada. Fluorescence bronchoscopy in the detection of preinvasive bronchial lesions in patients with sputum cytology suspicious or positive for malignancy. *Lung Cancer 32*, 19-25 (2001).

37   M. Sato, A. Sakurada, M. Sagawa, M. Minowa, H. Takahashi, T. Oyaizu, Y. Okada, Y. Matsumura, T. Tanita and T. Kondo. Diagnostic results before and after introduction of autofluorescence bronchoscopy in patients suspected of having lung cancer detected by sputum cytology in lung cancer mass screening. *Lung Cancer 32*, 247-253 (2001).

38   F. R. Hirsch, S. A. Prindiville, Y. E. Miller, W. A. Franklin, E. C. Dempsey, J. R. Murphy, P. A. Bunn, Jr. and T. C. Kennedy. Fluorescence versus white-light bronchoscopy for detection of preneoplastic lesions: a randomized study. *J Natl Cancer Inst 93*, 1385-1391 (2001).

39   P. N. Chhajed, K. Shibuya, H. Hoshino, M. Chiyo, K. Yasufuku, K. Hiroshima and T. Fujisawa. A comparison of video and autofluorescence bronchoscopy in patients at high risk of lung cancer. *Eur Respir J 25*, 951-955 (2005).

40   J. M. Kurie, J. S. Lee, R. C. Morice, G. L. Walsh, F. R. Khuri, A. Broxson, J. Y. Ro, W. A. Franklin, R. Yu and W. K. Hong. Autofluorescence bronchoscopy in the detection of squamous metaplasia and dysplasia in current and former smokers. *J Natl Cancer Inst 90*, 991-995 (1998).

41   P. Vermylen, P. Pierard, C. Roufosse, T. Bosschaerts, A. Verhest, J. P. Sculier and V. Ninane. Detection of bronchial preneoplastic lesions and early lung cancer with fluorescence bronchoscopy: a study about its ambulatory feasibility under local anaesthesis. *Lung Cancer 25*, 161-168 (1999).

42   Y. Kusunoki, F. Imamura, H. Uda, M. Mano and T. Horai. Early detection of lung cancer with laser-induced fluorescence endoscopy and spectrofluorometry. *Chest 118*, 1776-1782 (2000).

43   M. T. van Rens, F. M. Schramel, J. R. Elbers and J. W. Lammers. The clinical value of lung imaging fluorescence endoscopy for detecting synchronous lung cancer. *Lung Cancer 32*, 13-18 (2001).

44   N. Ikeda, H. Honda, T. Katsumi, T. Okunaka, K. Furukawa, T. Tsuchida, K. Tanaka, T. Onoda, T. Hirano, M. Saito, N. Kawate, C. Konaka, H. Kato and Y. Ebihara. Early detection of bronchial lesions using lung imaging fluorescence endoscope. *Diagn Ther Endosc 5*, 85-90 (1999).

45   K. Haussinger, F. Stanzel, A. Markus, C. T. Bolliger and J. Pichler. [Early diagnosis of bronchial carcinoma. Technical endoscopic progress--a step toward new screening concepts?]. *Pneumologie 53*, 77-82 (1999).

46   L. Fuso, G. Pagliari, V. Boniello, A. Trove, F. Varone, A. Longobardi, S. Basso and L. Trodella. Autofluorescence bronchoscopy to identify pre-cancerous bronchial lesions. *Monaldi Arch Chest Dis 63*, 124-128 (2005).

47   J. F. Beamis, Jr., A. Ernst, M. Simoff, R. Yung and P. Mathur. A multicenter study comparing autofluorescence bronchoscopy to white light bronchoscopy using a non-laser light stimulation system. *Chest 125*, 148S-149S (2004).

48   N. Baletic, Z. Petrovic, I. Pendjer and H. Malicevic. Autofluorescent diagnostics in laryngeal pathology. *Eur Arch Otorhinolaryngol 261*, 233-237 (2004).

49   N. Ikeda, H. Honda, A. Hayashi, J. Usuda, Y. Kato, M. Tsuboi, T. Ohira, T. Hirano, H. Kato, H. Serizawa and Y. Aoki. Early detection of bronchial lesions using newly developed videoendoscopy-based autofluorescence bronchoscopy. *Lung Cancer 52*, 21-27 (2006).

50   J. Usuda, H. Tsutsui, H. Honda, S. Ichinose, T. Ishizumi, T. Hirata, T. Inoue, K. Ohtani, S. Maehara, K. Imai, Y. Tsunoda, M. Kubota, N. Ikeda, K. Furukawa, T. Okunaka and H. Kato. Photodynamic therapy for lung cancers based on novel photodynamic diagnosis using talaporfin sodium (NPe6) and autofluorescence bronchoscopy. *Lung Cancer 58*, 317-323 (2007).

51   B. W. Pogue, J. D. Pitts, M. A. Mycek, R. D. Sloboda, C. M. Wilmot, J. F. Brandsema and J. A. O'Hara. In vivo NADH fluorescence monitoring as an assay for cellular damage in photodynamic therapy. *Photochem Photobiol 74*, 817-824 (2001).

52   T. Gabrecht, S. Andrejevic-Blant and G. Wagnieres. Blue-Violet Excited Autofluorescence Spectroscopy and Imaging of Normal and Cancerous Human Bronchial Tissue after Formalin Fixation. *Photochem Photobiol* 83, 450-8 (2006).

53   A. K. Banerjee, P. H. Rabbitts and J. George. Lung cancer . 3: Fluorescence bronchoscopy: clinical dilemmas and research opportunities. *Thorax 58*, 266-271 (2003).

54   T. C. Kennedy, S. Lam and F. R. Hirsch. Review of recent advances in fluorescence bronchoscopy in early localization of central airway lung cancer. *Oncologist 6*, 257-262 (2001).

55   M. Chiyo, K. Shibuya, H. Hoshino, K. Yasufuku, Y. Sekine, T. Iizasa, K. Hiroshima and T. Fujisawa. Effective detection of bronchial preinvasive lesions by a new autofluorescence imaging bronchovideoscope system. *Lung Cancer 48*, 307-313 (2005).

56   K. Ueno, Y. Kusunoki, F. Imamura, M. Yoshimura, S. Yamamoto, J. Uchida and Y. Tsukamoto. Clinical experience with autofluorescence imaging system in patients with lung cancers and precancerous lesions. *Respiration 74*, 304-308 (2007).

57   E. Edell, S. Lam, H. Pass, Y. E. Miller, T. Sutedja, T. Kennedy, G. Loewen, R. L. Keith and A. Gazdar. Detection and localization of intraepithelial neoplasia and invasive carcinoma using fluorescence-reflectance bronchoscopy: an international, multicenter clinical trial. *J Thorac Oncol 4*, 49-54 (2009).

58   P. Lee, R. M. van den Berg, S. Lam, A. F. Gazdar, K. Grunberg, A. McWilliams, J. Leriche, P. E. Postmus and T. G. Sutedja. Color fluorescence ratio for detection of bronchial dysplasia and carcinoma in situ. *Clin Cancer Res 15*, 4700-4705 (2009).

59   P. Lee, H. A. Brokx, P. E. Postmus and T. G. Sutedja. Dual digital video-autofluorescence imaging for detection of pre-neoplastic lesions. *Lung Cancer* 58, 44-9 (2007).

60   K. Nakanishi, Y. Ohsaki, M. Kurihara, S. Nakao, Y. Fujita, K. Takeyama, S. Osanai, N. Miyokawa and S. Nakajima. Color auto-fluorescence from cancer lesions: Improved detection of central type lung cancer. *Lung Cancer* 58, 214-9(2007).

61   K. Gono, T. Obi, M. Yamaguchi, N. Ohyama, H. Machida, Y. Sano, S. Yoshida, Y. Hamamoto and T. Endo. Appearance of enhanced tissue features in narrow-band endoscopic imaging. *J Biomed Opt 9*, 568-577 (2004).

62   J. B. Votruba, Tomas1 Javorsky, Stanislav2 Zavadil, Jiri2 Kostka, Franta2. Discriminating value of three bronchoscopic techniques - autofluorescence bronchoscopy, autofluorescence spectroscopy and narrow band imaging. *Journal of Thoracic Oncology Volume 2, Number 8, Supplement 4* (2007).
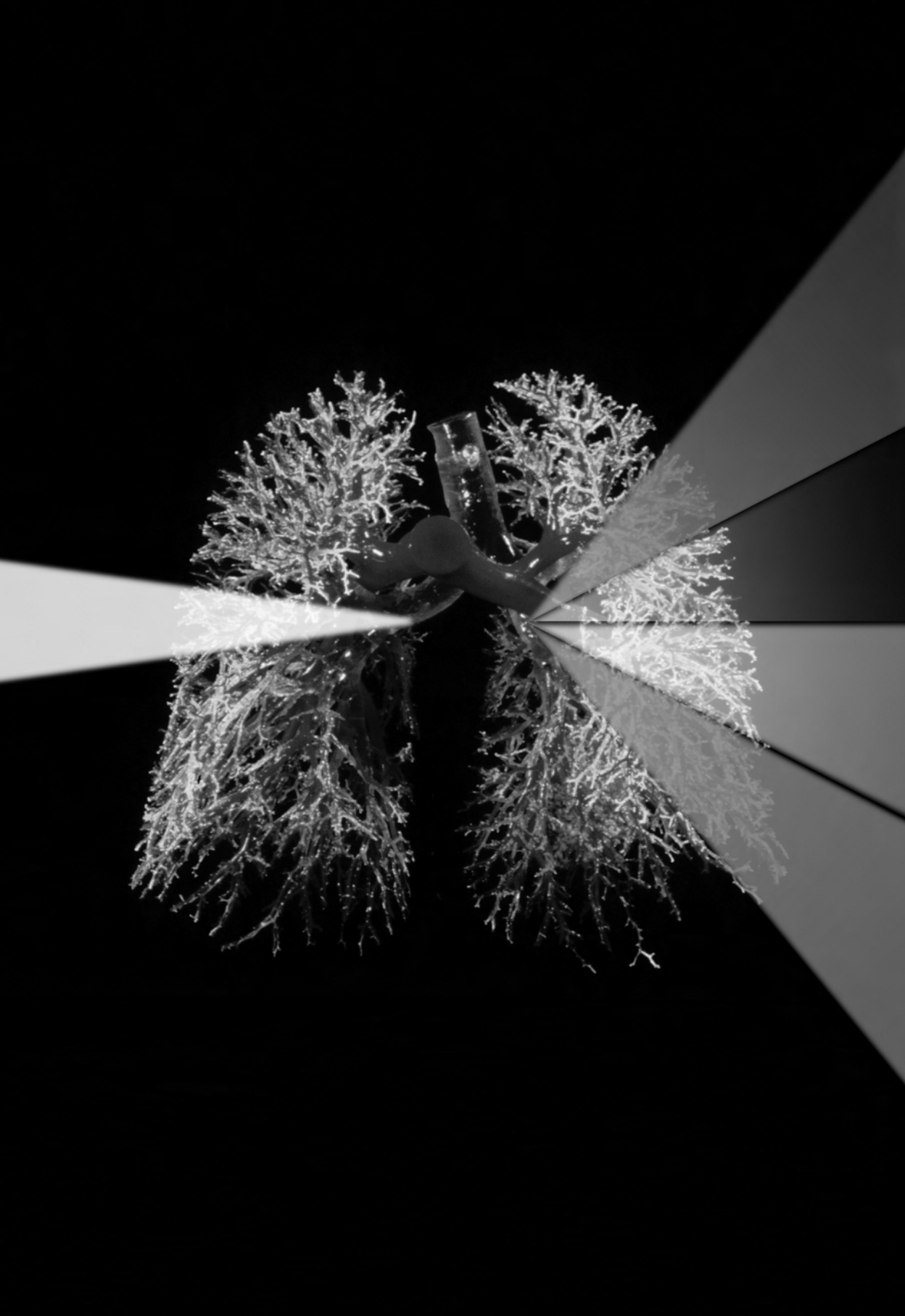
63   F. J. Herth, R. Eberhardt, D. Anantham, D. Gompelmann, M. W. Zakaria and A. Ernst. Narrow-band imaging bronchoscopy increases the specificity of bronchoscopic early lung cancer detection. *J Thorac Oncol 4*, 1060-1065 (2009).

64   B. D. Vincent, M. Fraig and G. A. Silvestri. A pilot study of narrow-band imaging compared to white light bronchoscopy for evaluation of normal airways and premalignant and malignant airways disease. *Chest 131*, 1794-1799 (2007).

65   L. Thiberville, M. Salaun, S. Lachkar, S. Dominique, S. Moreno-Swirc, C. Vever-Bizet and G. Bourg-Heckly. Confocal fluorescence endomicroscopy of the human airways. *Proc Am Thorac Soc 6*, 444-449 (2009).

66   S. M. Thiberville L, Lachkar S, Dominique S, Moreno-Swirc S, Vever-Bizet C, Bourg-Heckly G. in *World Conference on Lung Cancer 2009*   (San Francisco, 2009).

67   S. C. Whiteman, Y. Yang, D. Gey van Pittius, M. Stephens, J. Parmer and M. A. Spiteri. Optical coherence tomography: real-time imaging of bronchial airways microstructure and detection of inflammatory/neoplastic morphologic changes. *Clin Cancer Res 12*, 813-818 (2006).

68   L. M. Sakata, J. Deleon-Ortega, V. Sakata and C. A. Girkin. Optical coherence tomography of the retina and optic nerve - a review. *Clin Experiment Ophthalmol 37*, 90-99 (2009).

69   R. G. Mirza, M. W. Johnson and L. M. Jampol. Optical coherence tomography use in evaluation of the vitreoretinal interface: a review. *Surv Ophthalmol 52*, 397-421 (2007).

70   T. Gambichler, G. Moussa, M. Sand, D. Sand, P. Altmeyer and K. Hoffmann. Applications of optical coherence tomography in dermatology. *J Dermatol Sci 40*, 85-94 (2005).

71   M. U. Farooq, A. Khasnis, A. Majid and M. Y. Kassab. The role of optical coherence tomography in vascular medicine. *Vasc Med 14*, 63-71 (2009).

72   P. A. Testoni and B. Mangiavillano. Optical coherence tomography in detection of dysplasia and cancer of the gastrointestinal tract and bilio-pancreatic ductal system. *World J Gastroenterol 14*, 6444-6452 (2008).

73   J. M. Poneros. Diagnosis of Barrett's esophagus using optical coherence tomography. *Gastrointest Endosc Clin N Am 14*, 573-588, x (2004).

74   A. Karl, H. Stepp, E. Willmann, D. Tilki, D. Zaak, R. Knuchel and C. Stief. Optical coherence tomography (OCT): ready for the diagnosis of a nephrogenic adenoma of the urinary bladder? *J Endourol 22*, 2429-2432 (2008).

75   J. Schmidbauer, M. Remzi, T. Klatte, M. Waldert, J. Mauermann, M. Susani and M. Marberger. Fluorescence Cystoscopy with High-Resolution Optical Coherence Tomography Imaging as an Adjunct Reduces False-Positive Findings in the Diagnosis of Urothelial Carcinoma of the Bladder. *Eur Urol* epub ahead of print (2009).

76   D. S. a. C. Sheppard. <http://obel.ee.uwa.edu.au/research/oct>

77   M. Tsuboi, A. Hayashi, N. Ikeda, H. Honda, Y. Kato, S. Ichinose and H. Kato. Optical coherence tomography in the diagnosis of bronchial lesions. *Lung Cancer 49*, 387-394 (2005).

78   S. Lam, B. Standish, C. Baldwin, A. McWilliams, J. leRiche, A. Gazdar, A. I. Vitkin, V. Yang, N. Ikeda and C. MacAulay. In vivo optical coherence tomography imaging of preinvasive bronchial lesions. *Clin Cancer Res 14*, 2006-2011 (2008).

79   K. F. Shibuya, Taiki1; Wada, Hironobu1; Nagato, Kaoru1; Mohamed, Alaa1; Tamura, Hajime1; Yoshino, Mitsuru1; Hoshino, Hidehisa1; Moriya, Yasumitsu1; Yoshida, Shigetoshi1; Suzuki, Makoto1; Hiroshima, Kenzo2; Nakatani, Yukio2; Yoshino, Ichiro1. *Novel endoscopic microscopy using Endo-Cytoscopy system* (Department of Thoracic Surgery, Graduate School of Medicine, Chiba University, Chiba, Japan, 2009).

80   R. S. DaCosta, B. C. Wilson and N. E. Marcon. Fluorescence and spectral imaging. *ScientificWorldJournal 7*, 2046-2071 (2007).

81   M. P. Bard, A. Amelink, M. Skurichina, M. den Bakker, S. A. Burgers, J. P. van Meerbeeck, R. P. Duin, J. G. Aerts, H. C. Hoogsteden and H. J. Sterenborg. Improving the specificity of fluorescence bronchoscopy for the analysis of neoplastic lesions of the bronchial tree by combination with optical spectroscopy: preliminary communication. *Lung Cancer 47*, 41-47 (2005).

82   M. P. Bard, A. Amelink, V. N. Hegt, W. J. Graveland, H. J. Sterenborg, H. C. Hoogsteden and J. G. Aerts. Measurement of hypoxia-related parameters in bronchial mucosa by use of optical spectroscopy. *Am J Respir Crit Care Med 171*, 1178-1184 (2005).

83   J. G. Aerts, A. Amelink, C. van der Leest, J. P. Hegmans, A. Hemmes, B. D. Hamer, H. C. Sterenborg, H. C. Hoogsteden and B. N. Lambrecht. HIF1a expression in bronchial biopsies correlates with tumor microvascular saturation determined using optical spectroscopy. *Lung Cancer* 57, 317-21 (2007).

84   H. Zeng, M. Petek, M. T. Zorman, A. McWilliams, B. Palcic and S. Lam. Integrated endoscopy system for simultaneous imaging and spectroscopy for early lung cancer detection. *Opt Lett 29*, 587-589 (2004).
85   M. Tercelj, H. Zeng, M. Petek, T. Rott and B. Palcic. Acquisition of fluorescence and reflectance spectra during routine bronchoscopy examinations using the ClearVu Elite device: pilot study. *Lung Cancer 50*, 35-42 (2005).

HIF1a expression in bronchial biopsies correlates with tumor microvascular saturation determined using optical spectroscopy

J.G.J.V. Aerts[1,2]

A. Amelink[2,3]

C. van der Leest[2]

J.P.J.J. Hegmans[2]

A. Hemmes[2]

B. den Hamer[4]

H.C.J.M. Sterenborg[3]

H.C. Hoogsteden[2]

B.N. Lambrecht[2]

1 Department of Pulmonary Diseases, Amphia Hospital, Breda, The Netherlands

2 Department of Pulmonary Diseases, Erasmus MC, Rotterdam, The Netherlands

3 Center for Optical Diagnostics and Therapy, Department of Radiation Oncology, Erasmus MC, Rotterdam, The Netherlands

4 Department of Genetics, Erasmus MC, Rotterdam, The Netherlands

Summary

Tumor hypoxia is generally considered to be related to aggressive behaviour of a tumor. As in lung cancer direct determination of oxygenation is difficult, hypoxia-related proteins have been studied. A number of studies on these proteins show different results and the usefulness of these protein expressions remains questionable. In this article, we relate one of these hypoxia-related proteins (hypoxia-inducible factor, HIF1a) to a direct in vivo spectroscopic measurement of tumor blood saturation performed during bronchoscopy.

Seventeen samples from malignancies and non-malignant tissues were studied. Microvascular saturation levels in the no malignancy group equalled 87±11.5% (range 71-100%) and in the malignant group 43±21% (range 6-63%). This difference was statistically significant ($p < 0.0002$). There was a significant difference in the spectroscopically determined saturations between the biopsies with negative expression of HIF1a and the biopsies with positive expression of HIF1a ($p < 0.005$).

From these data, it can be concluded that HIF1a expression is related to a low microvascular blood saturation as determined in vivo by optical spectroscopy. This study may lead to a better acceptance of the usage of different techniques to establish hypoxia in order to study the effect of hypoxia on therapeutic interventions and prognosis of lung cancer.

1. Introduction

Tumor hypoxia has become of increasing interest in several forms of cancer and is generally considered to be related to a more aggressive behaviour of a tumor [1-3]. Tumor hypoxia is also related to a diminished response to radiotherapy and chemotherapy [4,5]. In lung cancer, direct determination of the tissue oxygen status in vivo was not possible until recently, due to the inaccessibility of the organ [1]. For that reason, endogenous hypoxia-related parameters have been determined in biopsies ex vivo. One of the most studied hypoxia-related parameter is hypoxia-inducible factor 1a (HIF1a) [1,2]. HIF1a is the oxygen-regulated subunit of hypoxia-induced factor 1 (HIF1). HIF1a is kept at low levels under normoxic conditions due to the continuous degradation via the ubiquitin-dependent proteasome pathway. Hypoxia results in an increase in the HIF1a protein levels, thereby activating genes involved in tumor metabolism, growth and angiogenesis. In recent years, a number of papers have been published relating the expression of hypoxia-related proteins like HIF1a to survival in patients with lung cancer [6]. Other hypoxia markers, such as CA IX have been studied as well, with comparable results [1,7]. However, the use of these endogenous hypoxia markers is still not firmly established in lung cancer due to the fact that a direct comparison between these hypoxia markers and cellular oxygen tension was not possible.

We recently developed and validated a new method to measure the microvascular saturation real-time and noninvasively by use of optical spectroscopy, that can be used during bronchoscopy. In an earlier study, we observed that lung carcinoma was associated with lower microvascular saturation than normal and metaplastic tissues [8].

The aim of the present pilot study was to establish whether a biologic marker for hypoxia, HIF1a, is related to the spectroscopically determined microvascular saturation.

2. Methods

2.1. Patients

Patients with known or suspected malignancies of the lung and with a medical indication for a bronchoscopy were invited to participate. All patients were older than 18 years and provided written informed consent. None of these patients were included in previous studies. The study was approved by the local Medical Ethics Review Board.

2.2. Examination procedure

The endoscopic examination of the bronchial tree was performed with a commercially available flexible fluorescence bronchoscope (Karl Storz® 11004BI, Germany). All lesions that appeared abnormal at blue and/or white light imaging were measured. The DPS fiber-probe was led through the working channel of the bronchoscope and placed in gentle contact with the bronchial mucosa. The duration of reflectance spectral acquisition was less than 1 s during which the light source of the bronchoscope was switched off. An average of three measurements was done on each location.

Bronchial biopsies of the lesions were obtained at exactly the same place of the spectroscopic measurement. First a biopsy for histological examination was obtained, then a biopsy was taken for determination of HIF1a expression and

afterwards, again a biopsy for histological examination was obtained. The biopsy for HIF1a expression was directly snap frozen in liquid nitrogen. For histological examination, the biopsies were transported in formaldehyde and fixed in paraffin. The pathological diagnoses were coded referring to the World Health Organisation Lung Cancer classification.

2.3. Differential path-length spectroscopy

The DPS technique has been previously described in great detail [8,9]. In short, spectra are measured using a custommade instrument using a fiberoptic probe small enough to be led through the working channel of a flexible bronchoscope. One fiber (delivery-and-collection (dc)-fiber) is used for both delivery and detection of light. The second fiber (collection (c)-fiber) is used for only detection of reflected light from the tissue. A tungsten-halogen lamp (Ocean Optics HL- 2000-FHSA, Duiven, The Netherlands) is used to light up the bronchial mucosa through the dc-fiber and the remitted light collected in the dc- and c-fiber is analysed in a dual channel spectrometer (Ocean Optics, SD2000). The difference of the dc- and c-fiber collection signals is the differential reflectance signal $R(\lambda)$. In the range of parameters relevant for biological tissue, we have previously reported that the differential reflectance signal $R(\lambda)$ can be modelled by [8]:

$$R(\lambda) = C_1 \lambda^{-b} \exp\{-0.32 C_{cor}(\lambda)\,\rho[StO_2 \mu_a^{HbO_2}(\lambda) + (1 - StO_2)\mu_a^{Hb}(\lambda)]\},$$

(1)

where $C1$ is a proportionality constant related to the density of scatterers in the tissue, b the so-called Mie parameter related to the size distribution of the scattering particles in the tissue [refs.], ρ the blood volume fraction, $StO2$ the microvascular blood oxygenation, $\mu_a^{HbO_2}$ (λ) the absorption coefficient of fully oxygenated whole blood, μ_a^{Hb} (λ) the absorption coefficient of fully deoxygenated whole blood and C_{cor} is a correction factor that accounts for the inhomogeneous distribution of blood in tissue [10] and is related to the vessel diameter (D_{vessel}).

Fitting the data to our equation yields values for the local blood oxygenation ($StO2$), local blood volume fraction (ρ), apparent average vessel diameter (D_{vessel}) and the Mie parameter (b). Since the path length of the photons which have travelled through the tissue is short (apparent differential path length = 320 μm), the optical properties extracted from the differential reflectance signal characterize the most superficial layer of the tissue (roughly within 160 μm of the tissue surface).

2.4. Western blot analysis of HIF1a expression

Frozen biopsies were pressed through a 40 μm mesh cell strainer (BD Biosciences, San Jose, CA, USA) using 100 μl of lysis buffer (20mM Tris pH 7.4, 150mM NaCl, 1mM EDTA, 0.1% NP40 and mini-complete protease inhibitors [Roche, Basel, S]). After 30 min incubation in ice, the protein suspension was centrifuged for 10 min at 12,000×g at 4 ∘C. The protein concentration was determined using 2D Quant (GE Healthcare-Amersham, Buckinghamshire, UK) and separated by one-dimensional SDS-PAGE. Proteins were electroblotted onto Immobilon P membranes (Millipore Corp, Etten-Leur, The Netherlands) and incubated with specific antibodies, followed by horseradish peroxidase-conjugated secondary antibodies and detected using SuperSignal West Pico

chemiluminescent substrate (Pierce Perbio Science, Etten-Leur, The Netherlands). Antibodies used in this study were anti- HIF1a (1:250, clone [BD transduction laboratories] and anti-beta-tubulin (1:2000, clone E7, Developmental Studies Hybridoma Bank, Iowa City, IA, USA) as control. Quantification of the expression levels were performed in duplicate by two independent observers denoted as negative/weak or positive/strong staining.

2.5. Statistical analysis
Variance analysis between saturation and negative and positive expression of HIF1a were tested using Wilcoxons rank sum test.

3. Results
Nine patients were included in this pilot study and 17 different locations that appeared endoscopically abnormal under white light or fluorescence bronchoscopy were measured and biopsied. Mean age was 62 years (range 50-90 years). All patients were analysed because of a suspicion for lung cancer. No desaturations during bronchoscopy were established using pulse-oximetry. The histology of these samples is denoted in Table 1.

Table 1 Histological diagnosis, saturation level and HIF1a expression levels in nine patients

Patient	Pathological diagnosis	Saturation level (%)	HIF1a expression levels
1	No dysplasia	84	Negative
	No dysplasia	100	Negative
2	No dysplasia	100	Negative
	No dysplasia	83	Negative
3	No dysplasia	100	Negative
4	No dysplasia	83	Negative
	Severe dysplasia	45	Positive
5	Metaplasia	87	Negative
	No dysplasia	76	Negative
	Large cell carcinoma	45	Negative
	No dysplasia	100	Negative
6	Large cell carcinoma	37	Positive
7	Small cell carcinoma	6	Positive
8	Adenocarcinoma	63	Positive
	No dysplasia	71	Negative
9	Squamous cell carcinoma	64	Positive
	No dysplasia	72	Negative

In all the subjects, the two biopsies taken for histological examination were compared. It was found that these biopsies showed a similar histology. Since the biopsy for HIF1a expression was taken in between those two, we are confident that the biopsy used for HIF1a expression will have a similar histology.

Due to the well-known low specificity of fluorescence bronchoscopy, histology varied from no dysplasia to invasive cancer. Microvascular blood saturation values ranged from 6 to 100%. In this pilot study, the data of non and mild dysplastic tissues were combined into a "no malignancy" group and the data of severe dysplasia and tumors into a "malignant" group for statistical purposes. Microvascular saturation levels in the no malignancy group (n = 11) equalled 87±11.5% (range 71-100%) and in the malignant group (n=6) 43±21% (range 6-63%). This difference was statistically significant ($p < 0.0002$). There was a significant difference in the spectroscopically determined saturations between the biopsies with negative expression of HIF1a and the biopsies with positive expression of HIF1a ($p < 0.005$; Fig. 1).
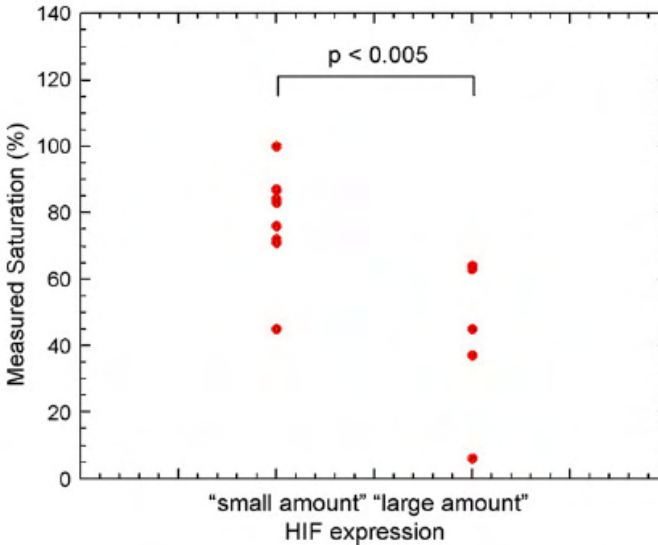
Fig. 1 Difference between HIF1a expression level expressed as small amount in case of absent or low expression and large amount in case of moderate or high expression in relation to the measured saturation

4. Discussion

We studied the relation between an indirect, ex vivo determined measure of hypoxia (HIF1a) and a real-time, non-invasive, in vivo measurement of blood oxygen saturation using optical spectroscopy. It was found that the expression of HIF1a was related to the optically determined microvascular oxygen saturation.

Determination of hypoxia-related proteins like HIF1a has been subjected to many studies in recent years. In contrast to many other tumors, the oxygen status in lung cancer cannot be determined directly (for instance with polarographic techniques) due to the inaccessibility of the bronchial tree. Only during operation, recently a study was published using an Eppendorf polarographic electrode, in which oxygen

tension was related to hypoxic markers, one of them being CA IX [11]. In their study, tissue oxygen tension correlated with expression of CA IX. In our study, patients with more advanced disease are studied which are in general associated with a lower oxygen tension. Also, our method is less invasive and can easily be done during bronchoscopy, but of course, is dependent on visualisation of the tumor during bronchoscopy.

The method used in this study is based on optical spectroscopy (differential path-length spectroscopy, DPS) to determine tumor blood-oxygen saturation [8,9,12,13]. In earlier studies using this technique, it was shown that malignancies were associated with a low microvascular saturation [8]. The determined values of microvascular saturation are highly reproducible. It is the subject of ongoing research to investigate saturation levels in premalignancies in order to increase specificity of fluorescence bronchoscopy. In lung tumors, we are evaluating the relation between microvascular saturation levels and survival. Also the relation between microvascular saturation levels and efficacy of therapy is the subject of study. One could theoretically predict that hypoxic tumors will be more resistant to radiotherapy, while the response to chemotherapy may also be related to microvascular saturation levels. Presently no data on these subjects are published.

DPS determines the tumors microvascular blood saturation as opposed to the tumors tissue oxygen tension as determined with HIF1a, a marker for cellular hypoxia. Although microvascular blood saturation and tissue oxygen tension may not be similar, they will be related. Certainly, if low blood saturation levels are measured, it cannot be expected that tissue oxygen tensions are high. In case of high blood saturation levels, however, tissue oxygen levels may still be low due to increased oxygen consumption and diffusion capacity problems.

Tumor hypoxia is becoming of increasing interest since a relation between hypoxia and metastases and survival has been described in several studies using hypoxia-related proteins, as reviewed in Ref. [2]. A higher expression of hypoxia-related proteins was shown to be related to a higher rate of metastases and a shorter survival. In this excellent review, the relation between hypoxia and tumor aggressiveness is discussed in great detail. The conclusions of the studies on expression of hypoxia-related proteins are not uniform [1]. In some of the studies, the relation between the protein expression and survival was not found, questioning the usefulness of these indirect measures of hypoxia [3,7]. As we do find a correlation between oxygen tension and the expression of hypoxia-related proteins, it is our hypothesis that this inconsistency is related to differences in the sampling of tissue for protein expression. Most of the samples studied for protein expression are samples from patients who have been operated. In a tumor, the tissue saturation will not be the same in the whole tumor [2]. In most of the ex vivo studies, it is not known where the sample for protein determination is taken from. The center of a tumor may be more hypoxic than its periphery causing high expression of hypoxia-related proteins in the center of the tumor, while the periphery of the tumor may be characterized by a low expression of hypoxia-related proteins.

We hypothesize that the presence of hypoxic areas on the periphery of a tumor are better predictors of invasive growth and thus of the rate of metastases than hypoxic areas in the centre of the tumor. For instance, squamous cell carcinomas are known to have necrotic centres, causing high expression of hypoxia-related proteins in the centres of these tumors, while these large necrotic tumors may
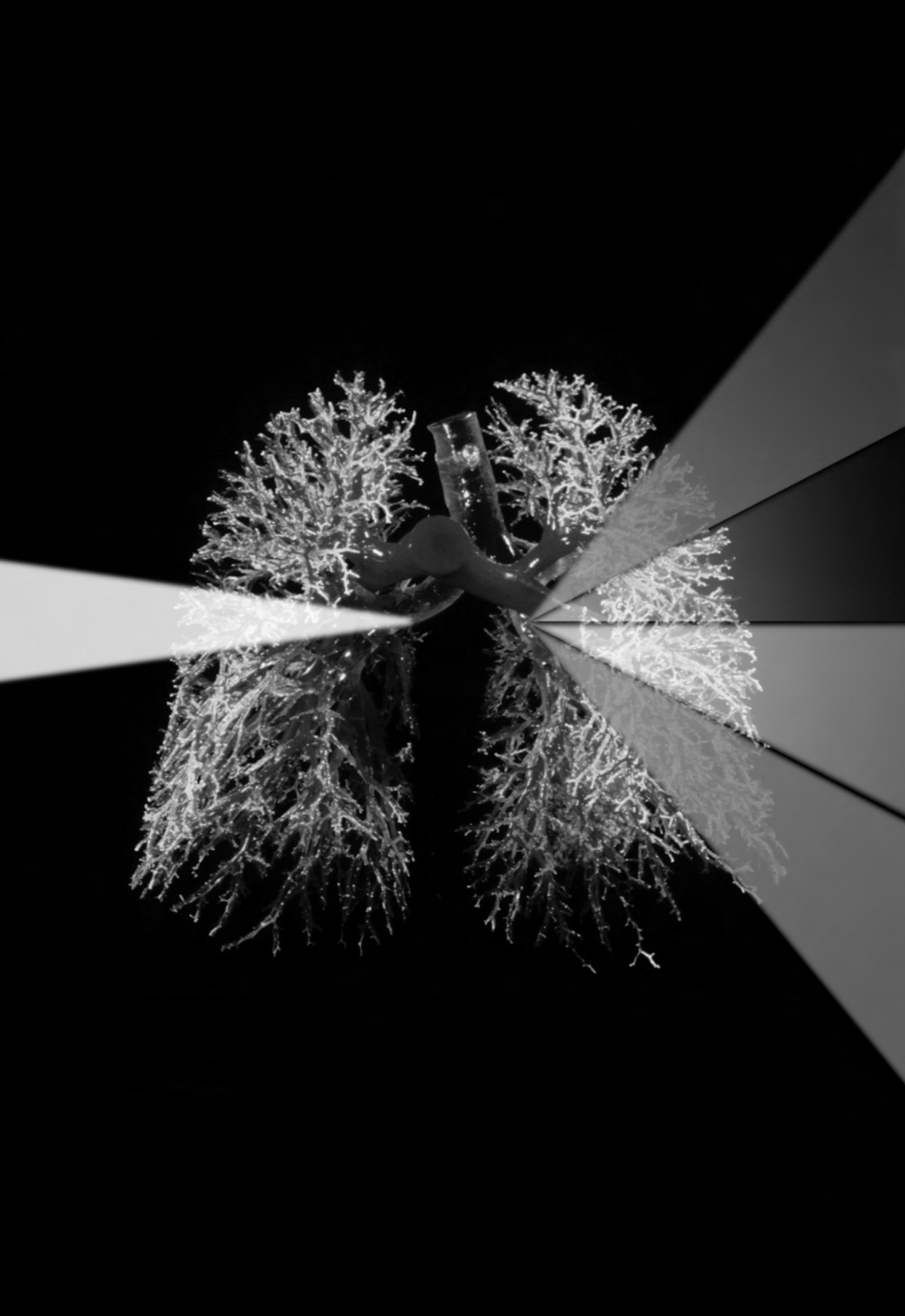
present without metastases. Interestingly, in a separate study, we found that squamous cell carcinomas, presenting with central necrosis were characterized by relatively high blood saturation at the periphery of the tumor. The average microvascular saturation measured with DPS of squamous cell carcinomas was found to be 61% ($n = 10$), while the average microvascular saturation of all other histological types ($n = 24$) was 43%.

In conclusion, two independent measures to determine hypoxia in tissue, either by ex vivo protein expression or by in vivo optical spectroscopic techniques, show a good correlation. The determination of hypoxia may be of importance, for example, in the choice of therapeutic agents. In a recent article on the effect of tyrapazamine, it was suggested that the absence of a beneficial effect of this agent might be related to the percentage of hypoxic cells in a tumor. Furthermore, hypoxic tumors may be more resistant to ionizing radiation [2].

Our results open the field for in vivo research on hypoxia, e.g. on the effect of different therapeutic options like angiogenesis inhibitors, hypoxia targeted agents like tyrapazamine or the effects of radiotherapy on hypoxic lung tumors.

References

[1] Kim SJ, Rabbani ZN, Dewhirst MW, Vujaskovic Z, Vollmer RT, Schreiber EG, et al. Expression of HIF-1alpha, CA IX, VEGF, and MMP-9 in surgically resected non-small cell lung cancer. Lung Cancer 2005;49(3):325—35.

[2] Hockel M, Vaupel P. Tumor hypoxia: definitions and current clinical, biologic, and molecular aspects. J Natl Cancer Inst 2001;93(4):266—76.

[3] Evans SM, Koch CJ. Prognostic significance of tumor oxygenation in humans. Cancer Lett 2003;195(1):1—16.

[4] Li L, Yu J, Xing L, Ma K, Zhu H, Guo H, et al. Serial hypoxia imaging with 99mTc-HL91 SPECT to predict radiotherapy response in nonsmall cell lung cancer. Am J Clin Oncol 2006;29(6):628—33.

[5] Song X, Liu X, Chi W, Liu Y, Wei L, Wang X, et al. Hypoxiainduced resistance to cisplatin and doxorubicin in non-small cell lung cancer is inhibited by silencing of HIF-1alpha gene. Cancer Chemother Pharmacol 2006;58(6):776—84.

[6] Giatromanolaki A, Koukourakis MI, Sivridis E, Turley H, Talks K, Pezzella F, et al. Relation of hypoxia inducible factor 1 alpha and 2 alpha in operable non-small cell lung cancer to angiogenic/ molecular profile of tumours and survival. Br J Cancer 2001;85(6):881—90.

[7] Kim SJ, Rabbani ZN, Vollmer RT, Schreiber EG, Oosterwijk E, Dewhirst MW, et al. Carbonic anhydrase IX in early-stage non-small cell lung cancer. Clin Cancer Res 2004;10(23): 7925—33.

[8] Bard MP, Amelink A, Hegt VN, Graveland WJ, Sterenborg HJ, Hoogsteden HC, et al. Measurement of hypoxia-related parameters in bronchial mucosa by use of optical spectroscopy. Am J Respir Crit Care Med 2005;171(10):1178—84.

[9] Amelink A, Sterenborg HJ, Bard MP, Burgers SA. In vivo measurement of the local optical properties of tissue by use of differential path-length spectroscopy. Opt Lett 2004;29:1087—9.

[10] van Veen RLP, Verkruysse W, Sterenborg HJCM. Diffusereflectance spectroscopy from 500 to 1060nm by correction for inhomogeneously distributed absorbers. Opt Lett 2002;27:246—8.

[11] Le QT, Chen E, Salim A, Cao H, Kong CS, Whyte R, et al. An evaluation of tumor oxygenation and gene expression in patients with early stage non-small cell lung cancers. Clin Cancer Res 2006;12(5):1507—14.

[12] Bard MP, Amelink A, Skurichina M, Noordhoek Hegt V, Duin RP, Sterenborg HJ, et al. Optical spectroscopy for the classification of malignant lesions of the bronchial tree. Chest 2006;129(4):995—1001.

[13] Bard MP, Amelink A, Skurichina M, den Bakker M, Burgers SA, van Meerbeeck JP, et al. Improving the specificity of fluorescence bronchoscopy for the analysis of neoplasticlesions of the bronchial tree by combination with optical spectroscopy, preliminary communication. Lung Cancer 2005;47(1): 41—7.

Chapter 4

Relation of lung cancer histology to peripheral microvascular saturation measured by optical spectroscopy

C. van der Leest[1,2]

A. Amelink[3]

M. Bard[4]

P. Mulder[5]

R. Djamin[1]

D. Sterenborg[3]

H.C. Hoogsteden[2]

J.G.J.V. Aerts[1,2]

1 Department of Pulmonary Diseases, Amphia Hospital, Breda, The Netherlands

2 Department of Pulmonary Diseases, Erasmus MC, Rotterdam, The Netherlands

3 Center for Optical Diagnostics and Therapy, Department of Radiation Oncology, Erasmus MC, Rotterdam, The Netherlands

4 Department of Pulmonary Diseases, Kennemer Gasthuis, Haarlem, The Netherlands

5 Department of Department of Epidemiology & Biostatistics, Erasmus MC, Rotterdam, The Netherlands

Abstract
Introduction: Lung cancer is historically divided into Non-Small Cell Lung Cancer (NSCLC) and Small Cell Lung Cancer (SCLC), due to differences in treatment options and prognosis.
Hypoxia is a well known parameter in many solid tumors and has been related to high metastatic rate and poor prognosis. Whether hypoxia is different between the histological subtypes of lung cancer is unknown. The aim of the study was to compare spectroscopic determined saturation levels of endobronchial NSCLC and SCLC tumors and relate this to survival.
Methods: Differential pathlength spectroscopy (DPS) was used during bronchoscopy. Hereby peripheral in vivo microvascular saturation data were obtained in different histological subtypes of lung tumors. DPS data were correlated with endobronchial tumors histology corrected for stage of disease.
Results: In 98 patients DPS data could be correlated to histological-confirmed endobronchial tumor tissue. No differences in oxygenation between NSCLC and SCLC were established. Adenocarcinomas and squamous cell carcinomas had a better peripheral oxygenation, StO_2 65% (± 20,0) and 58% (± 28,9) respectively, compared to large cell carcinoma and SCLC, StO_2 42% (± 28,9) and 38% (± 28,2) (p <0.05) respectively. No relation between peripheral microvascular tumor saturation and survival could be established.
Conclusion: Although differences in peripheral microvascular saturation, measured during bronchoscopy, between the histological subtypes of lung cancer can be observed, this is not related to survival.

Introduction

Based on treatment potentials, lung cancer is historically subdivided into two subtypes, Non-Small Cell Lung Cancer (NSCLC) and Small Cell Lung Cancer (SCLC)[1]. Compared to NSCLC, SCLC is in general associated with higher mitotic rate and higher metastatic potential[1]. For this reason, SCLC is considered metastasized at diagnosis and surgery is limited to a very selected population of patients which are also treated with adjuvant chemotherapy.

One of the key factors considered to be related to the aggressiveness of a tumor is hypoxia[2-4]. Hypoxia is a well known phenomenon in many solid tumors[5]. Three main reasons cause tumor hypoxia [6]. First, inadequate blood flow of tumor tissue. Hypoxia can be caused by inadequate vascular network and impaired blood vessels resulting in absence of flow regulation or stasis. Second, increased diffusion distance. By tumor expansion without increment of microvessel network the distance between the oxygen providing vessels and the cells become larger. Third, tumor associated anemia can cause reduction in oxygen supply to tumors[7-9].

Using reflectance spectroscopy it is possible to determine peripheral microvascular saturation of endobronchial tumors during bronchoscopy[10]. A previous study of our group showed lower peripheral microvascular saturation levels of endobronchial tumors compared to normal bronchial tissue[10] and this lower microvascular saturation was correlated with a higher hypoxia inducible factor 1-alpha (HIF1a) expression[11].

We studied the microvascular saturation levels of SCLC and NSCLC. Different histological subtypes of NSCLC were compared as well. Finally the relation between peripheral microvascular saturation and survival was studied.

Material and methods

Subjects

In this non-randomized open study, patients with suspect malignancies of the lung and therefore medical indication for bronchoscopy were invited to participate. All patients were above 18 years old. The study was approved by the Medical Ethics Review board of the Erasmus Medical Centre Rotterdam, the Netherlands. Survival follow up was performed by status research and contacting the General Practitioner.

Histology

Endobronchial tumors were classified according to the World Health Organization (WHO) criteria[1], by a dedicated pathologist who was blinded for the DPS results. Patients with histology confirmed lung cancer diagnosis were included. Patients with cytological confirmation of lung cancer were excluded.

Examination procedures

Bronchoscopy was performed with a pentax bronchoscope. Any macroscopically visible tumor lesions could be measured. The DPS fiber was led through the working channel of the bronchoscope and placed in gentle contact with the bronchial mucosa. The duration of one spectral measurement was less than one second. An average of three spectra was taken in order to take into account the heterogeneity of the tissue. After measurement, histology biopsies of the measured place were obtained.

Differential path length spectroscopy
The DPS technique has been previously described in great detail[10]. In short, spectra are measured using a custom made fiberoptic probe containing two fibers, small enough to be led through the working channel of a flexible bronchoscope. One fiber is used for both delivery and detection of light, the other is only used for detection of reflected light from the tissue. A Xenon lamp (Ocean Optics, HPX 2000) is used to light up the bronchial mucosa through the deliver and detection fiber and the remitted light collected in both fibers is analyzed in a dual channel spectrometer (Ocean Optics, SD2000). The difference between the two collecting signals is the differential reflectance signal. In the range of parameters relevant for biological tissue we previously reported that the differential reflectance signal $R(\lambda)$ can be modeled by[10].

$$R(\lambda) = C_1\lambda^{-b} \exp\{-0.32C_{cor}(\lambda)\ \rho[StO_2\mu_a^{HbO2}(\lambda) + (1-StO_2\mu_a^{Hb}(\lambda)]\},$$

where C_1 is a proportionality constant, b is a parameter related to the size of the scattering particles, C_{cor} is a correction factor that accounts for the inhomogeneous distribution of blood in tissue and its related vessel diameter D_{vessel}, ρ is the blood fraction, STO_2 is the microvascular blood oxygenation, $\mu_a^{HbO2}(\lambda)$ is the absorption coefficient of fully oxygenated whole blood, and $\mu_a^{Hb}(\lambda)$ is the absorption coefficient of fully deoxygenated whole blood.
Fitting the data to our equation yields values for the local blood oxygenation (%) and with this technique is it possible to measure direct in vivo saturation of the superficial layer of the bronchial mucosa and tumour tissue.
Since the path length of the photons which have travelled through the tissue is short (apparent differential path length = 320µm), the optical properties extracted from the differential reflectance signal characterize the most superficial layer of the tissue (roughly within 160µm of the tissue surface).

Statistical analysis
Differences of peripheral microvascular saturation between the histological types of cancer were evaluated with univariate analysis adjusted for stadium and gender. This was done by SPSS. T-tests between different histology and average saturation, adjusted for stadium and gender, were performed. Survival analyses were evaluated with the Kaplan Meier curves and a log rank scale. Log Rank test was used to asses the best discriminative StO_2 in relation to survival. P values less than 0.05 were regarded as significant.

Results
Between January 2004 and April 2008, 98 patients (73 men, 25 women) were included. In these patients, with histological biopsies confirmed lung cancer, DPS measurements were performed. Patients' data are shown in table 1. Endoscopic determined DPS saturation levels are shown in table 2. Average number of DPS measurements per tumor was 3.6 (range 1-10).
No differences in peripheral tumor microvascular saturation were established when NSCLC and SCLC as a group were compared, irrespective of stadium (table 3 and figure 1). Peripheral microvascular saturation levels were 51.2% (±29) in NSCLC and 37.5 (±28.2) in SCLC. The NSCLC group was divided into the three subgroups; Adenocarcinomas (ADC), squamous cell carcinomas (SCC) and large cell carcinomas (LCC). Comparing these subgroups and SCLC, irrespective of stadium, differences of peripheral tumor microvascular saturation were observed. ADC and SCC were better oxygenated, StO_2 65% and 58% respectively,

compared to LCC and SCLC, StO$_2$ 42% and 38% respectively (Table 3 and figure 2). No significant difference between stage I/II compared to III/IV was observed. The stage I and II tumors were mainly SCC (66.7%). A subgroup analysis between stage I/II SCC and stage III/IV SCC showed no significant results (p-value 0.219). The survival data in the SCC group were significant different between stage I/II and III/IV (p=0.009). Mean follow up of all the patients was 2.5 (±1.7) year.

Evaluation of survival data and peripheral tumor microvascular saturation showed no significant difference, although the curve was in favor of the tumors with higher microvascular saturation (figure 3). Univariate analysis was performed in order to exclude confounders. The univariate analyses, including gender and tumor stadium, showed no significant difference between the independent variants and the relation between peripheral tumor microvascular saturation and histology.

Discussion

We studied a hypoxia related parameter in relation to the different endoscopic visible lung tumors using DPS technology. In addition, we investigated the prognostic value of this parameter. It was found that SCLC and LCC are associated with the lowest blood oxygenation compared to ADC and SCC. There was no correlation between peripheral tumor microvascular saturation and overall survival.

SCLC represents one of the more aggressive types of lung cancer with necrosis and high mitotic count[1]. Rapid cell division rate is associated with increased cell metabolism and increased oxygen consumption and when neoangiogenesis flow becomes inadequate, blood flow diffusion distance increases, leading to tumor hypoxia [7]. Based on WHO criteria LCC is considered to be a NSCLC which does not fit into the criteria of either squamous or adenocarcinoma. LCC do not have clear cut morphological signs of differentiation, considering poorly angiogenetic architecture. Tumor bloodvessels with poor angiogenetic architecture become leaky and tortuous causing impaired blood flow [12, 13]. This impaired blood flow causes lower blood saturation.

Hypoxia is a known prognostic tumormarker in many solid tumors. In lung cancer these data are not definite. In our study we do not find peripheral microvascular saturation as a prognostic marker. Striking are the high saturation levels of the peripheral adeno and squamous cell subtypes. Although the microvascular saturation is lower compared to normal bronchial tissue, the microvascular saturation is unexpected high. Several other studies support the idea that NSCLC is a less hypoxic tumor. A study with the Eppendorf electrode showed a median pO2 of 16 mm Hg (range 0.7-46 mm Hg)[14]. One other hypoxia-related study, using a tracer 18F-fluoromisonidazol (^{18}F-FMISO), found only small areas of hypoxia in adeno and squamous cell carcinomas[15]. They hypothesized that the unique structure of the lung parenchyma, including the dual blood supply and the abundant oxygen-containing air spaces, might be the reason why some lung tumor types are less hypoxic than others.

The studies which measured lung tumor hypoxia with the Eppendorf [14] and the ^{18}F-FMISO [15] support our finding of a high microvascular saturation level in endobronchial adeno and squamous cell carcinoma tissue. As DPS measures only a small size of the peripheral tumor, we don't have data about central tumor areas. By using ^{18}F-FMISO all the hypoxic areas are visible including the centre of the tumor[16]. For complete information about tumor hypoxia, [18]FMISO is superior to DPS. However, ^{18}F-FMISO is a technique where the uptake of tracer 18F-

fluoromisonidazol is qualitative related to hypoxia and spatial resolution is a problem. DPS utilized reflectance spectra to provide quantitative hypoxia related data.

Localizing sub-populations with tumor hypoxia which are more resistant to radiotherapy and chemotherapy would enable to customize the treatment. Our results show that LCC and SCLC are the type of tumors with a lower saturation. An early study with tirapazamine, a hypoxic cytotoxin, showed promising results in patients with NSCLC[17]. Tirapazamine is an aromatic heterocycle di-*N*-oxide, which is activated to a toxic radical only at very low levels of oxygen[18]. A phase III study (CATAPULT I) showed a benefit of the combination cisplatin and tirapazamine over cisplatin alone. Unfortunately the next study (CATAPULT II) showed no benefit of cisplatin and tirapazamine over cisplatin and etoposide[18]. Both studies were done in patients with advanced stage NSCLC. Studies with tirapazamine in patients with SCLC have been reported as well. Two studies combined tirapazamine with concurrent chemo-radiotherapy treatment in patients with limited SCLC and showed promising median survival rates[19, 20]. Our low levels of peripheral microvascular saturation in SCLC support their positive study results.

Peripheral tumor microvascular saturation was not an independent prognostic marker in our study. This might be caused by the heterogeneous population. The patient population comprises all tumor stadia and therefore all treatment modalities. Patients were treated with either surgery, chemo-radiotherapy (concurrent or sequential), chemotherapy alone or best supportive care. Diversity in stadia and treatment has major influence on the prognosis. It was not possible to create a more homogeneous group, because the bronchoscopy including DPS measurements were performed in the beginning of the tumor work-up. Therefore, no information about histology diagnosis, stage of disease and treatment were available before including patients. The patient population is too small to perform sub-analysis for prognosis. Future study of a larger study population with a homogeneous treatment is necessary for more information about the prognostic value of peripheral microvascular saturation.

No differences in peripheral microvascular saturation between the different tumor stadia have been observed. One of the reasons for this is a limited number of stage I and II tumors. Secondly, most of the stage I and II tumors are SCC. This histological subtype is more often located in the central airways and therefore more often visible by bronchoscopy. There was no significant difference in microvascular saturation between squamous cell tumors of stadium I/II and stadium III/IV. Although the number of patients in this subanalysis is very limited, as survival was significant in the two groups, it supports the hypothesis that peripheral microvascular tumor saturation is not related to invasiveness of the tumor, and therefore not related to prognosis.

In conclusion, peripheral microvascular saturation measured in endobronchial tumors using DPS do not differ between NSCLC and SCLC. ADC and SCC contained higher peripheral microvascular saturation compared to LCC and SCLC. Peripheral microvascular saturation seems to be related to histological cell subtypes and is not prognostic in this analysis. Future studies should take into consideration the differences in peripheral tumor microvascular saturation in the different histological subtypes of lung cancer to investigate its impact on different treatments.

	NSCLC				SCLC	Total
	ADC	SCC	LCC	total		
number of patients	12	29	37	78	20	98
Men	7	24	30	61	12	73
Women	5	5	7	17	8	25
Mean Age (years)	64.7 ± 10.9	69.0 ± 8.0	70.9 ± 10.3	69.2 ± 9.7	64.2 ± 10.9	
Smoking history	10	29	36	75	20	95
Stage I	-	6	2	8	1	9
Stage II	-	2	1	3	-	3
Stage III	3	15	19	37	7	44
Stage VI	9	5	15	29	12	41
Unknown	-	1	-	1	-	1

Table 1: patients' characteristics

	NSCLC				SCLC
	ADC	SCC	LCC	total	
number of patients	12	29	37	78	20
Mean Sat (%) (SD)	64.8 ± 20.0	57.9 ± 28.9	41.6 ± 28.9	51.2 ± 29.0	37.5 ± 28.2
Median Sat (%)	71.7	57.8	41.3	54.9	35.2

Table 2: Endoscopic determined DPS saturation levels

histology	microvascular saturation p-value
NSCLC versus SCLC	0.158
ADC versus SCC	0.161
ADC versus LCC	0.002*
ADC versus SCLC	0.005*
SCC versus LCC	0.035*
SCC versus SCLC	0.095
LCC versus SCLC	0.928

Table 3: t-test adjusted for stadium and gender
Abbreviations: NSCLC total group of non-small cell carcinomas, ADC adenocarcinoma, SCC squamous cell carcinoma, LCC large cell carcinoma, SCLC small cell carcinoma
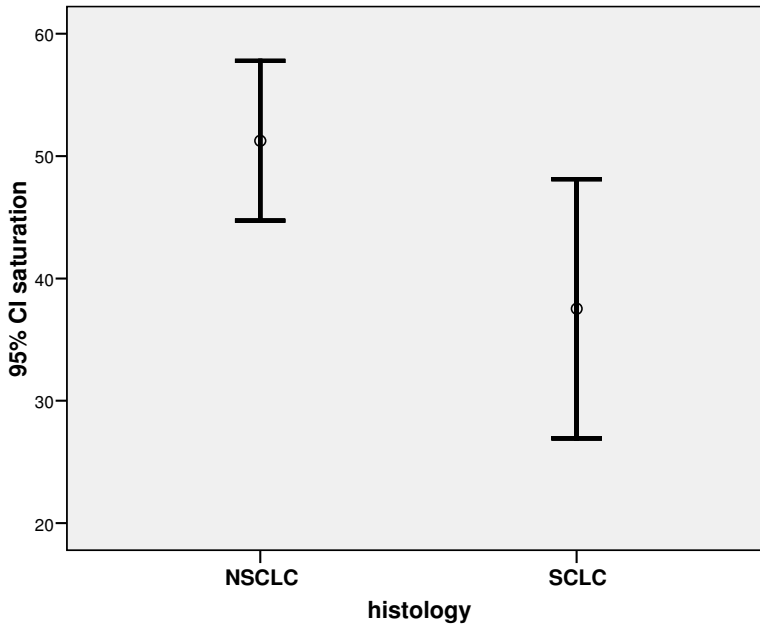

Figure 1: Mean and 95% confidence interval in peripheral saturation between NSCLC and SCLC

Relation of lung cancer histology to peripheral microvascular saturation measured by optical spectroscopy
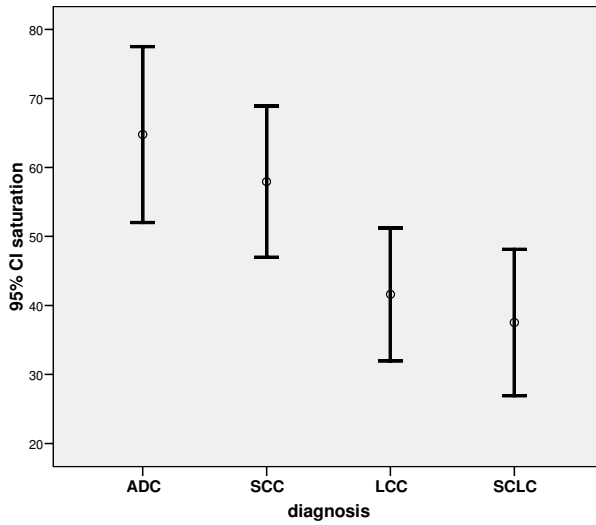

Figure 2: Mean and 95% confidence interval in peripheral saturation between the different histological lung tumors. Abbreviation: adenocarcinoma (ADC), squamous cell carcinoma (SCC), Large cell carcinoma (LCC), Small cell carcinoma (SCLC)
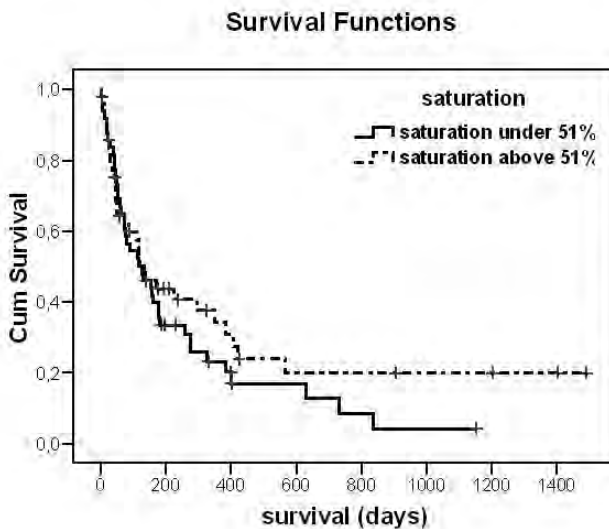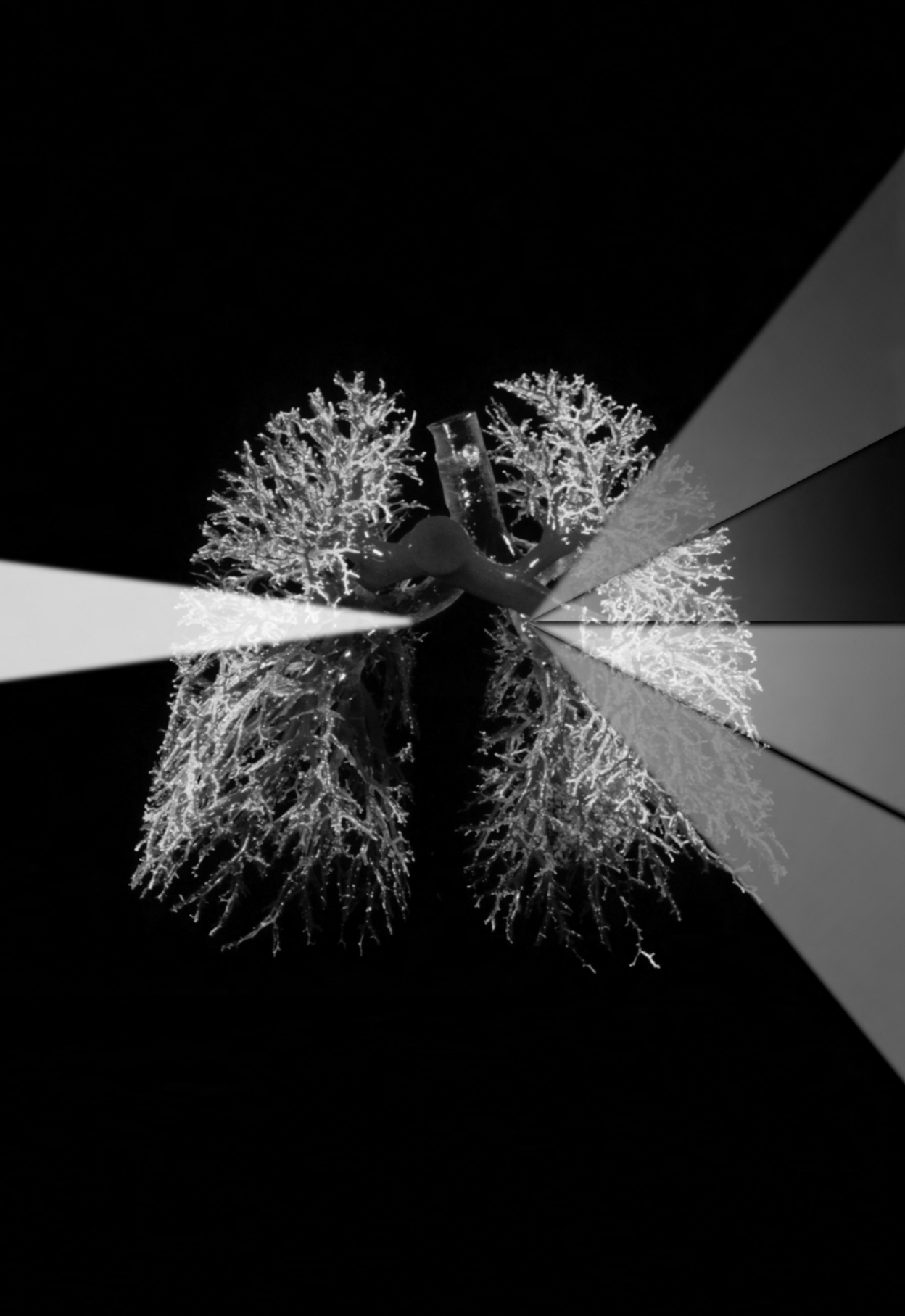

Figure 3: Kaplan Meier of survival between the different peripheral tumor saturation

References

1.   W.D Travis EB, H.K. Muller-Hermelink, C.C Harris. Pathology and genetics of Tumours of the Lung, Pleura, Thymus and Heart; 2004; 9-124.
2.   Brahimi-Horn C, Pouyssegur J. The role of the hypoxia-inducible factor in tumor metabolism growth and invasion. Bull Cancer 2006;93:E73-80.
3.   Gort EH, Groot AJ, van der Wall E, van Diest PJ, Vooijs MA. Hypoxic regulation of metastasis via hypoxia-inducible factors. Curr Mol Med 2008;8:60-7.
4.   Goudar RK, Vlahovic G. Hypoxia, angiogenesis, and lung cancer. Curr Oncol Rep 2008;10:277-82.
5.   Bertout JA, Patel SA, Simon MC. The impact of O2 availability on human cancer. Nat Rev Cancer 2008;8:967-75.
6.   Vaupel P, Harrison L. Tumor hypoxia: causative factors, compensatory mechanisms, and cellular response. Oncologist 2004;9 Suppl 5:4-9.
7.   Hockel M, Vaupel P. Tumor hypoxia: definitions and current clinical, biologic, and molecular aspects. J Natl Cancer Inst 2001;93:266-76.
8.   Vaupel P, Thews O, Hoeckel M. Treatment resistance of solid tumors: role of hypoxia and anemia. Med Oncol 2001;18:243-59.
9.   Vaupel P, Kelleher DK, Hockel M. Oxygen status of malignant tumors: pathogenesis of hypoxia and significance for tumor therapy. Semin Oncol 2001;28:29-35.
10.   Bard MP, Amelink A, Hegt VN, et al. Measurement of hypoxia-related parameters in bronchial mucosa by use of optical spectroscopy. Am J Respir Crit Care Med 2005;171:1178-84.
11.   Aerts JG, Amelink A, van der Leest C, et al. HIF1a expression in bronchial biopsies correlates with tumor microvascular saturation determined using optical spectroscopy. Lung Cancer 2007;57:317-21.
12.   Jain RK. Normalizing tumor vasculature with anti-angiogenic therapy: a new paradigm for combination therapy. Nat Med 2001;7:987-9.
13.   Jain RK. Normalization of tumor vasculature: an emerging concept in antiangiogenic therapy. Science 2005;307:58-62.
14.   Le QT, Chen E, Salim A, et al. An evaluation of tumor oxygenation and gene expression in patients with early stage non-small cell lung cancers. Clin Cancer Res 2006;12:1507-14.
15.   Cherk MH, Foo SS, Poon AM, et al. Lack of correlation of hypoxic cell fraction and angiogenesis with glucose metabolic rate in non-small cell lung cancer assessed by 18F-Fluoromisonidazole and 18F-FDG PET. J Nucl Med 2006;47:1921-6.
16.   Krohn KA, Link JM, Mason RP. Molecular imaging of hypoxia. J Nucl Med 2008;49 Suppl 2:129S-48S.
17.   Weitman S, Mangold G, Marty J, et al. Evidence of enhanced in vivo activity using tirapazamine with paclitaxel and paraplatin regimens against the MV-522 human lung cancer xenograft. Cancer Chemother Pharmacol 1999;43:402-8.
18.   Reddy SB, Williamson SK. Tirapazamine: a novel agent targeting hypoxic tumor cells. Expert Opin Investig Drugs 2009;18:77-87.
19.   Le QT, Moon J, Redman M, et al. Phase II study of tirapazamine, cisplatin, and etoposide and concurrent thoracic radiotherapy for limited-stage small-cell lung cancer: SWOG 0222. J Clin Oncol 2009;27:3014-9.
20.   Le QT, McCoy J, Williamson S, et al. Phase I study of tirapazamine plus cisplatin/etoposide and concurrent thoracic radiotherapy in limited-stage small cell lung cancer (S0004): a Southwest Oncology Group study. Clin Cancer Res 2004;10:5418-24.

Chapter 5

Integration of single fiber reflectance spectroscopy into ultrasound-guided endoscopic lung cancer staging of mediastinal lymph nodes

S.C. Kanick[1]

C. van der Leest [2,3]

J.G.J.V. Aerts[2,3]

H.C. Hoogsteden[2]

Slávka Kaščáková[1]

H.J.C.M. Sterenborg[1]

A. Amelink[1]

1 Center for Optical Diagnostics and Therapy, Department of Radiation Oncology, Erasmus MC, Rotterdam, The Netherlands
2 Department of Pulmonary Diseases, Erasmus MC, Rotterdam, The Netherlands
3 Department of Pulmonary Diseases, Amphia Hospital, Breda, The Netherlands

Chapter 5

Integration of single-fiber reflectance spectroscopy into ultrasound-guided endoscopic lung cancer staging of mediastinal lymph nodes

Stephen Chad Kanick
Erasmus Medical Center
Center for Optical Diagnostics and Therapy
Department of Radiation Oncology
Rotterdam 3015 GE
The Netherlands

Cor van der Leest
Joachim G. J. V. Aerts
Amphia Hospital
Department of Pulmonary Diseases
Breda, The Netherlands
    and
Erasmus Medical Center
Department of Pulmonary Diseases
Rotterdam 3000 CA
The Netherlands

Henk C. Hoogsteden
Erasmus Medical Center
Department of Pulmonary Diseases
Rotterdam 3000 CA
The Netherlands

Slávka Kaščáková
Henricus J. C. M. Sterenborg
Erasmus Medical Center
Center for Optical Diagnostics and Therapy
Department of Radiation Oncology
Rotterdam 3015 GE
The Netherlands

Arjen Amelink
Erasmus Medical Center
Center for Optical Diagnostics and Therapy
Department of Radiation Oncology
Rotterdam 3015 GE
The Netherlands
    and
Erasmus Medical Center
Department of Pulmonary Diseases
Rotterdam 3000 CA
The Netherlands

Abstract. We describe the incorporation of a single-fiber reflectance spectroscopy probe into the endoscopic ultrasound fine-needle aspiration (EUS-FNA) procedure utilized for lung cancer staging. A mathematical model is developed to extract information about the physiological and morphological properties of lymph tissue from single-fiber reflectance spectra, e.g., microvascular saturation, blood volume fraction, bilirubin concentration, average vessel diameter, and Mie slope. Model analysis of data from a clinical pilot study shows that the single-fiber reflectance measurement is capable of detecting differences in the physiology between normal and metastatic lymph nodes. Moreover, the clinical data show that probe manipulation within the lymph node can perturb the *in vivo* environment, a concern that must be carefully considered when developing a sampling strategy. The data show the feasibility of this novel technique; however, the potential clinical utility has yet to be determined. © *2010 Society of Photo-Optical Instrumentation Engineers.* [DOI: 10.1117/1.3290822]

1 Introduction

Lung cancer causes the most cancer-related deaths in both men and women worldwide.[1] For patients diagnosed with limited stage non-small-cell lung cancer (NSCLC), treatment options are dependent on the presence of metastatic cancer in the mediastinal lymph nodes.[2–4] For patients diagnosed with

NSCLC, treatment in the absence of metastatic cancer involves surgical resection of the tumor; however, in the presence of metastatic cancer, the treatment of choice is systemic chemotherapy combined with radiotherapy.[2] Following diagnosis of NSCLC, the mediastinal lymph nodes are imaged, usually with a computed tomography (CT) scan and/or positron emission tomography (PET) scanning, but the specificity of these imaging modalities are not reliable enough to properly diagnose cancer, and histopathological examination of

Address all correspondence to: Stephen Chad Kanick, Erasmus Medical Center, Center for Optical Diagnostics and Therapy, Department of Radiation Oncology, Rotterdam 3015 GE, The Netherlands. Tel: 31-10-7032102; E-mail: s.kanick@erasmusmc.nl

Integration of single fiber reflectance spectroscopy into ultrasound-guided endoscopic lung cancer staging of mediastinal lymph nodes
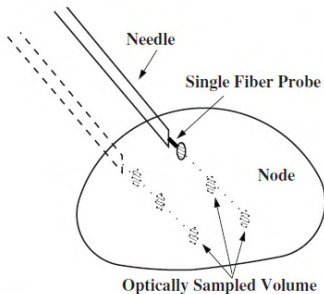
Fig. 1 Schematic of proposed sampling strategy.

any enlarged lymph node is required. The gold standard procedure for mediastinal staging is surgical biopsy of the lymph node[2] (termed mediastinoscopy). A novel alternative method to stage lymph nodes is the endoscopic ultrasound fine-needle aspiration (EUS-FNA), which utilizes an ultrasound probe to visualize the lymph node being sampled, offering the clinician access to mediastinal lymph nodes with lower costs and less patient morbidity than mediastinoscopy.[2–4] However, EUS-FNA has a low sensitivity and is associated[2] with a false negative (FN) rate of $\approx 23\%$ (compared with the 9% FN rate of mediastinoscopy). The high EUS-FNA FN rate is attributable to localized malignant areas within the node that were not sampled during the biopsy. This complication necessitates the sampling of multiple sites within the node or requires the presence of a cytologist on-site. On average, five sampling sites within the node are biopsied during EUS-FNA, a total that cannot be easily increased because more samples would require more punctures into the node and longer procedure times; factors that would negatively affect patient comfort.

Incorporation of a fiber optic reflectance device into the EUS-FNA procedure may assist in the identification of malignant regions within the lymph nodes during biopsy, potentially reducing the FN rate of the current procedure. The fiber optic device would enable rapid optical sampling from multiple local tissue regions throughout the lymph node, with optical properties accurately estimated within small volumes (≈ 0.1 mm^3) of tissue optically interrogated during measurement. The schematic in Fig. 1 shows a proposed sampling strategy for EUS-FNA with the incorporated optical device, with the optical fiber sampling multiple (≈ 10 to 50) samples acquired within the same time required for one biopsy acquisition in the current procedure. This strategy would result in characterization of a larger volume of the lymph node than is achieved with the current procedure, reducing the chance that malignant areas are not biopsied.

Reflectance spectra measured in the UV-VIS wavelength range contain information about tissue absorption and scattering properties;[5] information that can be used[6–8] to describe tissue physiology (e.g., vascular oxygen saturation, blood volume fraction) and morphology (e.g., tissue/cell/organelle size and density), and can be used to differentiate between normal and malignant tissue. Classical reflectance spectroscopic devices that utilize multiple optical fibers to deliver and collect

light during measurement[6–8] are too large to fit through the EUS-FNA biopsy needle (with an inner diameter of ≈ 460 μm). This application requires the use of a single optical fiber with fiber diameters in the range of 200 to 400 μm that could be incorporated into the narrow channel of the EUS-FNA device.

The concept of single-fiber (SF) reflectance spectroscopy has been previously proposed,[9,10] but these studies were limited to qualitative analysis of spectra because they lacked an accurate description of the relationship between the photon path length and the tissue optical properties. Recently, our group developed a novel empirical relationship between the SF photon path length and both the absorption coefficient and reduced scattering coefficient within an optically sampled turbid medium.[11] This advancement enables quantitative analysis of SF reflectance spectra measured in the UV-VIS wavelength range that provides information about the wavelength-dependent optical properties and enables quantitative extraction of tissue physiological and morphological parameters.

The aims of this study are to investigate the feasibility and identify the technical challenges associated with incorporating an SF spectroscopy device into the EUS-FNA procedure for lung cancer staging. A mathematical model is developed to analytically describe the SF reflectance spectra measured in lymph node tissue *in vivo*; work that requires characterization of the basis set of chromophores in lymph tissue. The model is applied to a set of clinical pilot data and used to extract physiological and morphological parameters from the SF reflectance spectra measured in normal and metastatic lymph nodes. This paper also presents the practical and technical challenges associated with the novel technique.

2 Methods

2.1 Clinical Study

Recently, we conducted a clinical pilot study to utilize the combined EUS-FNA with incorporated SF spectroscopy technique during a staging procedure for lung cancer, with data collected at the Erasmus Medical Center and Amphia hospitals (both located in the Netherlands). The experimental protocol was approved by the Institutional Review Board (IRB) at both locations. Data acquired from an initial patient enrolled within the study were used to develop a mathematical model for analysis of the lymph node spectra; in that case, multiple spectra were acquired from a single lymph node that was subsequently determined to contain metastatic cancer by cytology. The mathematical model was then applied to data acquired from 12 patients enrolled in the clinical pilot study, with multiple spectra recorded from seven normal nodes and eight nodes containing metastatic cancer as confirmed by cytology (throughout this paper lymph nodes containing metastatic cancer are referred to as metastatic lymph nodes). Each node was sampled with a new sterile SF reflectance probe. SF measurements were performed with the SF probe extended through the EUS-FNA needle and allowed to rest with no external pressure applied to the probe during spectral acquisition. Previously it has been shown that pressure exerted by a fiber optic probe on tissue during measurements can have effects on the tissue physiology.[12] This study considers the effects of probe pressure on the measured physiological param-
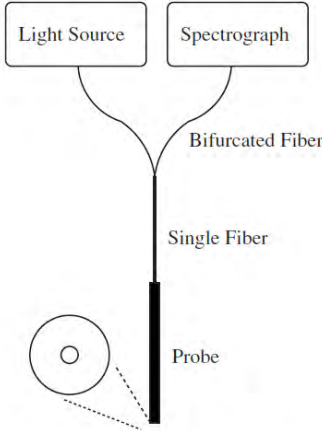
77

Fig. 2 Schematic of SF reflectance probe machinery.

eters by performing a subset of measurements on two lymph nodes while pressure was applied to the SF probe tip during measurement.

The experimental setup utilized here has been described in detail previously.[11] In brief, the setup utilized a single optical fiber (internal core diameter of 320 μm) connected to a bifurcated fiber with one arm leading from a halogen light source (HL-2000-FHSA; Ocean Optics; Duiven, the Netherlands) and the second arm leading to a spectrophotometer (SD 2000; Ocean Optics; Duiven, the Netherlands). Figure 2 shows a schematic of the fiber probe. Spectral reflections at the probe tip due to the refractive index mismatch between fiber and sample are minimized by polishing the SF probe tip at an angle of 15 deg. A calibration procedure was described previously[11] to account for other internal reflections, variability in lamp-specific output, and in fiber-specific transmission properties.

2.2 Mathematical Model of SF Reflectance Spectra

SF reflectance spectra ($\mathbf{R}_{SF}$) were analyzed using an analytical model to describe the wavelength-dependent optical properties, and in turn, extract physiological and morphological information (throughout this manuscript, terms shown in bold are wavelength dependent). Previously, a similar model was utilized[6–8] for analysis of other tissues (e.g., lung, breast, and oral mucosa), and is given as

$$\mathbf{R}_{SF} = \left[a_1 \left(\frac{\lambda}{\lambda_0} \right)^{a_2} + a_3 \left(\frac{\lambda}{\lambda_0} \right)^{-4} \right] e^{-\mu_a^{\text{tissue}} \langle \mathbf{L}_{SF} \rangle}. \quad (1)$$

Here, the term within the square brackets is the background scattering model that is a combination of Mie and Rayleigh scattering, given by wavelength-dependent power law functions with fitted parameters specifying the Mie amplitude (a_1), Mie slope (a_2), and Rayleigh amplitude[13] (a_3). Attenuation due to absorption within the tissue is modeled using the modified Beer-Lambert law and is a function of both the tis-

sue absorption coefficient (μ_a^{tissue}) and the SF photon path length ($\langle \mathbf{L}_{SF} \rangle$). The basis set of chromophores in lymph tissue is not well characterized, therefore, our initial model assumed that absorption was attributable to oxygenated and deoxygenated hemoglobin (HbO$_2$ and Hb, respectively) within the local microvasculature (μ_a^{vasc}), and is given in Ref. 6 as

$$\mu_a^{\text{tissue}} = \mu_a^{\text{vasc}} = \rho C_v [\text{StO}_2 \mu_a^{\text{HbO}_2} + (1 - \text{StO}_2) \mu_a^{\text{Hb}}]. \quad (2)$$

Here, ρ is the blood volume fraction, StO$_2$ is the microvascular hemoglobin oxygen saturation, C_v is a factor that accounts for the effect of discrete blood vessels on the absorption coefficient and enables estimation of the average vessel diameter d_v. Previously,[11] we showed that the photon path length is dependent on μ_a, the reduced scattering coefficient (μ_s'), and the fiber diameter (d_{fiber}), and is given as

$$\langle \mathbf{L}_{SF} \rangle = \frac{1.34 d_{\text{fiber}} \exp(0.17 d_{\text{fiber}})}{(\mu_s' d_{\text{fiber}})^{0.23} [0.52 + (\mu_a^{\text{tissue}} d_{\text{fiber}})^{0.52}]}. \quad (3)$$

This model structure requires specification of μ_s' at one wavelength, for which we choose $\mu_s'(800 \text{ nm}) = 1 \text{ mm}^{-1}$, and the background scattering model estimates the wavelength-dependent change in μ_s'; the effect of this assumption on model estimates is considered in Sec. 4.

Inspection of the data showed that absorption from an unknown chromophore was present within the SF reflectance spectra. Absorption from this unknown chromophore was accounted for by fitting absorption of an uncharacterized chromophore (μ_a^{unknown}) with a Gaussian curve; a procedure that was described previously.[13] This fitting technique estimated the wavelength of the absorption maximum for μ_a^{unknown}, which was similar to that of bilirubin as observed *in vivo*.[14] The observation of bilirubin in measurements of *in vivo* tissue is reasonable because it is an endogenous compound that is a heme breakdown product and is found bound to albumin in human serum. Absorption from albumin-bound bilirubin within the SF spectra was considered by incorporating the contribution of bilirubin into Eq. (2), as

$$\mu_a^{\text{tissue}} = \mu_a^{\text{vasc}} + \mu_{a,\text{spec}}^{\text{bil-al}} C_{\text{bil-al}}. \quad (4)$$

Incorporation of Eq. (4) into Eq. (1) allowed the model to estimate the albumin-bound bilirubin concentration ($C_{\text{bil-al}}$).

Model analysis of measured SF spectra yielded estimates of StO$_2$, ρ, d_v, $C_{\text{bil-al}}$, and Mie slope (a_2). The Mie amplitude (a_1) was not compared between measurements on different nodes because the value of a_1 was dependent on the specific distance between the probe and spectralon during calibration measurements, a factor that was not uniformly controlled for all probes used in this study. Parameter estimation was achieved using a Levenberg-Marquardt algorithm to minimize the chi-squared metric between measured reflectance data and model predictions, and confidence intervals on parameter estimates were calculated from the square root of the diagonal of the covariance matrix.[13] Statistical comparison of parameters estimated in normal and metastatic nodes was performed using a nonparametric Wilcoxon rank sum test, with significance determined by calculated p values. In this study, spectra

that showed evidence of a blood pool within the detection volume were identified as $\rho > 40\%$ and excluded from the comparative analysis.

2.3 Bilirubin-Specific Absorption Coefficient

Bilirubin, human serum albumin (HSA), and 99% dimethyl sulfoxide (DMSO) were obtained from Sigma-Aldrich (Zwijndrecht, The Netherlands). Phosphate-buffered saline (PBS) was purchased from Gibco-Invitrogen (DH Breda, the Netherlands). Two stock solutions of bilirubin (concentrations: 0.2 and 3 mM) were prepared by dissolving bilirubin in DMSO and the solutions were stored in the dark at 4 °C until use. Stock solution of HSA (concentration: 0.25 mM) was prepared in PBS (pH 7.4). The solutions of bilirubin-HSA complexes were prepared by mixing the stock solutions of bilirubin and HSA in PBS (pH=7.4). The final concentration of HSA in complexes was kept constant (1 μM) and the concentration of bilirubin was varied between 0.25 and 20 μM. Complexes containing bilirubin concentrations in the range 0.25 to 3 μM were prepared with the 0.2-mM bilirubin stock solution, while complexes containing bilirubin concentrations in the range 5 to 20 μM were prepared with the 3-mM bilirubin stock solution. The bilirubin-HSA complexes prepared in PBS had a maximum residual content of DMSO of 1.5%; this percentage is too low to have an effect on the complexes within solution. After preparation, the bilirubin-HSA complexes were stored in the dark in a water bath at 37 °C for 12 h to enable a complete equilibrium of the drug with the albumin. The bilirubin/HSA binding kinetics are known to be temperature dependent,[15] so the 37 °C temperature was chosen to mimic the biological conditions in vivo.

Absorption spectra were recorded using a quartz cuvette (1×1 cm) in an UV-VIS spectrophotometer (UV-2101 PC, Schimadzu Deutschland GmbH, Duisburg, Germany) in the wavelength range 240 to 800 nm with a slit width combination that resulted in a spectral resolution of 0.5 nm. A distinct shift of the absorption maximum of bilirubin to a longer wavelength position was observed when bound to HSA, compared with bilirubin free (unbound) in the PBS. Therefore, it was important to consider the amount of bound and unbound bilirubin within the solutions, a factor that depended on the bilirubin/HSA concentration ratio. No changes in the wavelength position of the absorption maximum were observed for solutions with bilirubin concentrations $\leqslant$1 μM, a concentration that corresponds to a bilirubin/HSA ratio of 1:1. For molar ratios of bilirubin/HSA higher than 1:1, a spectral shift to shorter wavelength was observed that indicates saturation of the HSA binding sites and presence of free, unbound bilirubin molecules within the solution. This procedure enabled the determination of the specific absorption coefficient of bilirubin bound to HSA ($\mu_{a,\text{spec}}^{\text{bil-al}}$).

3 Results

3.1 Mathematical Model of R_{SF} in Lymph Tissue In Vivo

Figure 3(A) shows a representative single fiber reflectance (R_{SF}) spectrum from the first (metastatic) lymph node sampled in the pilot study. We measured R_{SF} at a resolution of 3 pixels/nm, and the data were smoothed by averaging data
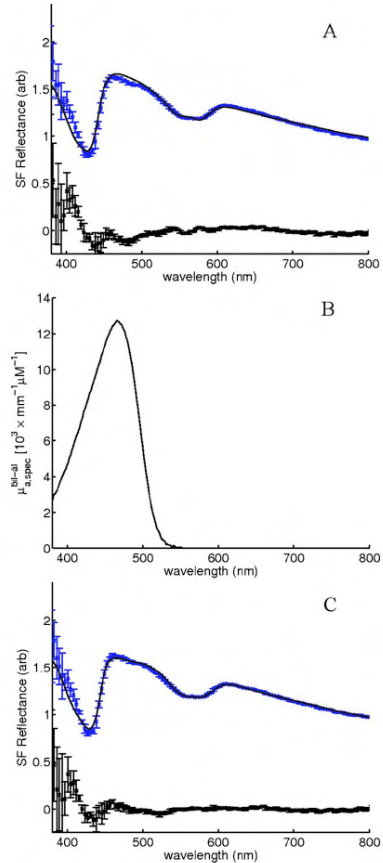
Fig. 3 SF reflectance model fit and 2× the residual with (A) absorption attributed to oxygenated and deoxyenated hemoglobin, (B) $\mu_{a,\text{spec}}^{\text{bil-al}}$ as measured in this study, and (C) model fit with bilirubin included in the basis set of chromophores.

points into bins of 10 pixels, which enabled the calculation of a standard deviation that represents noise within the signal.[11] The line through the data set shows the mathematical model of the spectra (with absorption attributable to oxygenated and deoxygenated hemoglobin) and the dashed line below shows 2× the residual error (=data—model predictions). This model provided estimates of StO_2 (30.3 $\pm$ 3.7%), ρ (1.5 $\pm$ 0.1%), d_v (29.0 $\pm$ 4.0 μm), and Mie slope (−1.159 $\pm$ 0.041). The Rayleigh amplitude estimate approached zero, indicating that this spectrum could be described by only Mie scattering (a finding that was confirmed in measurements on subsequent nodes). Although the fit in Fig. 3(A) seems reasonable, a detailed inspection of the residual error shows deviation between the model fit and the data in the 400- to 500-nm wavelength

79

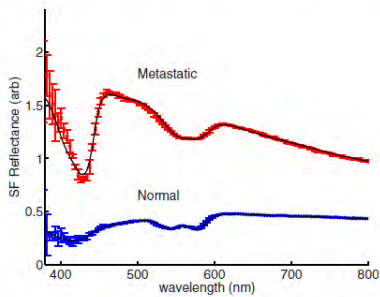**Fig. 4** Representative SF spectra and model fits from measurements on normal and metastatic lymph nodes, as confirmed by cytological examination.

Table 1 Mean physiological and morphological parameters extracted from SF reflectance measurements of normal and metastatic lymph nodes *in vivo*.

Parameter	Normal (7 nodes)	Metastatic (8 nodes)
Hemoglobin saturation (%)	83.9 ± 10.0	46.8 ± 24.9^a
Blood volume fraction (%)	13.5 ± 7.6	3.2 ± 2.6^a
Average vessel diameter (μm)	13.9 ± 10.9	8.9 ± 5.0
Bilirubin (μM)	23.2 ± 12.4	10.2 ± 5.5
Mie slope	-0.71 ± 0.34	-1.13 ± 0.38

^{a}Indicates significant differences with $p < 0.01$ for the Kruskal Wallis test.

range. Deviation in the 400- to 450-nm range is attributable to the Soret band of hemoglobin, an issue that was described in detail previously.[16] Deviations in the 450- to 500-nm range are attributed to improper specification of the basis set of chromophores, an issue that can have a profound effect on the estimated parameters.[13] Therefore, we followed a systematic procedure to account for the absorption of an uncharacterized chromophore ($\mu_a^{unknown}$) with a Gaussian curve. Inclusion of the Gaussian resulted in a model fit that no longer showed the distinct deviation in the 450- to 500-nm wavelength range (data not shown). Interestingly, the Gaussian predicted an absorption maximum at 470 nm, an observation that suggested bilirubin as the potential unknown absorber.

Figure 3(B) shows the specific absorption coefficient of albumin-bound bilirubin as measured in this study (with an absorption maximum of 0.0127 mm^{-1} μM^{-1} at 466 nm). The $\mathbf{R}_{SF}$ model was reconfigured with bilirubin added as a chromophore contributing to the total tissue absorption coefficient; model predictions are shown in Fig. 3(C). The resulting model fit showed excellent agreement with the data and reduced the mean residual error between model and data by 64%. The model with bilirubin added to the chromophore set provides an estimate of C_{bil-al} (15.2 ± 2.0 μM) as well as different parameter estimates for StO$_2$ ($11.8 \pm 1.8\%$), ρ ($1.9 \pm 0.1\%$), and d_v (50.1 ± 4.1 μm) compared with estimates from the model fit without bilirubin; other parameters did not change by more than 10%. These observations suggest that bilirubin contributes meaningfully to the total absorption detected within the lymph node *in vivo*, and that incorporation of bilirubin into the basis set of chromophores influences the estimated values of the other model parameters. As a result, bilirubin concentration was added to the set of physiological parameters extracted from the SF measurements in lymph tissue.

3.2 Model Analysis of Clinical Pilot Data

Figure 4 shows representative $\mathbf{R}_{SF}$ spectra from both normal and metastatic lymph nodes, and the line through each data set shows the mathematical model for each respective spectrum. These spectra show differences that are attributable to the differences in tissue composition and morphology. Parameters estimated by the fitted mathematical model indicated

major differences between these two representative spectra in StO$_2$ (85.9 ± 2.3 versus $11.9 \pm 1.8\%$), ρ ($7.6 \pm 0.2\%$ versus $2.0 \pm 0.1\%$), and d_v (20.8 ± 17.0 versus 50.0 ± 4.1 μm) for the normal and metastatic nodes, respectively. Data for all nodes measured in the clinical pilot study are shown in Table 1, which displays the mean values for each of the five parameter factors for all spectra measured in both normal and metastatic nodes. Significant differences between normal and metastatic nodes were found in StO$_2$ and ρ (with p values of <0.01). Differences in the mean values of d_v, C_{bil-al}, and Mie slope were not significant. These results indicate that physiological differences between normal and metastatic nodes could be detected by the SF reflectance measurement.

3.3 Effect of SF Probe on Lymph Node Environment

To observe the effect that manipulation of the SF probe has on the lymph node environment, we performed rapid measurements over a time frame with pressure applied to the probe, maintained for a time interval, and then released. Figure 5 shows temporal profiles of StO$_2$ and ρ as measured in one normal [Fig. 5(A)] and one metastatic [Fig. 5(B)] lymph node. The x axis of each plot provides the time with respect to the onset of the application of pressure. The data for time <0 s show measurements with the probe placed into the lymph node, but no additional pressure being applied. Horizontal dashed lines indicate the onset of pressure (at time=0 s) and the subsequent release of pressure at 26 s in Fig. 5(A) and at 22 s in Fig. 5(B). The data in both plots show decreases in both StO$_2$ and ρ as pressure is applied to the probe and maintained; this temporal functionality was also observed for d_v (data not shown). These observations showed a distinct effect of pressure on physiology, and are attributed to the pressure compressing the tissue surrounding the probe tip, which impairs blood flow to the local vasculature. Pressure-induced changes to morphology (scattering) were not considered to be substantial ($<20\%$), and showed no temporal functionality. The data in the plot in Fig. 5(B) also show dramatic increases in the volume of blood sampled by the probe after the release of probe pressure; an observation that indicates the onset of bleeding and formation of a blood pool. These results indicate that the pressure exerted by the SF probe can have major effects on the physiological environment of the lymph node being sampled.
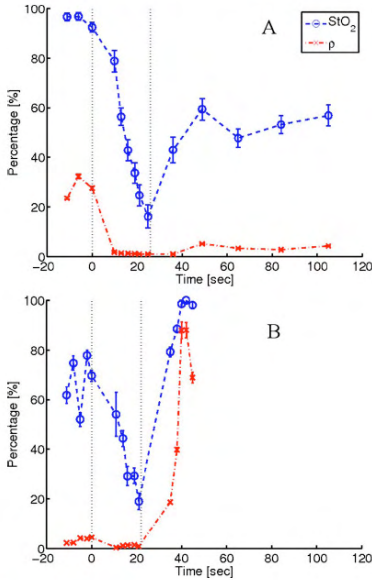
Fig. 5 Effect of single fiber probe pressure on physiological environment, with changes observed in hemoglobin saturation and blood volume fraction over time for one (A) normal and one (B) metastatic lymph node. The x axis shows time with respect to the onset of pressure by the probe on the lymph tissue. Horizontal dashed lines indicate the onset and release of pressure.

4 Discussion

This study shows the feasibility and presents the technical aspects of incorporating an SF reflectance spectroscopy device into the EUS-FNA technique for lung cancer staging *in vivo*. Preliminary clinical data are used to develop an analytical model of R_{SF} measured in lymph tissue *in vivo*. A systematic mathematical methodology is used to characterize the basis set of chromophores in lymph tissue using a Gaussian curve.[13] The estimated absorption maximum for the Gaussian was similar to that of bilirubin as observed *in vivo*.[14] However, previous studies have utilized a specific absorption coefficient of bilirubin as measured in chloroform for analysis of *in vivo* spectra,[17] a problem because the absorption maximum of bilirubin in chloroform is[18] at ≈ 453 nm, while bilirubin bound to serum albumin shows an absorption maximum at ≈ 466 nm. Our attempts to utilize the specific absorption coefficient of bilirubin as measured in chloroform yielded poor model fits that showed observable features within the residual (data not shown). It is well-known that the specific absorption coefficient of a compound depends on the surrounding matrix; this motivated measurement of bilirubin absorption in an environment that mimics the *in vivo* situation, i.e., in the presence of albumin. Incorporation of the albumin-bound bilirubin spectra into the model resulted in a high-quality fit, with a large reduction in the mean error about the model and with an

observable improvement in the residual plot. Physiological parameter estimates were also affected by the inclusion of bilirubin in the model. Specifically, we observed changes in StO_2 (30.3 versus 11.8%), ρ (1.5 versus 1.9%), and d_v (29.0 versus 50.1 μm), as calculated by the model without and with bilirubin incorporated, respectively. These results highlight the impact that improper specification of the *in vivo* chromophore set can have on estimates of model parameters.[13] While this study does not obtain independent confirmation of the presence of bilirubin within the sampled lymph nodes, the data strongly suggest that bilirubin is an important source of absorption within lymph tissue *in vivo*. Definitive confirmation of these results would require analysis of the bilirubin content within the tissue extracted during the EUS-FNA procedure; while this is beyond the scope of the current study, it could be incorporated into a future protocol.

Analysis of R_{SF} spectra measured in this clinical pilot study were capable of detecting differences in the physiology between normal and metastatic lymph nodes. The data shown in Table 1 indicate that metastatic nodes presented lower StO_2 and lower ρ than normal nodes. Previous studies that investigated the vascular supply of metastatic lymph nodes reported the presence of aberrant vessels, displacement of vessels, and avascular areas, with the primary source of perfusion from the peripheral vasculature.[19,20] In advanced stages of metastatic lymph nodes, the regular vascular network throughout the center of the lymph node may be destroyed or displaced due to the tumor cells, a problem that can be exacerbated by central necrosis or keratinization within the node.[21] These observations are consistent with the description of a compromised vascular network that provides an explanation of the decreases in StO_2 and ρ observed in metastatic lymph nodes compared with normal nodes within the current study. Interestingly, studies of the physiological environment of tumors in the breast, lung, and oral cavity[6–8] show reduced StO_2 and increased ρ compared with normal functioning tissue in each case. The difference in changes to ρ between normal and tumor tissue and normal and metastatic lymph nodes can be described by the difference in the respective local environments. Solid tumors have an increased ρ compared with normal tissue because the tumor cells up-regulate angiogenesis, increasing blood supply to meet the needs of highly proliferating cells.[22] In metastatic lymph nodes, neoplastic cells infiltrate the node from outside and are usually located in the peripheral areas; therefore, when the metastatic site(s) up-regulate angiogenesis, the effect is not uniform throughout the node and results in increased peripheral vascularization.[21] The subsequent proliferation of the metastatic site(s) in the peripheral areas of the node exacts a mechanical pressure to the center of the node, compressing blood vessels and increasing the resistance to blood flow,[23] factors that result in a reduction in ρ (and StO_2) within the node.

It is important to put the results associated with the comparison of the physiology between normal and metastatic lymph nodes into the proper clinical context. The EUS-FNA is utilized in lung cancer staging to provide definitive confirmation about the presence of metastatic cancer within lymph nodes that appear enlarged on a CT scan. The current study compares the tissue parameters of normal (not enlarged) lymph nodes with metastatic (enlarged) lymph nodes; how-

ever, it is the discrimination between benign nodes that are enlarged due to infection or nonmalignant disease and nodes enlarged due to presence of metastatic regions that is the clinically relevant question. Previously, it has been reported that lymph nodes enlarged due to immune response present vessel dilation and hypervascularity, with a relationship between perfusion and volume of the enlarged nodes.[24] These observations suggest that differences in the vascular networks between benign enlarged and metastatic lymph nodes may translate into differences in physiology that are detectable by the SF reflectance measurement. However, this hypothesis has yet to be tested experimentally and will be addressed by a future study.

The authors anticipate the need to address some specific technical challenges prior to widespread clinical acceptance of the combined EUS-FNA and SF spectroscopy technique. One such concern is the lack of a relationship between the SF reflectance intensity and μ_s'. The spectral analysis algorithm presented in this paper requires an assumption of μ_s' at a single wavelength [we chose $\mu_s'(800 \text{ nm}) = 1 \text{ mm}^{-1}$] and the wavelength-dependent changes in scattering across the spectra are described by a background scattering model. The error introduced to parameter estimates due to this assumption was quantified by varying the assumed $\mu_s'(800 \text{ nm})$ across a wide range that is representative of biological tissue ($0.5-2.0 \text{ mm}^{-1}$), with resulting changes to the estimates of ρ, StO_2, d_v, and Mie slope of 20%, <1%, 14%, and <1%, respectively. While these results indicate the error is small, it is desirable to not require the assumption within the model, so we are currently developing a stable optical phantom that can be used to calibrate a measured SF reflectance intensity to a value of μ_s'.

Another technical challenge is avoiding the perturbation of the lymph tissue *in vivo* environment with the optical probe during sampling. The sampling strategy described in Fig. 1 involves manipulation of the SF probe throughout the lymph node being sampled in an attempt to characterize a larger volume of the node than is achieved by the current procedure. Manipulation of the probe to different locations within the node requires the application of pressure to the probe tip. However, the data in Fig. 5 indicate that the application of pressure can compress the surrounding tissue and induce major changes in the tissue physiology; specifically to the microvasculature. This is problematic because pressure applied to a normal node can result in reduced ρ and StO_2, factors that were associated with metastatic nodes; this phenomenon is displayed in Fig. 5(A). Moreover, the pressure effects do not introduce any unique characteristics into the measured spectra, making it difficult to develop a system to provide online identification and correction. Note that pressure-induced changes in scattering were not substantial and showed no time dependence. Another concern associated with probe manipulation is tissue damage that results in bleeding. This can lead to the optical detection of a blood pool instead of native tissue, as observed in Fig. 5(B). However, this is not expected to be a serious problem for the technique, because the presence of blood pools can be identified by establishing a threshold blood volume fraction (as was performed in this study). In this study, the authors utilized a sampling strategy that is expected to minimize the effect of pressure on the

measurements with spectra acquired in the following manner: the EUS-FNA probe was inserted into the node, the SF probe extended and was allowed to rest with no external pressure being applied during the SF measurement. Therefore, while we have confidence that these pressure effects did not influence the data set presented in Table 1, the implementation of the sampling strategy outlined in Fig. 1 may prove to be infeasible.

In conclusion, this paper showed the successful incorporation of the EUS-FNA with incorporated SF reflectance spectroscopy as demonstrated in the clinical theater. A mathematical model was developed to extract physiological and morphological parameters from the SF reflectance spectra measured in lymph nodes *in vivo*; analysis included incorporation of albumin-bound bilirubin into the basis set of chromophores. Model analysis was performed on spectra measured in a clinical pilot study and results indicate that the SF measurement is sensitive to differences in tissue physiology between normal and metastatic lymph nodes. Moreover, clinical observations show that probe pressure can have major effects on the physiological environment of the lymph node; effects that must carefully be considered when developing a sampling strategy. The data presented in this study show the feasibility of this novel technique, however, the clinical utility of this technology will be based on the ability to assist in the classification of enlarged lymph nodes as either benign or metastatic; a question that will be investigated in future studies.

References

1. U.S. Cancer Statistics Working Group, Department of Health and Human Services, Centers for Disease Control and Prevention, and National Cancer Institute (2007).
2. F. C. Detterbeck, M. M. DeCamp Jr., L. J. Kohman, and G. A. Silvestri, "Invasive staging: the guidelines," *Chest* 123, 167S–175 (2003).
3. G. Caddy, M. Conron, G. Wright, P. Desmond, D. Hart, and R. Y. Chen, "The accuracy of EUS-FNA in assessing mediastinal lymphadenopathy and staging patients with NSCLC," *Eur. Respir. J.* 25, 410–415 (2005).
4. M. A. Eloubeidi, A. Tamhane, V. K. Chen, and R. J. Cerfolio, "Endoscopic ultrasound-guided fine needle aspiration of mediastinal lymph node in patients with suspected lung cancer after positron emission tomography and computed tomography scans," *Ann. Thorac. Surg.* 80, 1231–1239 (2005).
5. D. T. Delpy and M. Cope, "Quantification in tissue near-infrared spectroscopy," *Philos. Trans. R. Soc. London, Ser. B* 352, 649–659 (1997).
6. R. L. P. van Veen, A. Amelink, M. Menke-Pluymers, C. van der Pol, and H. J. C. M. Sterenborg, "Optical biopsy of breast tissue using differential path-length spectroscopy," *Phys. Med. Biol.* 50, 2573–2581 (2005).
7. M. P. L. Bard, A. Amelink, V. Noordhoek Hegt, W. J. Graveland, H. J. C. M. Sterenborg, H. C. Hoogsteden, and J. G. J. V. Aerts, "Measurement of hypoxia-related parameters in bronchial mucosa by use of optical spectroscopy," *Am. J. Respir. Crit. Care Med.* 171, 1178–1184 (2005).
8. A. Amelink, O. P. Kaspers, H. J. C. M. Sterenborg, J. E. vander Wal, J. L. N. Roodenburg, and M. J. H. Witjes, "Non-invasive measure-

ment of the morphology and physiology of oral mucosa by use of optical spectroscopy," *Oral Oncol.* **44**, 65–71 (2008).

9. T. P. Moffit and S. A. Prahl, "In-vivo sized-fiber spectroscopy," *Proc. SPIE* **3917**, 225–231 (2000).

10. M. Canpolat and J. R. Mourant, "Particle size analysis of turbid media with a single optical fiber in contact with the medium to deliver and detect white light," *Appl. Opt.* **40**, 3792–3799 (2001).

11. S. C. Kanick, H. J. C. M. Sterenborg, and A. Amelink, "Empirical model of the photon path length for a single fiber reflectance spectroscopy device," *Opt. Express* **17**, 860–871 (2009).

12. R. Reif, M. S. Amorosino, K. W. Calabro, O. A'Amar, S. K. Singh, and I. J. Bigio, "Analysis of changes in reflectance measurements on biological tissues subjected to different probe pressures," *J. Biomed. Opt.* **13**, 010502 (2008).

13. A. Amelink, D. J. Robinson, and H. J. C. M. Sterenborg, "Confidence intervals on fit parameters derived from optical reflectance spectroscopy measurements," *J. Biomed. Opt.* **13**, 054044 (2008).

14. S. L. Jacques, I. Saidi, A. Ladner, and D. Oelberg, "Developing an optical fiber reflectance spectrometer to monitor bilirubinemia in neonates," *Proc. SPIE* **2975**, 115–127 (1997).

15. R. Brodersen, "Bilirubin. Solubility and interaction with albumin and phospholipid," *J. Biol. Chem.* **254**(7), 2364–2369 (1979).

16. A. Amelink, T. Christiaanse, and H. J. C. M. Sterenborg, "Effect of hemoglobin extinction spectra on optical spectroscopic measurements

17. of blood oxygen saturation," *Opt. Lett.* **34**, 1525–1527 (2009).

17. L. Lyngsnes Randeberg, E. Bruzell Roll, L. T. Norvang Nilsen, T. Christensen, and L. O. Svaasand, "*In vivo* spectroscopy of jaundiced newborn skin reveals more than a bilirubin index," *Acta Paediatr.* **94**, 65–71 (2005).

18. H. Du, R. A. Fuh, J. Li, A. Corkan, and J. S. Lindsey, "Photochem-CAD: a computer-aided design and research tool in photochemistry," *Photochem. Photobiol.* **68**, 141–142 (1998).

19. A. Tschammler, H. Wirkner, G. Ott, and D. Hahn, "Vascular patterns in reactive and malignant lymphadenopathy," *Eur. Radiol.* **6**, 473–480 (1996).

20. T. Chikui, K. Yuasa, S. Maemura, and S. Kanda, "Change of angio-structure and hemodynamics in lymph node metastases in rabbits," *Oral Surg. Oral Med. Oral Pathol. Oral Radiol. Endod.* **93**, 350–357 (2002).

21. M. Ying and A. T. Ahuja, "Ultrasound of neck lymph nodes: how to do it and how do they look?" *Radiology* **12**, 105–117 (2006).

22. R. K. Jain, "Determinants of tumor blood flow: a review," *Cancer Res.* **48**, 2641–2658 (1988).

23. A. T. Ahuja and M. Ying, "Sonographic evaluation of cervical lymph nodes," *AJR, Am. J. Roentgenol.* **184**, 1691–1699 (2005).

24. P. G. Herman, D. Lyonnet, R. Fingerhut, and R. N. Tuttle, "Regional blood flow to the lymph node during the immune response," *Lymphology* **9**, 101–104 (1976).
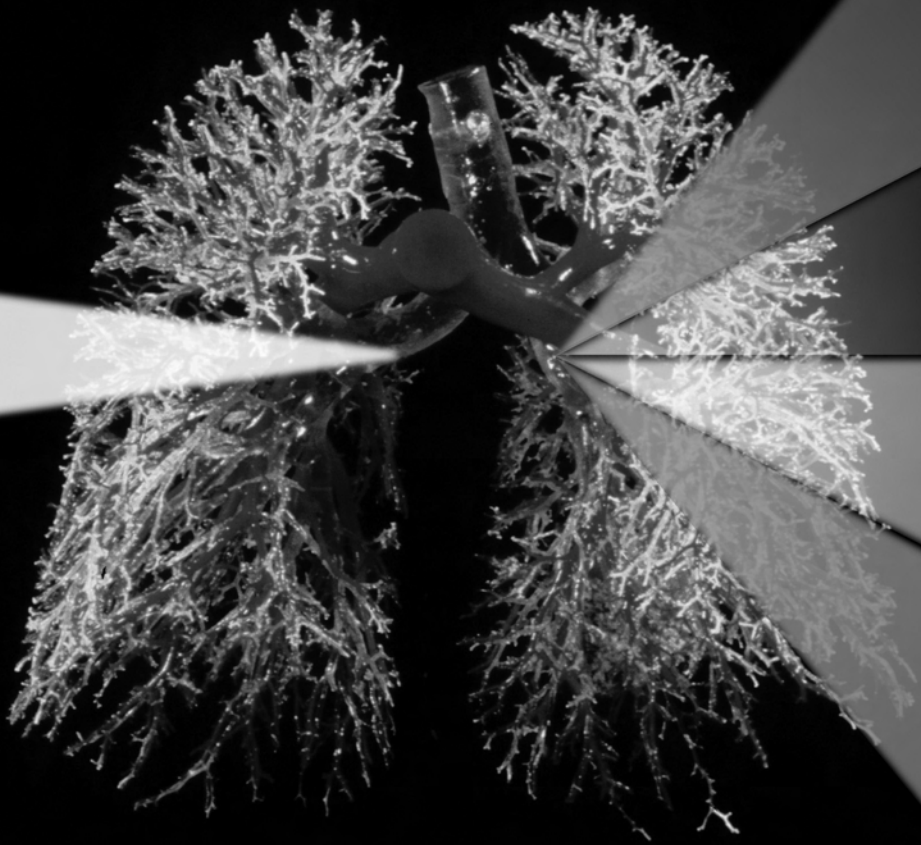
Characterization of mediastinal lymph node physiology in vivo by optical spectroscopy during endoscopic ultrasound-guided fine-needle aspiration

C. van der Leest[1,2]

S.C. Kanick[3]

R.S. Djamin[1]

A.M. Janssens[1]

H.C. Hoogsteden[2]

H.J.C.M. Sterenborg[3]

A. Amelink[3]

J.G.J.V. Aerts[1,2]

1 Department of Pulmonary Diseases, Amphia Hospital, Breda, The Netherlands

2 Department of Pulmonary Diseases, Erasmus MC, Rotterdam, The Netherlands

3 Center for Optical Diagnostics and Therapy, Department of Radiation Oncology, Erasmus MC, Rotterdam, The Netherlands

Abstract

Introduction: Esophageal endoscopic ultrasound guided fine needle aspiration (EUS-FNA) is a minimally-invasive staging procedure for mediastinal lymph nodes in patients diagnosed with lung cancer. But, a substantial false negative rate necessitates that patients returning a negative EUS-FNA result must undergo a subsequent surgical staging procedure. This study incorporates a fiberoptic reflectance spectroscopy device into the EUS-FNA procedure to asses the vascular physiology within the sampled lymph node. The aim of this pilot study was to determine the feasibility of incorporating a reflectance spectroscopy device into the EUS-FNA clinical procedure and to gather preliminary information about the vascular physiology within the center of normal and metastatic lymph nodes.
Methods: This study included 10 patients with proven or suspected lung cancer and an indication for EUS-FNA. The procedure was performed on seven normal (unenlarged, positron emission tomography negative) nodes and seven suspicious (enlarged, positron emission tomography positive), with the malignant status of all nodes cytologically confirmed. Reflectance spectra were acquired using a single optical fiber that fits through the end of the EUS-FNA biopsy needle, with an outer fiber diameter of 0.38 mm.
Results: The procedure was successfully performed and did not introduce complications. Model-based analysis of single fiber reflectance spectra provided quantitative information about the vascular physiology within the sampled lymph node. We observed that metastatic lymph nodes were characterized by lower microvascular oxygen saturation (50% versus 84%, $p<0.01$) and lower blood volume fraction (5.6% versus 13.5%, $p<0.01$) than normal nodes.
Conclusions: Single fiber reflectance spectroscopy has the potential to detect abnormal lymph node physiology.

Introduction

For patients diagnosed with lung cancer, treatment options are dependent on the presence of metastatic cancer in the mediastinal lymph nodes [1]. In the absence of clearly identifiable distant metastases, imaging modalities such as Computer Tomography (CT) and Positron Emission Tomography (PET) are used to identify suspicious nodes (based on size and metabolic activity); however, the sensitivity and specificity of these techniques are not sufficient to properly diagnose the presence of metastatic cancer, and tissue acquisition from an enlarged lymph node is needed for definitive confirmation [2-3]. The gold standard procedure for mediastinal staging is an invasive surgical biopsy of the lymph node, termed mediastinoscopy [4,5]. An alternative staging approach uses endoscopic ultrasound techniques, that are introduced through the esophagus or through the bronchial tree [6]. These techniques provide echo visualization of lymph nodes and allow incorporation of fine-needle aspirations (FNA) for minimally-invasive tissue acquisition. For staging of mediastinal lymph nodes, the EUS-FNA (endocopic ultrasound-guided FNA) procedure is considered less-invasive, less-expensive, and less-likely to introduce complications than surgical staging procedures [6-12]. However, EUS-FNA has a large false negative (FN) rate (~17-22 %) compared with mediastinoscopy [4,5,7-12]; a substantial limitation that is attributed to localized malignant areas within the node that were not sampled during EUS-FNA tissue acquisition. The EUS-FNA FN rate is not reduced substantially by increasing the number of aspirations from the current standard (reasonable accuracy is obtained after approximately 3 [13]), and the inclusion of on-site cytopathology may not improve sensitivity [9] but also introduces additional practical and economic considerations. Because of the substantial EUS-FNA FN rate, the clinical guidelines recommend that patients receiving a negative cytology result from EUS-FNA biopsy of suspicious nodes must undergo a subsequent surgical staging procedure for definitive confirmation of the diagnosis [4,5]: a procedure that is (retrospectively) unnecessary in approximately 77-81% of patients, because the negative EUS-FNA result was indeed correct. Hypothetically, a method that provided additional, complementary information about the malignant status of lymph nodes could improve EUS-FNA FN rate, reducing unnecessary spending of resources and avoiding unnecessary delay before the onset of treatment administration.

Previous studies investigating the physiology of lymph node metastases have observed systematic effects of the metastatic sites on the vasculature within the node [14-18]. These studies observed the presence of aberrant vessels, displacement of vessels, and avascular areas in the center of the node, with the primary source of perfusion from the peripheral vasculature. Such observations indicate a compromised vascular network within the center of the node, changes that would affect local tissue blood content and blood oxygen saturation. These physiological changes provide a hypothetical basis to differentiate between normal and metastatic lymph nodes; specifically, these physiological aspects (microvascular saturation and blood content) can be measured by fiber-optic reflectance spectroscopy. This pilot study aims to incorporate a fiber-optic measurement technique into the EUS-FNA procedure that would return unique quantitative information about node vascular physiology, information that would be complementary to the cytological observations, and potentially improve the EUS-FNA FN rate.

Reflectance spectroscopy in the visible-near infrared wavelength region provides information about the wavelength dependent optical properties that allow estimation of tissue physiological parameters [19]. The dominant absorption bands of hemoglobin in the visible wavelength region allow both the blood content and hemoglobin saturation to be estimated from the reflectance measurement. Previously, our group developed differential path length spectroscopy (DPS) to quantitatively determine tissue physiological characteristics [20]. DPS utilizes a unique probe geometry that provides knowledge of the photon path length [21] and allows accurate description of optical properties in small volumes of tissue; the accuracy of this technique has been extensively validated [22] and clinically investigated [23-27]. However, DPS probes include multiple optical fibers and are too large to be incorporated into the biopsy needle at the end of the EUS-FNA catheter (which has an internal diameter of ~0.45 mm). This clinical application requires the use of a fiber optic probe with an outer fiber diameter (<0.4 mm) that could be incorporated into the narrow channel of the EUS-FNA device. Our group has addressed this problem by developing a novel quantitative analysis technique for reflectance spectra measured by a probe that uses a single optical fiber to deliver and collect light during the measurement [28-29]; these studies presented a mathematical model of the single fiber (SF) photon path length that is accurate over a wide range of optical properties and allows quantitative analysis of SF reflectance spectra. Recently [30], we described the detailed technical aspects associated with incorporating SF reflectance probes into the EUS-FNA procedure for mediastinal lymph node staging: aspects that included the characterization of the chromophores (absorbing compounds) present within lymph node tissue, the development of a mathematical model of SF reflectance spectra measured within the lymph node *in vivo*, and a detailed analysis of the effects of probe pressure on the measured spectra. In this work we describe the clinical aspects of a pilot study that incorporated SF reflectance spectroscopy into EUS-FNA staging of mediastinal lymph nodes and present a novel optical sampling strategy that addresses the sampling error associated with the current EUS-FNA biopsy technique. The specific aims of this pilot study are to show the feasibility of conducting the technique in a clinical setting and to gather preliminary information about the vascular physiology within the center of normal (non-suspicious) and metastatic (suspicious) lymph nodes in patients undergoing EUS-FNA.

Methods
Subjects
The Medical Ethics Committee of the Erasmus Medical Centre (Rotterdam, The Netherlands) approved this observational study. Patients were recruited from the Erasmus Medical Centre and from the Amphia Hospital (Breda, The Netherlands) between December 2008 and April 2009. Patients who had an indication for an EUS-FNA procedure (i.e. presented enlarged lymph nodes on CT scan, or positive lymph nodes on a PET scan, or had a primary tumor or had an enlarged left adrenal gland that was reachable by EUS-FNA) were asked to participate. According to published guidelines for mediastinal staging [4,5], all reachable nodes were sampled with FNA to optimally stage the mediastinum; not all FNA sampled lymph nodes were measured by reflectance spectroscopy. Written informed consent to perform the procedure was obtained from all patients before inclusion.

Classification of Lymph Nodes
In this study both unenlarged non-suspicious (normal) lymph nodes and enlarged suspicious lymph nodes containing metastatic cancer were included (throughout this article lymph nodes containing metastatic cancer are referred to as metastatic). Suspicious lymph nodes were defined as visible on CT-scan with a short-axis diameter of more than 10 mm and were PET positive.
Non-suspicious (normal) lymph nodes were defined as PET negative with a short-axis diameter of less than 10 mm. This pilot study included only nodes with a very defined clinical suspicion for a diagnosis and, therefore, excluded PET negative lymph nodes with short-axis diameter of more than 10 mm. The classification of each node was confirmed by cytology. Normal nodes were observed during minimal 6-month follow-up examinations (except in one who underwent surgical staging) to confirm no suspicious enlargement of the node had occurred.

Single Fiber Reflectance Device
SF reflectance spectra were measured using a custom-made instrument shown in Figure 1. The SF probe contained a single optical fiber for both light delivery and light collection and was small enough (outer diameter of 0.38 mm) to be fed through the biopsy needle channel of the EUS-FNA. The proximal end of the SF probe connects to a bifurcated fiber, with one arm leading to a tungsten-halogen lamp (HL-2000-FHSA; Ocean Optics; Duiven, The Netherlands) and the other arm leading to a spectrophotometer (SD 2000; Ocean Optics). The distal end of the SF probe, which is in contact with the tissue during measurement, is polished at an angle of 15 degree to minimize the collection of specular reflection that is caused by refractive index mismatch between the fiber and tissue. During measurement, light in the visible near infrared wavelength range (400-900 nm) travels from the lamp to the SF probe tip, exits the fiber and scatters throughout the tissue. Light that is remitted from the tissue and is collected by the fiber returns a wavelength-dependent reflectance intensity (R_{SF}). A calibration procedure was described previously [28] to account for internal reflections and for variability in lamp-specific output and in fiber-specific transmission characteristics.

Examination procedure
EUS-FNA procedures were performed in an outpatient setting with monitoring of heart rate and oxygen saturation. Lidocain gel was orally administered (10 mL) before the EUS-FNA procedure to provide local throat and esophageal anesthesia. The patient was oriented into left lateral decubitus and midazolam was intravenously administered (2.5-5.0 mg) for mild sedation before introduction of the endoscope (Olympus GF-UCT160-OL5). On placement of the endoscope within the esophagus in proximity to the targeted lymph node, a sterile single-use needle (Cook Echo-1-22) was introduced through the esophagus and into the lymph node using echo guidance. After needle placement, the guide wire was removed from the needle channel, and a sterilized single-use SF probe was introduced into the FNA channel. The fiber optic probe was extended approximately 3 mm through the EUS-FNA needle into the center of the lymph node and allowed to rest with no external pressure applied to the probe during spectral acquisition. Manipulation of the probe to different locations within the node during measurement can exert pressure-induced changes to the endogenous physiology within the node [30]; a confounding factor that is avoided using the current sampling strategy of a limited

number of SF measurement sites near the center of the node. Multiple spectral acquisitions were performed with a specified minimum of 3 measurements and additional measurements obtained based on the judgment of the clinician conducting the procedure (range: 3-11, average 7). After reflectance measurements, the fiber optic probe was removed and the routine FNA performed to obtain cytologic aspirations. In this study, 1 to 2 lymph nodes per patient were measured with SF reflectance spectroscopy during each EUS-FNA procedure; a new FNA needle and a new fiber optic probe were used for each node sampled to avoid blood and tissue contamination between nodes. On average, each EUS-FNA procedure lasted 30 minutes. After the procedure, patients were observed for 1 hour and then visited by the endoscopist to reveal any side-effects. Three days after the procedure, all patients were returned for an outpatient visit to receive test results and to reveal any further side-effects.

Mathematical Analysis of Spectra
SF reflectance spectra (R_{SF}) were analyzed using a previously developed [27] mathematical model that describes the wavelength-dependent effects of scattering and absorption on the reflectance intensity collected by the SF device in lymph node tissue. The model is given as:

$$R_{SF} = \left[a_1 \left(\frac{\lambda}{\lambda_0} \right)^{a_2} \right] e^{-\mu_a^{tissue} \langle L_{SF} \rangle}$$

(1)

Here, the term in square brackets is a background scattering model that follows Mie theory dependence, with fitted parameters describing the Mie amplitude (*a*1) and Mie slope (*a*2); Rayleigh scattering was shown to not contribute to R_{SF} measured in lymph node tissue [30].
The model describes attenuation because of absorption through the modified Beer-Lambert law that includes the product of the absorption coefficient within the lymph node tissue (μ_a^{tissue}) and the SF photon path length ($\langle L_{SF} \rangle$). Our previous study [30], described the basis set of chromophores within lymph tissue as oxygenated and deoxygenated hemoglobin (HbO$_2$ and Hb, respectively) and albumin-bound bilirubin. The summed contribution of each of these components to μ_a^{tissue} is given as follows

$$\mu_a^{tissue} = \left[\rho C_v \left(StO_2 \mu_a^{HbO2} + (1 - StO_2) \mu_a^{Hb} \right) \right] + \mu_a^{bilirubin} C_{bilirubin}$$

(2)

Here ρ is the blood volume fraction, StO$_2$ is the microvascular saturation, μ_a^{HbO2} is the specific absorption coefficient of oxygenated hemoglobin, μ_a^{Hb} is the specific absorption coefficient of deoxygenated hemoglobin, and $\mu_a^{bilirubin}$ and $C_{bilirubin}$ are the specific absorption coefficient and concentration of albumin-bound bilirubin, respectively. Within tissue, whole blood (and in turn Hb and HbO$_2$) is located within the vasculature. This heterogeneous distribution affects the spectral shape

of the absorption detected by reflectance spectroscopy: an effect that is characterized by the C_v term [31], which is given as, $C_v = \{1 - \exp(\mu_a^{blood} D_v)\}/\{\mu_a^{blood} D_v\}$, and includes an estimate of the average vessel diameter (D_v). Application of the Beer-Lambert law in Equation (1) requires knowledge of $\langle L_{SF} \rangle$, a factor that is complicated by the dependence of the collected photon paths on both the absorption and scattering properties within the optically sampled tissue volume. Recently [28,29], our group developed an empirical model that accurately describes $\langle L_{SF} \rangle$ in terms of the SF diameter (d_{fiber}), reduced scattering coefficient (μ_s'), and absorption coefficient (μ_a'), and is given as follows

$$\langle L_{SF} \rangle = \frac{1.54 d_{fiber}}{\left(d_{fiber} \mu_s'\right)^{0.18} \left(0.61 + .d_{fiber} \mu_a\right)^{0.61}}$$

(3)

Fitting the measured R_{SF} data with the model given in Equation (1) yielded estimates for the microvascular saturation (StO$_2$), blood volume fraction (ρ), average vessel diameter (D_v), bilirubin concentration (C_{bil}), and Mie slope (a_2); the scattering amplitude (a_1) did not provide unique information because of differences in calibration procedure between probes [30].

Statistical Analysis
The difference of SF-estimated physiological parameters between normal and metastatic lymph nodes was evaluated with a Kruskal-Wallis test. This non-parametric test was selected because of the small number of data points. The values of *P* less then 0.05 were regarded as significant. Spectra that showed evidence of a blood pool within the detection volume were identified as ρ more than 40% and not included in the statistical analysis.

Results
Lymph Node Staging
Ten patients were included (six men and four women) with an average age of 68 (±11.8) years. Spectroscopic measurements took place in 14 lymph nodes that were classified before the EUS-FNA based on CT and PET scans and subsequently confirmed through cytology (seven normal and seven metastatic). Cytologic conclusions of the metastatic lymph nodes were two adenocarcinomas, one undifferentiated large cell carcinoma (large cell), and four small cell carcinomas. Table 1 includes a detailed breakdown of patient-specific factors for each sampled lymph node.
Tolerance of the EUS-FNA with combined SF measurements was excellent in all patients, and no adverse events of the spectroscopy procedure were observed; addition of SF measurements extended no procedure by longer than 5 minutes. During the procedure, reflectance spectra and extracted physiological parameter estimates were visible less than 1 second after each measurement, information

that would immediately indicate if the probe tip was located in a blood pool, necessitating repositioning of the probe and measurement of additional spectra. This was the case in two normal nodes and one metastatic node.

Single Fiber Reflectance Spectra
Figure 2 displays representative SF reflectance spectra collected from measurements of a metastatic (top) and a normal (bottom) lymph node, both from a single patient (patient 9, nodes 12 and 13 from Table 1). The plots show measured data points and the line represents the model fit from Equation (1). The absorption bands of hemoglobin are visible in the spectra as the dips between 500 and 600 nm; the magnitude and shape of these spectral features inform model estimates of blood volume fraction (ρ) and microvascular saturation (StO$_2$). Table 1 includes a summary of ρ and StO$_2$ estimates for each lymph node sampled by SF, with SDs calculated from multiple spectra measured within each node.
Inspection of these data show that metastatic lymph nodes are associated with lower StO$_2$ (50% versus 84%) and lower ρ (5.6% versus 13.5%) than normal nodes; comparison of the mean values of these parameters between normal and metastatic nodes indicates significant differences (p<0.01 for each). Although other optical parameters (specifically, D_v, C_{bil} and a_2) extracted from SF spectra showed differences in the mean between normal and metastatic nodes, these differences were not significant and are not presented in detail in this paper.

Discussion
This work presents the first clinical pilot study incorporating SF reflectance spectroscopy into the EUS-FNA procedure for staging of mediastinal lymph nodes. The incorporation of the SF technique was feasible, quickly performed in the clinical setting, and did not introduce complications or extend the procedure by more than 5 minutes. SF reflectance spectra provided quantitative information about the tissue physiology within the lymph nodes. We observed differences in the mean values of the model estimates of microvascular saturation and blood volume fraction between normal and malignant nodes, with metastatic lymph nodes characterized by a lower blood volume fraction and lower microvascular saturation: observations that are associated with a compromised vascular supply.
Previous studies have described the disruptive effect that metastatic cancer within lymph nodes has the vascular supply and perfusion within the node. During the development of metastatic sites within lymph nodes, malignant cells invade the node through the afferent lymphatic vessels and then enter the subscapular sinus and cortex of the node, an infiltration route that usually results in metastatic sites located in the peripheral areas of the node [15,32]. As these metastatic sites proliferate and locally upregulate angiogenesis, they increase the vascularity in the peripheral areas of the node [14,15,33,34]. These morphological changes exert a mechanical (hydrostatic) pressure on the center of the node, compromising the central blood supply. Larger metastases destroy or displace the regular vascular network throughout the centre of the lymph node, a feature that can be exacerbated by central necrosis or keratinization within the node [16,17]. It is not well known if these changes are tumor-type specific or if these changes are representative of metastatic infiltration from all tumortypes. Previous studies using Doppler techniques reported abnormal vascular characteristics of metastatic

nodes, including the presence of aberrant vessels, displacement of vessels, and avascular areas, with the primary source of perfusion from the peripheral vasculature [14,16-18,33,34]. Our fiberoptic measurements estimated a reduction in blood volume fraction and microvascular saturation in the center of metastatic nodes as compared with normal nodes, observations that are consistent with the previous descriptions in the literature of vascular physiology within metastatic lymph nodes. These observations support the concept that reflectance spectroscopy can detect abnormal vascular physiology associated with metastatic lymph nodes.

For EUS-FNA staging of lung cancer patients, the clinically relevant problem is the classification of suspicious nodes as either reactive (benign) or metastatic. Lymph nodes undergoing a reactive immune response may appear suspiciously enlarged on CT and/or show increased activity on PET [35]. These reactive nodes are known to present vessel dilation and hypervascularity with the highest perfusion in the center of the node and proportionality between perfusion and volume of the enlarged nodes [36]: factors that would result in an increase in blood volume fraction while maintaining a high microvascular saturation within the node. Doppler techniques have been used to qualitatively observe and distinguish between increased perfusion within reactive nodes [36,37] and decreased perfusion within the center of metastatic nodes [14,33,34]; such differences in the vascular networks are expected to translate into differences in physiology that are quantitable by SF reflectance measurements. Moreover, these findings suggest that differences in vascular characteristics between reactive and metastatic nodes are more pronounced than what was observed between normal and metastatic nodes in this study. These factors suggest that only a limited number of SF reflectance measurements made near the center of a node would be required to quantify the regional effect of metastatic disease (or the regional effect of benign infection) on the node physiology. Such a fiberoptic sampling strategy specifically would not require optical sampling of localized malignant areas within a node and, therefore, would directly address the sampling error associated with the current EUS-FNA biopsy technique. It is important to note that whereas the tumorload required to change node physiology is currently unknown, but the nodes undergoing sampling within this scheme (will) have appeared enlarged on imaging scans (or are PET positive) and, therefore, if the tumorload is responsible for node enlargement or enhanced metabolic activity, it is reasonable to assume that the node physiology has been altered accordingly. Nevertheless, the sensitivity of the SF reflectance measurement to changes in vascular physiology associated with the size of the tumorload within metastatic nodes should be carefully investigated in an expanded clinically relevant data set.

Although the preliminary data presented in this study are promising, this pilot study is limited in scope and requires further clinical investigation. This pilot study included a restricted patient population, with reflectance measurements aquired only from nodes with a very defined clinical suspicion for a diagnosis, normal (unenlarged, PET negative) and metastatic (enlarged, PET positive), while excluding small suspicious nodes (unenlarged, PET positive). This population was selected to gather preliminary insight into the vascular physiology associated with the limiting normal/metastatic cases, and moreover, this strategy avoided the inclusion of nodes enlarged because of immune reaction into the normal designation used in this study. Future work will involve a clinical investigation within a large population of patients presenting suspicious nodes investigated by

EUS-FNA. Another limitation of this pilot study was the determination of normal nodes without surgical staging procedures to confirm the absence of metastases. Instead, this study confirmed normal nodes using cytologic analysis of aspirate acquired during EUS-FNA and conducing subsequent follow-up examinations to confirm that nodes identified as normal did not increase in size. This methodology can not conclusively rule out the inclusion of a false negative within the presented set of normal nodes. Further investigation is required to make concrete conclusions about the clinical utility of the vascular information extracted from reflectance measurements of lymph nodes.

In conclusion, SF reflectance spectroscopy allows real-time analysis of the vascular physiology in lymph nodes undergoing EUS-FNA staging procedures. Incorporation of the SF technique into the EUS-FNA was well-tolerated, and simple to use, and the measured spectra provided unique quantitative information about lymph node vasculature. The SF reflectance technique has the potential to improve the quantitative understanding of vascular physiology within lymph nodes, understanding this factor till date has been based on qualitative Doppler techniques. The data presented in this study demonstrate the feasibility and potential utility of SF measurements of vascular changes associated with the presence of metastases within lymph nodes. Moreover, the results obtained within this pilot study support the rationale for a novel fiberoptic sampling strategy during EUS-FNA, which involves the detection of regional effects of metastatic sites on lymph node physiology: a sampling strategy that would not require direct optical sampling of metastatic sites within nodes. In addition, the SF technology is extensible to any accessible lymph node and may provide information about nodal vascular physiology during staging of mediastinal and hilar lymph nodes through the bronchial tree.

Patient	Node	Gen	Age	Site	Diam (mm)	PET	Class	Cytology	EUS use	StO$_2$ (%) Mean	Stdev	ρ (%) Mean	Stdev
1	1	F	48	LN 7	40-20	pos	M	adeno	staging	10.8	5.0	1.6	0.5
2	2	M	53	LN 7	15-0.8	neg	N	normal	staging	81.1	4.4	16.4	6.2
	3	M	53	LN 4 L	0.4-0.4	neg	N	normal	staging	79.3	0.8	15.3	1.4
3	4	M	82	LN 7	13-0.5	neg	N	normal	staging	91.4	0.6	8.4	1.9
	5	M	82	LN 4 L	30-20	pos	M	large cell	staging	47.4	22.7	0.12	0.03
4	6	F	82	LN 5	0.7-2.3	pos	M	adeno	staging	48.8	11.4	1.9	1.0
5	7	F	72	LN 4 L	1.4-1.8	pos	M	SCLC	staging	34.2	14.1	5.8	1.9
6	8	M	63	LN 7	2.9-1.7	pos	M	SCLC	staging	54.9	19.9	5.9	1.7
7	10	M	58	LN 7	3.2-1.3	pos	M	SCLC	staging	87.7	11.7	6.6	2.9
8	11	M	76	LN 7	1.8-0.6	neg	N	normal	enlarged adrenal gland	75.3	3.1	3.2	0.6
9	12	M	75	LN 7	1.8-0.3	neg	N	normal	staging	95.8	1.8	26.6	3.3
	13	M	75	LN 4L	3.6-4	pos	M	SCLC	staging	69.0	9.2	3.1	1.0
10	14	F	67	LN 7	1.5-0.1	neg	N	normal	primary tumor punc	69.9	4.5	8.7	0.8
	15	F	67	LN 4L	1.8-0.2	neg	N	normal	primary tumor punc	94.4	3.2	16.1	3.2

Table 1. Characteristics of patients and lymph nodes included in the current pilot study. Nodes were classified (Class) as normal (N) or metastatic (M). Note both normal and metastatic nodes were measured in patients 3 and 9. Patient 2 had a positive cytology for a lymph node located at location LN 5/6 that was not measured by SF reflectance spectroscopy.
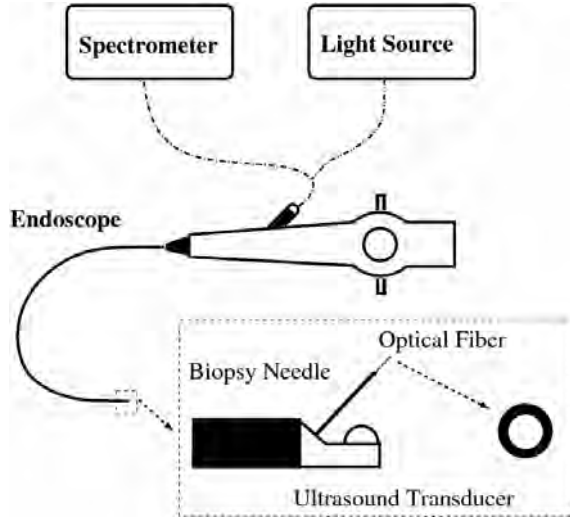
Figure 1. Setup used for optical measurements made during EUS-FNA staging of mediastinal lymph nodes. This measurement utilizes a single optical fiber to deliver white light to the lymph tissue *in vivo* and collect light remitted light to the spectrophotometer.
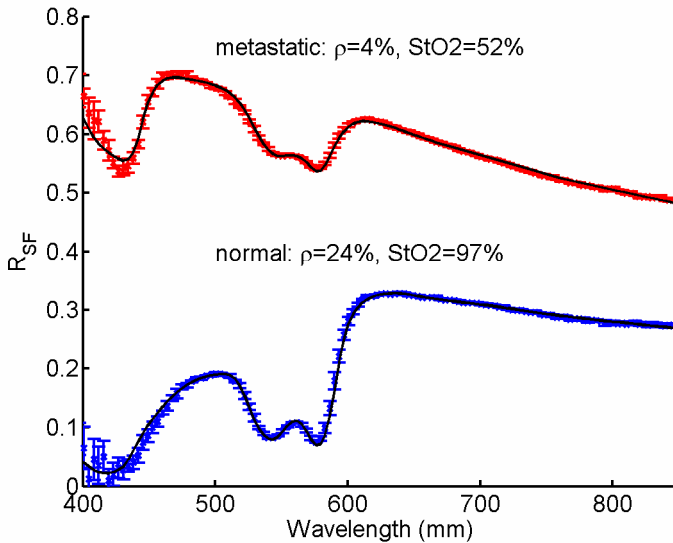
Figure 2. Single fiber reflectance spectra and model fit as measured in metastatic (top) and normal (bottom) lymph nodes within the same patient (patient 9, nodes 12 and 13 in Table 1). Spectra are shifted on horizontal axis for clarity (arbitrary units). These spectra show differences in both the oxygenation (StO_2) and volume fraction (ρ) of blood.

References

[1] Groome PA, Bolejack V, Crowley JJ, Kennedy C, Krasnik M, Sobin LH, Goldstraw P. The IASLC Lung Cancer Staging Project: validation of the proposals for revision of the T, N, and M descriptors and consequent stage groupings in the forthcoming (seventh) edition of the TNM classification of malignant tumours. *J Thorac Oncol* 2007;2:694-705.

[2] Gupta NC, Tamim WJ, Graeber GG, Bishop HA, Hobbs GR. Mediastinal lymph node sampling following positron emission tomography with fluorodeoxyglucose imaging in lung cancer staging. *Chest 2001;*120:521-7.
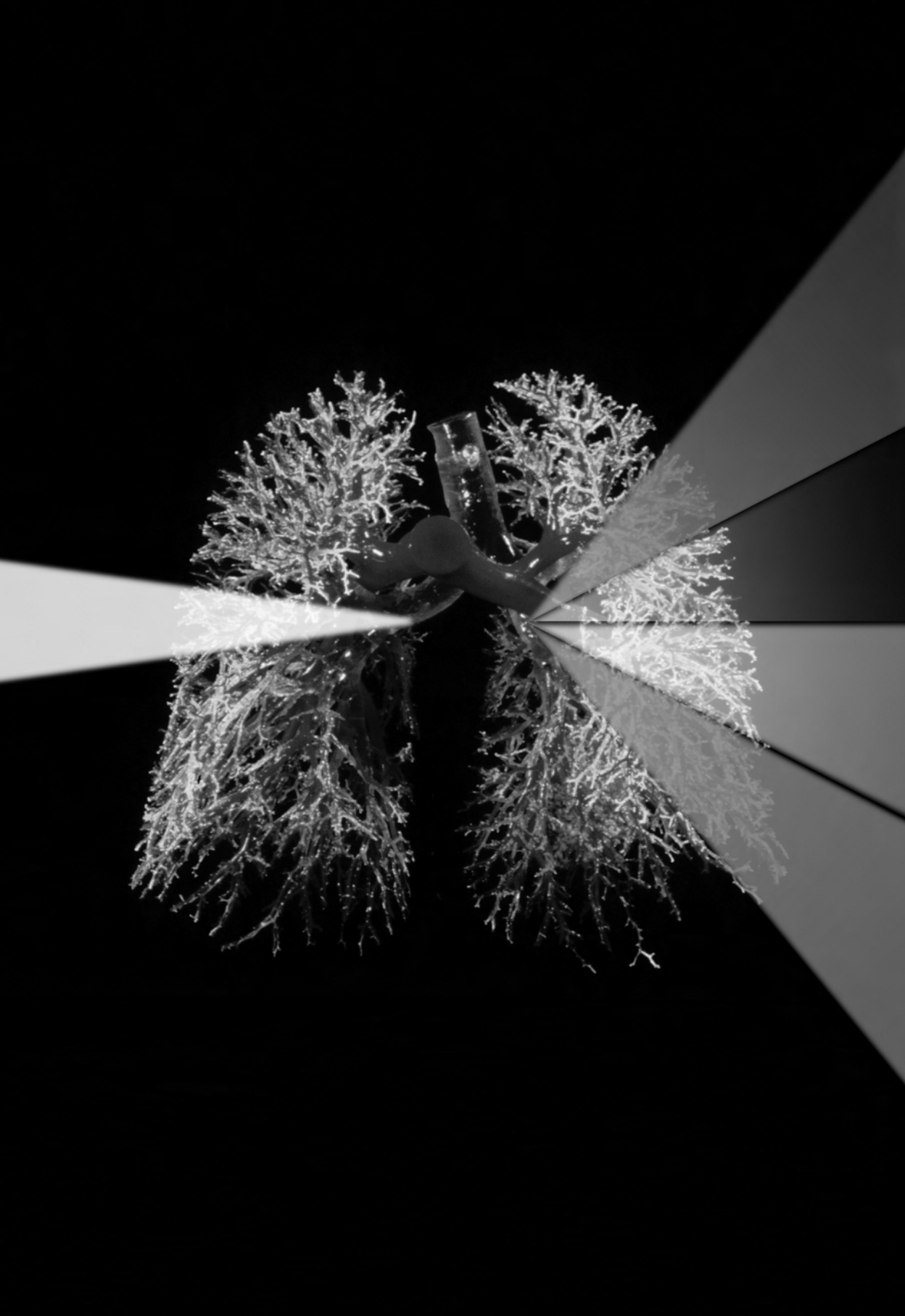
[3] Sanli M, Isik AF, Zincirkeser S, Elbek O, Mete A, Tuncozgur B, Elbeyli L. Reliability of positron emission tomography-computed tomography in identification of mediastinal lymph node status in patients with non-small cell lung cancer. *J Thorac Cardiovasc Surg* 2009;138:1200-1205.

[4] Detterbeck FC, Jantz MA, Wallace M, Vansteenkiste J, Silvestri GA. Invasive mediastinal staging of lung cancer: ACCP evidence-based clinical practice guidelines (2nd edition). *Chest* 2007; 132:202S-220S.

[5] De Leyn P, Lardinois D, Van Schil PE, Rami-Porta R, Passlick B, Zielinski M, Waller DA, Lerut T, Weder W. ESTS guidelines for preoperative lymph node staging for non-small cell lung cancer. Eur J Cardiothorac Surg 2007;32:1-8.

[6] Annema JT and Rabe KF. State of the art lecture: EUS and EBUS in pulmonary medicine. *Endoscopy* 2006;38:S118–S122.

[7] Caddy G, Conron M, Wright G, Desmond P, Hart D, Chen RY. The accuracy of EUS-FNA in assessing mediastinal lymphadenopathy and staging patients with NSCLC. *Eur Respir J* 2005;25:410–415.

[8] Singh P, Camazine B, Yashodeep J, et al. Endoscopic ultrasound as a first test for diagnosis and staging of lung cancer. A prospective study. *Am J respire Crit Care Med* 2007;175:345-354.

[9] Micames CG, McCrory DC, Pavey DA, Jowell PS, Gress FG. Endoscopic ultrasound-guided fine-needle aspiration for non-small cell lung cancer staging. Chest 2007; 131: 539-548.

[10] Tournoy KG, De Ryck F, Vanwalleghem LR, Vermassen F, Praet M, Aerts JG, Van Maele G, van Meerbeeck JP. Endoscopic ultrasound reduces surgical mediastinal staging in lung cancer: a randomized trial. *Am J Respir Crit Care Med* 2008;177:531-535.

[11] Talebian M, von Bartheld MB, Braun J, Versteegh MI, Dekkers OM, Rabe KF, Annema JT. EUS-FNA in the preoperative staging of non-small cell lung cancer. *Lung Cancer* 2009; (in press).

[12] Annema JT, Bohoslavsky R, Burgers S, et al. Implementation of endoscopic ultrasound for lung cancer staging. *Gastrointest Endosc* 2009; (in press).

[13] Boujaoude J, Mounassa L, Abboud B, et al. Did the presence of cytopathologist reduced optimal number of EUS-guided fine needle passes needed to obtain a correct diagnosis? *Gastrointest Endosc.* 2009; 69 S235-S236.

[14] Tschammler A, Wirkner H, Ott G, Hahn D. Vascular patterns in reactive and malignant lymphadenopathy. Eur Radiol 1996;6:473-480.

[15] Chikui T, Yuasa K, Maemura S, Kanda S. Change of angiostructure and hemodynamics in lymph node metastases in rabbits. *Oral Surg Oral Med Oral Pathol Oral Radiol Endod* 2002;93:350-357.

[16] Ahuja AT, Ying M. Sonographic evaluation of cervical lymph nodes. *AJR AM J Roentenal* 2005;184:1691-1699.

[17] Ying M, Ahuja AT. Ultrasound of neck lymph nodes: How to do it and how do they look? *Radiography* 2006;12:105-117.

[18] Esen G. Ultrasound of superficial lymph nodes. *Eur J Radiol* 2006; 58:345-359.

[19] Wilson BW, Jacques SL. Optical reflectance and transmittance of tissues: Principles and applications. *IEEE J Quantum Electron.* 1990;26:2186–2199.

[20] Amelink A, Bard M, Burgers J, Sterenborg HJCM. In vivo measurement of the local optical properties off tissue using differential pathlength spectroscopy. *Opt Lett* 2004;29:1087-1089.

[21] Kanick S, Sterenborg HJCM, Amelink A. Empirical model description of photon path length for differential path length spectroscopy: combined effect of scattering and absorption. *J Biomed Opt* 2008;13:064042.

[22] Amelink A, Christiaanse T, Sterenborg HJCM. Effect of hemoglobin extinction spectra on optical spectroscopic measurements of blood oxygen saturation. Opt Lett 2009;34:1525-1527.

[23] van Veen R, Amelink A, Menke-Pluymers M, van der Pol C, Sterenborg HJCM. Optical biopsy of breast tissue using differential path-length spectroscopy. *Phys Med Biol* 2005;50:2573-2581.

[24] Bard M, Amelink A, Noordhoek Hegt V, Graveland W, Sterenborg HJCM, Hoogsteden H, Aerts J. Measurement of hypoxia-related parameters in bronchial mucosa by use of optical spectroscopy. *Am J Respir Crit Care Med* 2005; 171:1178-1184.

[25] Bard M, Amelink A, Skurichina M, Noordhoek Hegt V, Duin R, Sterenborg HJCM, Hoogsteden H, Aerts J. Optical spectroscopy for the classification of malignant lesions of the bronchial tree. *Chest* 2006;129:995-1001.

[26] Amelink A, Kaspers O, Sterenborg HJCM, van der Wal J, Roodenburg J, Witjes M. Non-invasive measurement of the morphology and physiology of oral mucosa by use of optical spectroscopy. *Oral Oncology* 2008;44:65-71.

[27] Amelink A, Haringsma J, Sterenborg HJCM. Non-invasive measurement of the oxygen saturation of the microvascular blood in Barrett's dysplasia by use of optical spectroscopy. *Gastrointest Endosc* 2009;70:1-6.

[28] Kanick SC, Sterenborg HJCM, Amelink, A. Empirical Model of the Photon Path Length for a Single Fiber Reflectance Spectroscopy Device. *Opt Exp* 2009;17:860-871.

[29] Kanick SC, Robinson, DJ, Sterenborg HJCM, and Amelink, A. Monte Carlo analysis of single fiber reflectance spectroscopy: photon path length and sampling depth. *Phys Med Biol* 2009; 54:6991-7008.

[30] Kanick SC, van der Leest C, Aerts JG, Kascakova S, Sterenborg HJCM, Amelink A. Integration of Single Fiber Reflectance Spectroscopy into Ultrasound-Guided Endoscopic Lung Cancer Staging of Mediastinal Lymph Nodes. *J Biomed Opt* 2009;15:017004.

[31] van Veen RLP, Verkruysse W, Sterenborg HJCM. Diffuse-reflectance spectroscopy from 500 to 1600 nm by correction for inhomogeneously distributed absorbers. *Opt Lett* 2002;27:246-248.

[32] Yanagita S, Natsugoe S, Uenosono Y, etc. Morphological distribution of metastatic foci in sentinel lymph nodes with gastric cancer. Ann Surg Oncon 2007;15:770-776.

[33] Tschammler A, Ott G, Schang T, Seelbach-Goebel B, Schwager K, Hahn D. Lymphadenopathy: differentiation of benign from malignant disease-color Doppler US assessment of intranodal angioarchitecture. *Radiology* 1998;208:117-123.

[34] Ahuja AT, Ying M, Ho SSY, Metreweli C. Distribution of intranodal vessels in differentiating benign from metastatic neck nodes. *Clin Radiol* 2001; 56:197-201.

[35] Tournoy KG, Maddens S, Gosselin R, Van Maele G, van Meerbeeck JP, Kelles A. Integrated FDG-PET/CT does not make invasive staging of the intrathoracic lymph nodes in non-small cell lung cancer redundant: a prospective study. *Thorax* 2007; 62: 696-701.

[36] Herman PG, Lyonnet D, Fingerhut R, and Tuttle RN. Regional blood flow to the lymph node during the immune response. *Lymphology* 1976;9:101-104.

[37] Hall JD, Kahaleh M, White GE, Talreja J, Northup PG, Shami VM. Presence of lymph node vasculature: a new EUS criterion for benign nodes? *Dig Dis Sci* 2009;54:118-121.

Role of PET scanning in small cell lung cancer with emphasis on soft tissue lesions

C. van der Leest[1,2]

J. Baas[3]

R.J. Versteijlen[4]

J. Los[5]

N. van Walree[1]

J.G.J.V. Aerts[1,2]

1 Department of Pulmonary Diseases, Amphia Hospital, Breda, The Netherlands

2 Department of Pulmonary Diseases, Erasmus MC, Rotterdam, The Netherlands

3 Department of Nuclear Medicine, Amphia Hospital, Breda, The Netherlands

4 Department of Radiology, Amphia Hospital, Breda, The Netherlands

5 Department of Pathology, Amphia Hospital, Breda, The Netherlands

Summary

Background: Although several studies indicate an additional value of PET in small cell lung cancer (SCLC), the acceptance is limited.
Objectives: To study the additional value of soft tissue lesions detection with PET scanning in patients with SCLC.
Methods: A retrospective analysis of patients, in whom both CT and PET scanning were available in the staging work-up.
Results: Sixty-three patients were included. Thirty-six patients were staged as limited disease by CT scan, 2 patients were up staged to extended disease after PET scanning due soft tissue lesions. CT scan staged 27 patients as extended disease. In 3 patients, soft tissue lesions found with CT scanning were not confirmed with PET scanning, resulting in a down staging. These findings resulted in 5 of 63 patients (7.9%) a change in staging (95% CI 1.2-14.6).
Conclusion: PET scanning seems a valuable tool in detecting soft tissue lesions and improving staging of SCLC.

Introduction

Lung cancer is the second most common cancer in men and women, and is the leading cause of cancer related death. In industrialized countries the mortality rate in lung cancer exceeds breast, colorectal and prostate cancer combined [1]. Small cell lung carcinoma (SCLC) accounts for approximately 15% of all the diagnosed lung cancers [2,3]. SCLC is an aggressive type of lung cancer, associated with high metastases rate. Common metastasis localisations are brains, bones and soft tissue lesions like liver and adrenal glands. Although TNM staging is recommended in SCLC [4], for therapeutic reasons it is divided into limited and extended disease. Limited disease is characterized by tumors confined to one hemithorax. Involvement of supraclavicular nodes is acceptable if they encompass the same radiation portal as the primary tumor. All other disease is classified as extensive disease [5]. Standard treatment is (concomitant) chemotherapy and radiotherapy in patients with a limited stage SCLC, and chemotherapy alone in patients with extended SCLC. Sixty to seventy percent of all diagnosed SCLC is extended disease.

Current diagnostic staging modalities include contrast enhanced computerized tomography (CT) scan of chest and upper abdomen, bone scanning and CT scan or magnetic resonance imaging (MRI) of the brain [6,7]. Bone scanning and CT or MRI of the brain is able to detect bone and brain metastasis respectively. For detection of soft tissue metastasis we have to rely on the CT scan. Although positron emission tomography (PET) imaging improves accuracy of staging in patients with NSCLC [8], the role in staging patients with SCLC is less well defined [7]. Several studies [9-16] have suggested that PET scanning, added to the conventional staging, is more sensitive for detection of extended disease, but PET scanning is not a standard procedure yet.

In the Netherlands CT and PET scanning are regularly performed in patients without clinical signs of metastatic disease in case of a suspicion of lung cancer to reduce time to diagnosis and treatment. Therefore we were able to collect data of patients in whom the diagnosis SCLC was established. As no standard bone-scanning was performed our data are only related to the detection of soft tissue lesions. Our aim was, to study the additional value of PET scanning in detection of soft tissue lesions in patients with SCLC.

Patients and Methods

We retrospectively analysed data of patients who were diagnosed with SCLC in the Amphia General Hospital in Breda, the Netherlands between June 2004 and January 2008. As the present study is a retrospective observational study, the national law in our country requires neither institutional review board approval nor informed consent. Patients who received a CT scan and a PET scan were seen because of an abnormal chest radiograph. When no signs of extensive metastatic disease were apparent, CT scan, bronchoscopy and PET scan were planned during the first consultancy to reduce time to diagnosis.

All patients who received CT scan and PET scan in the work up to diagnose SCLC were reviewed. Cytology or histology was obligatory in all patients. CT scanning was performed between 2004 and august 2007 by a General Electric type: CTI, spiral scan, single slice, 7 mm coupes. Hereafter CT scanning was carried out by a Siemens Definition 64 slice dual source, 5 mm slice coupes. Contrast enhanced imagines were made of the thorax and the upper abdomen, including

the adrenals and the liver. CT head was performed in patients without evidence of extended disease or in case of clinical suspicion. PET scanning in the Amphia General Hospital started in 2004. Whole body PET-imaging was performed 60 minutes after intravenous injection of 300 – 500 MBq 2-deoxy-2-[18]fluoro-D-glucose, after a six hour fasting period, on a Siemens Ecat Exact PET-scanner. None of the patients was diabetic or had a fasting blood glucose level above 120mg/dL. Scans were performed using a two-dimensional acquisition mode from the thigh to the skull base with seven bed positions. Each bed position was composed of 1 min of transmission scanning and 5 min of emission scanning. Due to low sensitivity the cerebrum was not analysed by PET scanning.

Results
In total 63 patients diagnosed with SCLC underwent CT and PET scanning in a primary work up between June 2004 and January 2008. Male female ratio was 1.6. Average age at diagnosis was 67 years. After CT thorax/abdomen and CT cerebrum, limited stage was diagnosed in 36 patients (57 %), extended stage was diagnosed in 27 patients (43 %) (Figure 1). Average time interval between CT scan and PET was 8 days (range -6 to 36 days). Follow up was at least 1 year and results were based on the response assessed by CT.
PET down staged three patients. Lesions found with CT scanning were not confirmed with PET scanning. All lesions (2 adrenal glands and 1 liver lesion) were soft tissue lesions. Follow up CT scan showed unchangeable lesions after chemotherapy.
PET scanning was responsible for up staging in 2 patients due to detection of extrathoracic soft tissue lesions (cervical region and liver metastases). Follow up by PET and CT scans showed regression after chemotherapy.
In total 5 patients (7.9 %) of 63 patients (95% CI 1.2 – 14.6) had a stage shift due to soft tissue lesions that were not detected or wrongly interpreted by CT scan (table 1). PET scanning showed in 20 patients (31.7%) additional bone lesions. One patient, staged as limited by CT scan, showed additional liver lesions but also skeletal lesions. This scan was not considered as an additional value scan, because the bone lesions could also be detected by a bone scan. Two patients who were limited staged, also after PET scanning, showed brain metastasis after CT cerebrum.
No differences in the results between the 2 different CT–scanning modalities could be established.

Discussion
In this retrospective study PET scanning lead to a stage shift in 7.9% due to soft tissue lesions. In 3 patients who were diagnosed as extended disease with CT-scanning, PET scanning was negative in these CT-suspicious lesions. In 2 patients additional soft tissue lesions were found with PET scanning, resulting in an upstaging.
Accurate staging is essential in the work-up of SCLC. Chemotherapy in combination with thoracic irradiation can promote long-term survival in patients with limited stage, but risk of complications such as irradiation pneumonitis or oesophagitis is high. This causes worsening of patient's quality of life or even treatment related death.

False positive lesions detected on CT-scan cause under treatment and poor survival. It is considered unacceptable to stage patients solely based on imaging, and pathological conformation is required. In clinical practice this conformation is not always possible for several reasons like, a lesion which is not assessable for puncture. PET is a non-invasive tool, which can be helpful in these patients. A negative PET excludes metastases and could avoid 3 unnecessary punctures in this study.

Positive PET is not proving for metastases and pathological confirmation is required. In this study, similarly to Niho *et al.* [15], we did not confirm pathologically the additional metastases detected by PET scanning. The lesions were followed up during treatment and this was considered as proof of origin. Follow up was at least one year and results were based on the response assessed by CT.

Skeletal lesions are frequently missed by CT (sensitivity is reported 30%) [17]. In our series additional bone lesions were established in 20 patients (31.7%). Bone scintigraphy was not performed regularly added to PET. Because PET scanning was done upfront, no confirmatory bone scanning was performed, which can be considered controversial. Formally in case of limited disease SCLC a bone scanning should have been performed. The reason that no standard bone scintigraphy was performed is based on studies suggesting that PET might even be superior to bone scan in detecting bone metastasis [10,14,17]. Fischer *et al.* reported in patients with SCLC sensitivity of detection of bone metastasis by bone scintigraphy and PET scanning of 75% and 80% respectively [17]. Another study revealed 84% identical metastatic bone lesion detection between bone scan and PET scan [14]. Our results about a stage shifting after PET in patients with bone metastases cannot be related to general practice.

The total stage shift is lower compared to Fischer *et al.* [17] and Brink *et al.* [10] who concluded that PET induced a stage shifting in 17% and 12% of respectively 29 and 120 patients diagnosed with SCLC. In these studies unexpected bone metastasis detected by PET scanning were also included in the analysis.

By doing a retrospective analysis a selection bias is present. To reduce time to diagnosis and treatment CT scan and PET scan were planned simultaneously on the first consultancy. Especially in those patients without clear signs of metastatic disease, PET scanning was done. This explains the higher than expected number of limited disease compared to extended disease and also the number of limited metastatic sides.

Because the study is retrospective some drawbacks, like missing histopathology on positive soft tissue lesions and selection bias, are inevitable. Despite these drawbacks we believe that our results are of value for the general oncologist, and do add to the present literature in the way that we do present a rather large series.

It is known that PET/CT is superior to PET imaging alone [18]. PET/CT decreases imaging time per patient and significantly reduces the number of equivocal PET interpretations. PET/CT also has the ability to improve accuracy of PET image interpretation [19]. In this study, PET scanning was performed by a stand alone PET scan.

As PET has a low sensitivity for the detection of brain metastases, this was not analysed in this study. Patients underwent routinely a CT cerebrum to analyse the presence of cerebral lesions. Two patients who were limited staged also after PET scanning, showed brain metastasis after CT cerebrum.

Conclusion

In conclusion, although our study has some limitations, PET adds to the accuracy of diagnosing soft tissue metastases in patients with SCLC disease resulting stage shift in 5 of 63 patients (7.9%) (95% CI 1.2-14.6). For bone metastases its value above CT-scanning is apparent but, as no comparison with bone scanning was performed, no conclusions on the comparison of PET with bone scanning can be drawn. Additional prospective investigations about optimal staging procedures in small cell lung cancer should be performed.

Stage shift after PET scanning due to soft tissue lesions				
patient	CT scan result	PET scan result	Comment	Follow up
1	Extended stage	Limited stage	Adrenal masses on CT, negative on PET	Follow up CT showed still enlarged left adrenal
2	Extended stage	Limited stage	Liver lesion detected by CT scan, PET is negative	Follow up CT showed still enlarged liver lesion
3	Extended stage	Limited stage	Adrenal masses on CT, negative on PET	Follow up CT showed still enlarged left adrenal
4	Limited stage	Extended stage	Positive lesions in the liver by PET scan	Follow up PET showed disappearing of liver lesions
5	Limited stage	Extended stage	PET detected additional a lesion in the cervical region	Follow up CT scan showed lesion regression

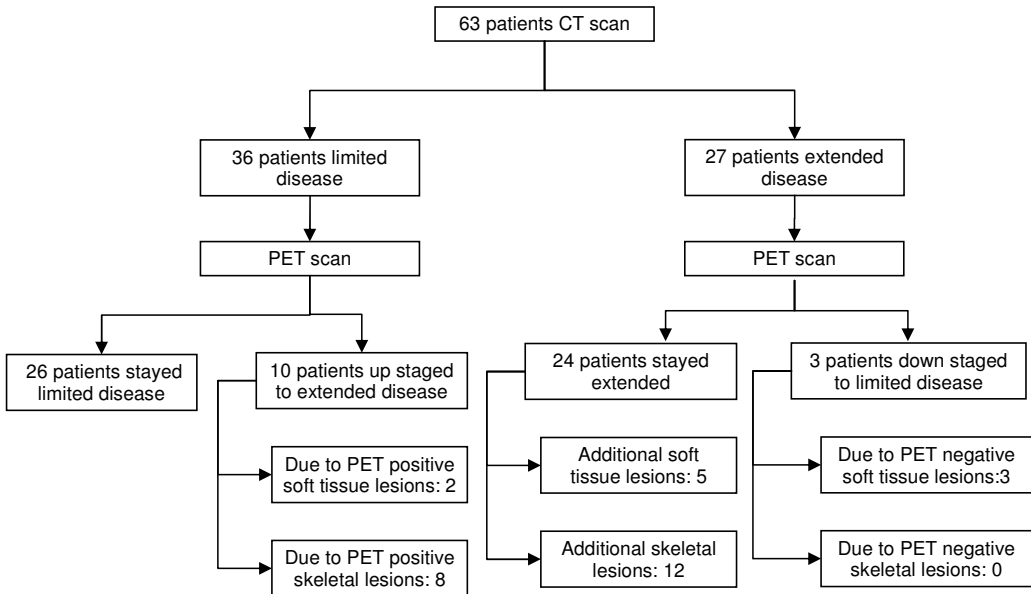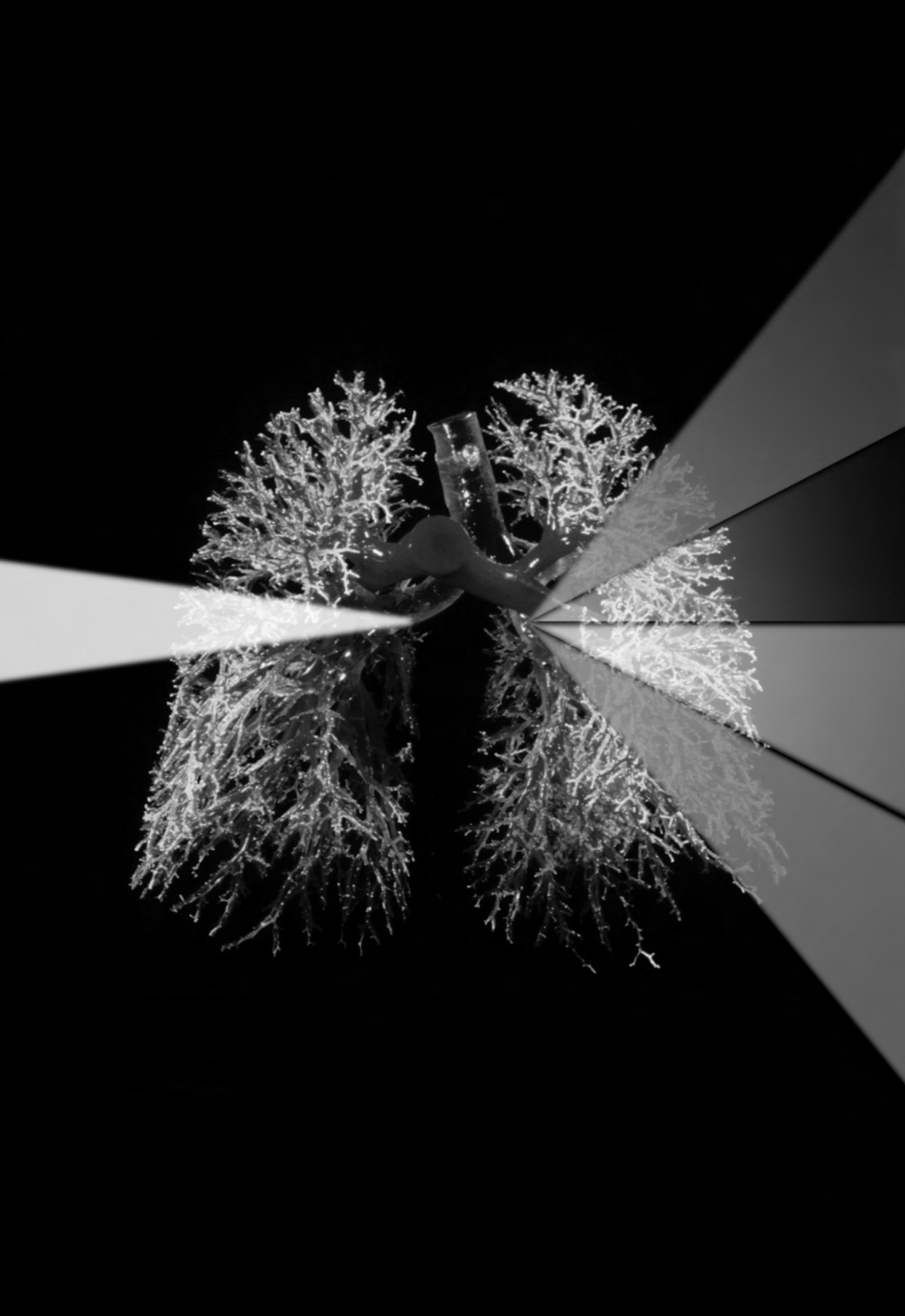Table 1: Five patients with stage shift after PET scanning due to soft tissue lesions

Figure 1: sixty-three patients diagnosed with SCLC staged by CT and PET scan

References

1. Jemal A, Siegel R, Ward E, Murray T, Xu J, Thun MJ. Cancer statistics, 2007. CA Cancer J Clin;57(1):43-66, 2007.
2. Janssen-Heijnen ML, Coebergh JW. The changing epidemiology of lung cancer in Europe. Lung Cancer;41(3):245-258, 2003.
3. Serke M, Schonfeld N. [Diagnosis and staging of lung cancer]. Dtsch Med Wochenschr;132(21):1165-1169, 2007.
4. Shepherd FA, Crowley J, Van Houtte P et al. The International Association for the Study of Lung Cancer lung cancer staging project: proposals regarding the clinical staging of small cell lung cancer in the forthcoming (seventh) edition of the tumor, node, metastasis classification for lung cancer. J Thorac Oncol;2(12):1067-1077 2007.
5. Zelen M. Keynote address on biostatistics and data retrieval. Cancer Chemother Rep 3;4(2):31-42, 1973.
6. Seidenfeld J, Samson DJ, Bonnell CJ, Ziegler KM, Aronson N. Management of small cell lung cancer. Evid Rep Technol Assess (Full Rep) (143):1-154, 2006.
7. Samson DJ, Seidenfeld J, Simon GR et al. Evidence for management of small cell lung cancer: ACCP evidence-based clinical practice guidelines (2nd edition). Chest;132(3 Suppl):314S-323S, 2007.
8. Pieterman RM, van Putten JW, Meuzelaar JJ et al. Preoperative staging of non-small-cell lung cancer with positron-emission tomography. N Engl J Med;343(4):254-261, 2000.
9. Bradley JD, Dehdashti F, Mintun MA, Govindan R, Trinkaus K, Siegel BA. Positron emission tomography in limited-stage small-cell lung cancer: a prospective study. J Clin Oncol;22(16):3248-3254, 2004.
10. Brink I, Schumacher T, Mix M et al. Impact of [18F]FDG-PET on the primary staging of small-cell lung cancer. Eur J Nucl Med Mol Imaging;31(12):1614-1620, 2004.
11. Shen YY, Shiau YC, Wang JJ, Ho ST, Kao CH. Whole-body 18F-2-deoxyglucose positron emission tomography in primary staging small cell lung cancer. Anticancer Res;22(2B):1257-1264, 2002.
12. Blum R, MacManus MP, Rischin D, Michael M, Ball D, Hicks RJ. Impact of positron emission tomography on the management of patients with small-cell lung cancer: preliminary experience. Am J Clin Oncol;27(2):164-171, 2004.
13. Schumacher T, Brink I, Mix M et al. FDG-PET imaging for the staging and follow-up of small cell lung cancer. Eur J Nucl Med;28(4):483-488, 2001.
14. Kut V, Spies W, Spies S, Gooding W, Argiris A. Staging and monitoring of small cell lung cancer using [18F]fluoro-2-deoxy-D-glucose-positron emission tomography (FDG-PET). Am J Clin Oncol;30(1):45-50, 2007.
15. Niho S, Fujii H, Murakami K et al. Detection of unsuspected distant metastases and/or regional nodes by FDG-PET [corrected] scan in apparent limited-disease small-cell lung cancer. Lung Cancer;57(3):328-333, 2007.
16. Kamel EM, Zwahlen D, Wyss MT, Stumpe KD, von Schulthess GK, Steinert HC. Whole-body (18)F-FDG PET improves the management of patients with small cell lung cancer. J Nucl Med;44(12):1911-1917, 2003.
17. Fischer BM, Mortensen J, Langer SW et al. A prospective study of PET/CT in initial staging of small-cell lung cancer: comparison with CT, bone scintigraphy and bone marrow analysis. Ann Oncol;18(2):338-345, 2007.
18. Schoder H, Erdi YE, Larson SM, Yeung HW. PET/CT: a new imaging technology in nuclear medicine. Eur J Nucl Med Mol Imaging;30(10):1419-1437, 2003.
19. Lardinois D, Weder W, Hany TF et al. Staging of non-small-cell lung cancer with integrated positron-emission tomography and computed tomography. N Engl J Med;348(25):2500-2507, 2003.

SUVmax during PET scanning in small cell lung cancer; similar information as in non-small cell lung cancer?

C. van der Leest[1,2]

E.F. Smit[3]

J. Baas[4]

R.J. Versteijlen[5]

H.C. Hoogsteden[2]

N. van Walree[1]

J.G.J.V. Aerts[1,2]

1 Department of Pulmonary Diseases, Amphia Hospital, Breda, The Netherlands
2 Department of Pulmonary Diseases, Erasmus MC, Rotterdam, The Netherlands
3 Department of Pulmonary Diseases, Vrije Universiteit, Amsterdam, The Netherlands
4 Department of Nuclear Medicine, Amphia Hospital, Breda, The Netherlands
5 Department of Radiology, Amphia Hospital, Breda, The Netherlands

Abstract

Introduction: Small cell lung cancer (SCLC) is an aggressive tumor with poor prognosis. Positron Emission Tomography (PET) scanning is widely used in staging of Non-Small Cell Lung Cancer (NSCLC), and the SUVmax value seems to have a prognostic value. Limited results of the prognostic and predictive value of SUVmax in SCLC are available.

Methods: a prospective study in 75 chemonaive patients diagnosed with SCLC and a PET scan before treatment was performed. SUVmax values of the primary tumor were related to the overall survival (OS) and the progression free survival (PFS). To investigate SUVmax, patients were divided in a low SUVmax and high SUVmax group according to the median SUVmax level. Separate analyses in limited and extended disease patients were performed.

Results: Significant lower SUVmax values of the primary tumor were observed in patients with limited disease (LD) compared to extended disease (ED). By subdividing the total population in low and high SUVmax groups, no significant differences in OS and PFS were observed. Analysis in the patients staged as LD, between high and low SUVmax revealed no significant in OS and PFS. In patients stages as ED, significant differences in OS and PFS survival were found between the low and high SUVmax groups. The patients with ED and a high SUVmax value had a significant better OS (p-value 0.005) and a longer PFS (0.002).

Conclusion: In patients with SCLC, SUVmax was higher in ED compared to LD. A high SUVmax is a predictive factor for prolonged PFS and OS, probably due to a beneficial effect of chemotherapy which we ascribe to the increased chemosensitivity in these patients. In LD SUVmax was found not to be a predictive factor.

Introduction

Small cell lung carcinoma (SCLC) accounts for approximately 15% of all the diagnosed lung cancers [1, 2]. This type of lung cancer associated with a high mitotic rate and widespread metastatic disease. Consequently, prognosis in these patients is poor and overall survival rates are disappointingly low.

Historically, SCLC is classified as either limited disease (LD) or extended disease (ED) which is mainly based on treatment options. Limited disease is defined as a disease confined to the ipsilateral hemithorax which can be encompassed by a single radiotherapy port [3], ED is defined as a disease beyond that ipsilateral thorax. Recently it has been advocated to stage SCLC similar to non-small cell lung cancer (NSCLC) according to the TNM system [4].

A number of parameters have been studied as possible prognostic factors in SCLC [5, 6], but none are reliable enough to base treatment decision on. In patients with NSCLC it was shown that metabolic activity on 18FDG PET is correlated with survival [7-11]. There is a suggestion that 18FDG PET scanning also carries prognostic information in SCLC [12]. In recent years fluorine-18 fluorodeoxyglucose positron emission tomography 18FDG-PET improved staging of SCLC [3, 13-17]. Because SCLC staging with PET scanning is acceptable, this study could be performed. In the present prospective study we evaluate whether the standardized uptake value (SUVmax) of 18FDG of the primary tumor during PET scanning has prognostic and predictive value in both limited and extended disease with respect to progression free survival (PFS) and overall survival (OS).

Patients and methods

This is a single center prospective study. All patients with a histological or cytological confirmation of the diagnosis SCLC and a PET scan before treatment were included between January 2007 and December 2008. The decision to perform a PET scan was made by the treating physician. Staging was performed by standard procedure: patients history and physical examination, chest X-ray, CT Thorax and abdomen, CT brain and when clinical indicated bone scintigraphy. This study was approved by the institutional board of the Amphia Hospital (Breda, The Netherlands). Patients were divided into LD and ED. LD was defined as disease restricted to one hemi thorax with regional lymph node metastases. These included hilar and mediastinal ipsilateral and contralateral as well as ipsi- and contralateral supraclavicular lymph nodes. All patients with sites of disease beyond the definition of limited disease were defined as ED. Ipsilateral pleural effusion was considered as ED. The PET scan caused stage shifting in 6 patients (8%). Two patients were down staged by virtue of FDG negative enlarged adrenal glands and 4 patients were upstaged.

PET imaging

Whole body PET-imaging was performed 60 minutes after intravenous injection of 300 – 500 MBq 18-F-fluorodeoxyglucose (FDG), after a six hour fasting period, on a Siemens Ecat Exact PET-scanner. None of the patients was diabetic or had a fasting blood glucose level above 120 mg/dL. Scans were performed using a two-dimensional acquisition mode from the thigh to the skull base with seven bed positions. Each bed position was composed of 1 min of transmission scanning and 5 min of emission scanning.

The images were reviewed on an interactive video display provided by the equipment manufacturer. The maximum standard uptake values (SUVmax) was quantitative used to determine FDG PET activity. SUVmax was defined as maximum tumor concentration of FDG divided by the injected dose, corrected for the body weight of the patients: (SUVmax = maximum activity concentration/[injected dose/body weight]). The SUVmax was the peak SUV in one pixel with the highest counts within the region of interest. The region of interest was only the primary tumor. With use of the CT scan, primary tumor was localized by the radiologist. To obtain the SUVmax, all images were analyzed by a single investigator.

Treatment and follow up
Treatment modalities were evaluated for each patient (table 1). First line chemotherapy was either Cisplatin-Etoposide or Carboplatin-Etoposide. Prophylactic cranial irradiation was administered to all patients without radiological signs of brain metastases. The primary end point was OS, defined as the date of the PET scan to the date of death. Patients who were still alive were censored.
Progression-free survival (PFS) was defined as the date of the PET scan to date of first progression or date of death in patients without progression. Progression was defined as local regional and/or new metastasis observed by Chest X-ray, CT or PET scan. All patients were evaluated at a 6-8 weeks interval.

Data analysis
Differences in SUVmax between LD and ED were evaluated using a two-tailed Student's t test. Patients were subdivided into high and low SUVmax according to median SUVmax level. Multivariate linear regression models were used to adjust the association between high and low SUVmax and PFS or OS for age, gender and performance score by the Eastern Cooperative Oncology Group (ECOG). Survival time was estimated by the Kaplan-Meier method and the survival difference between groups was assessed by the log-rank test. The SPSS 15.0 for Windows software was used for statistical analyses. A p-value of <0.05 was considered significant.

Results
Patient characteristics
75 patients, 29 women and 46 men, with a mean age of 66 years (range 49 - 81) were included. Follow up was at least 12 months. Of these patients 19 were still alive at the end of the study, 52 died and 4 were lost to follow up. Among these patients LD was staged in 35 patients and ED in 40 patients. Of the patients diagnosed with LD, 26 were treated with chemotherapy and radiotherapy (concurrent or sequential), 4 underwent surgery, 3 did not receive any treatment and 2 were lost of follow up. These last 5 patients were excluded from PFS analysis. The patients with LD received a median of 4 chemotherapy cycles (range 1-4). Median OS of the patients with LD was 12.1 months.
Of the patients with ED 28 received chemotherapy, 10 had no treatment and 2 were lost to follow up. These last 12 patients were excluded from PFS analysis. Median number of chemotherapy cycles in this group was 3.0 (range 1-5). Median OS of the treated ED patients was 7.0 months.

SUVmax and follow up

SUVmax of the primary tumor was higher in the patients with ED compared to LD (figure 1) (p-value= 0.02). Median SUVmax value of the primary tumor of the study population was 11.3.

OS difference was not present between high and low SUVmax in all treated patients (p= 0.342) Also no OS differences between high and low SUVmax was present in all non-treated patients (p= 0.291). In the patients with LD no significant differences in PFS and OS were established between high and low SUVmax (table 2). When taking into account only the patients who were treated with chemo radiotherapy (n=26) again no differences could be established.

In patients with ED, OS was significant longer in the group of patients with the high SUVmax (*p-value* 0.005). In the patients with ED and no treatment, there was no difference in OS between a high or low SUVmax (p=0.196), but this group (n=10) is too small to draw conclusions. Distribution of SUVmax between ED with or without treatment was equally. When looking at patients with ED and treated with chemotherapy both OS (p = 0.008) and PFS (p= 0.002) were favorable for the high SUVmax population (figure 3 and 4).

Discussion

We studied whether SUVmax had prognostic or predictive value in patients diagnosed with SCLC. SUVmax value were higher in ED compared to LD. Results showed no prognostic or predictive value of SUVmax in the total group. In LD no relation between SUVmax and OS or PFS were found. In ED, SUVmax did have a predictive value. Patients with ED who were treated with chemotherapy and a high SUVmax had both prolonged OS and PFS.

The general assumption is that the high mitotic activity of SCLC results in a high SUVmax and we hypothesized that a higher SUVmax be associated with more advanced disease. This hypothesis was supported by our result as the SUVmax in ED was significantly higher compared to SUVmax in LD.

Surprisingly we found a higher SUVmax in patients with ED to be associated with a better survival after chemotherapy. Our data in patients with ED are in contrast to published data in NSCLC, where a low SUV is in general associated with a better prognosis [9, 10, 18-20]. Most of these studies are performed in early stage NSCLC and therefore cannot necessarily be extrapolated to more advanced stages of the disease.

OS and PFS in our group are, as in general in SCLC, shorter then NSCLC. We found that the high metabolic rate in ED is associated with a better response to chemotherapy which increases survival. This is supported by Lee *et al.* [21] where 85 chemonaive patients with advanced NSCLC were included. Response rate and survival were analyzed according to SUVmax. Response rate on chemotherapy in the patients with NSCLC was better in patients with high SUVmax values. They concluded similar to our results that tumors with a high SUVmax were a predictive factor for OS. We found differences in OS and PFS which we hypothesize to be related to the tumor behavior of SCLC. SCLC is a tumor with high mitotic activity and for this reason high SUV values are present. As in general a high mitotic rate makes a tumor chemosensitive, chemotherapy response is often very good. Based on our findings we suggest that chemotherapy response will be higher in patients with high SUVmax. This will cause a delay in disease recurrence and

increase overall survival in the high SUVmax group compared to the lower SUVmax group.

In a study by Lee *et al* [12], the role of 18FDG-PET as prognostic factor in SCLC was studied, in a population of 76 patients. They investigated the relationship between OS and the SUVmax of the primary lesion. Just like us, they did not found significant results for the complete group. Whether they looked at the subpopulations LD and ED and the SUVmax of the primary lesion is not mentioned in their paper. They determined an alternative SUV parameter, the meanSUVmax, which showed in the complete group a better PFS and OS in patients with a low meanSUVmax compared to the patients with a high meanSUVmax. Patients with LD and a high meanSUVmax showed significant shorter OS and PFS compared to LD with low meanSUVmax. Identical results were observed in ED.

For a number of reasons the usage of SUVmax was preferred above a meanSUVmax in our study. Firstly, metabolic activity of lung cancer lesions varies depending on the sites of metastatic disease. SUVmax value is higher in bone metastasis compared to lymph node metastasis or solid organ metastasis [22]. This will have major influences on a meanSUVmax value. Secondly, in most published data, SUVmax of the primary tumor is used as the discriminated factor and consequently our results can be compared to these studies.

The number of patients with ED compared to LD is lower then expected in the general population of patients with SCLC. All patients were referred for PET scanning during the diagnostic work, but the decision for PET scanning was made by the patients treating physician. In patients with clear evidence of metastatic no PET scan will be performed, which may be the reason of the lower number of included patients with ED.

PET scan is nowadays a standard tool in the work-up of NSCLC. It is not implemented in the standard work-up of SCLC yet. But, as the number of studies on the better accuracy of staging with PET scanning is increasing, we think that PET scanning will be standard of care in the near future. Based on the results of the present study analysis of metabolic activity may give additional predictive value. In conclusion, we investigated the value of SUVmax in patients with SCLC. Patients diagnosed with an ED and a high SUVmax value had a better PFS and OS compared to ED and a low SUVmax. Further research has to be done on this subject to establish whether SUVmax can contribute in treatment options. For instance, it could be studied whether SUVmax might be a parameter in the decision of the number of chemotherapy cycles for SCLC patients staged with ED.

	number of patients
Total	75
Gender	
Male	46
Female	29
Age	
<65	36
>65	39
ECOG	
0-2	62
>2	13
Stage	
LD	35
ED	40
Treatment LD	
Surgery	4
Chemo/RT concurrent	19
Chemo/RT sequential	7
None	3
Unknown	2
Treatment ED	
Chemotherapy	28
None	10
Unknown	2
Status LD	
Alive	13
Death	20
Lost of follow up	2
Status ED	
Alive	6
Death	32
Lost of follow up	2

Table 1: patients' characteristics

	SUVmax mean	SUVmax range	Mean OS ± SD (days)	P-value	Mean PFS ± SD (days)	P-value
LD total	9.65	1.18 - 18.40	368 ± 172		275 ± 145	
Low SUVmax	6.60	1.18 - 11.05	359 ± 171		281 ± 146	
High SUVmax	12.88	11.47 - 18.40	379 ± 178	0.427	268 ± 150	0.78
ED total	11.88	4.75 - 25.99	189 ± 154		144 ± 83	
Low SUVmax	8.16	4.75 - 10.94	114 ± 110		99 ± 61	
High SUVmax	14.35	11.47 - 25.99	239 ± 161	0.005	181 ± 81	0.002
ED with treatment	11.20	4.75 - 19.41	210 ± 144		144 ± 83	
Low SUVmax	7.82	4.75 - 10.11	138 ± 116		99 ± 61	
High SUVmax	13.70	11.47 - 19.41	264 ± 142	0.008	181 ± 81	0.002

Table 2: Results of SUVmax between LD low and high SUVmax and ED low and high SUVmax. Low and high SUVmax was determined by the median SUVmax of 11.3. P-values adjusted for age, gender and ECOG
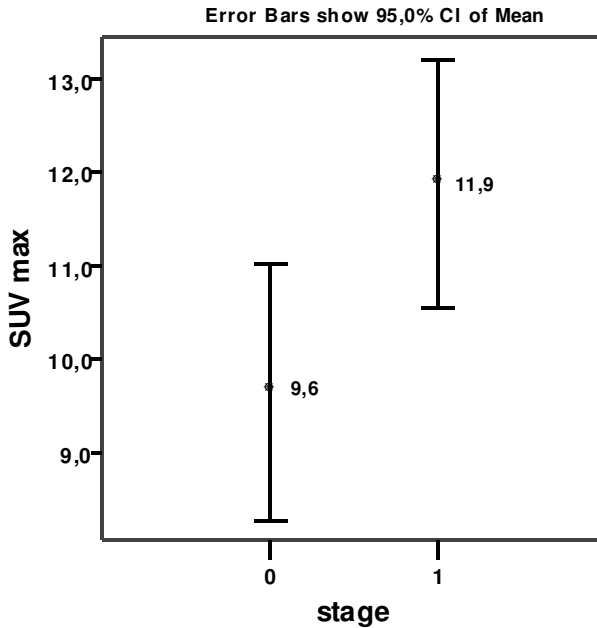
Figure 1: Error bars (95 CI of mean) significance differences in SUVmax between LD (0) and ED (1) (p-value 0.02)
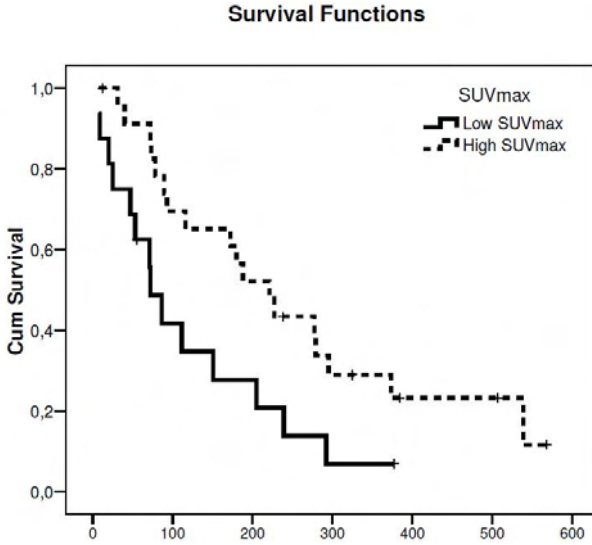
Figure 2: Overall survival curve, all patients diagnosed ED. Lower curve (0) are the patients with a low SUVmax, upper curve (1) are the patients with a high SUVmax (p= 0.005)

Figure 3: Overall survival curve, all patients diagnosed ED and treated with chemotherapy. Lower curve (0) are the patients with a low SUVmax, upper curve (1) are the patients with a high SUVmax (p= 0.008)

Figure 4: Progression-free survival curve, all patients diagnosed ED and treated with chemotherapy. Lower curve (0) are the patients with a low SUVmax, upper curve (1) are the patients with a high SUVmax (p= 0.002)
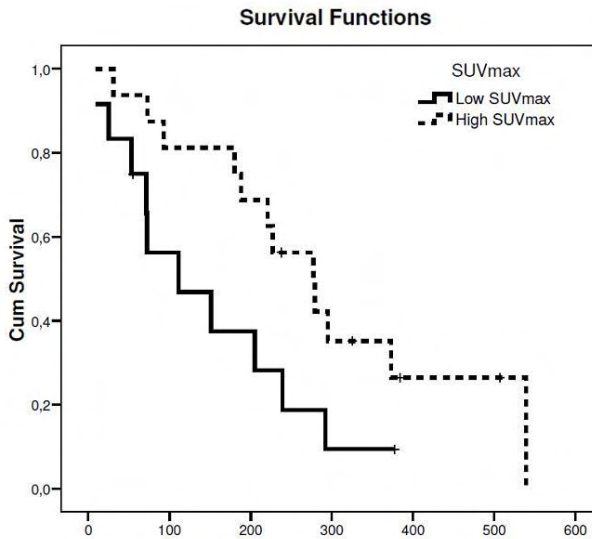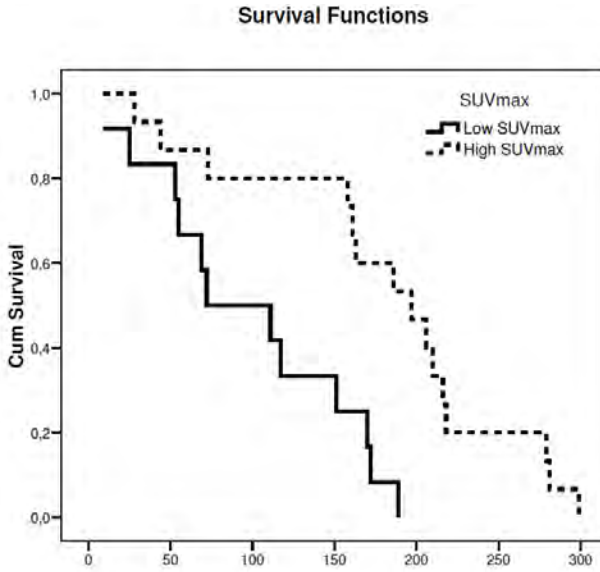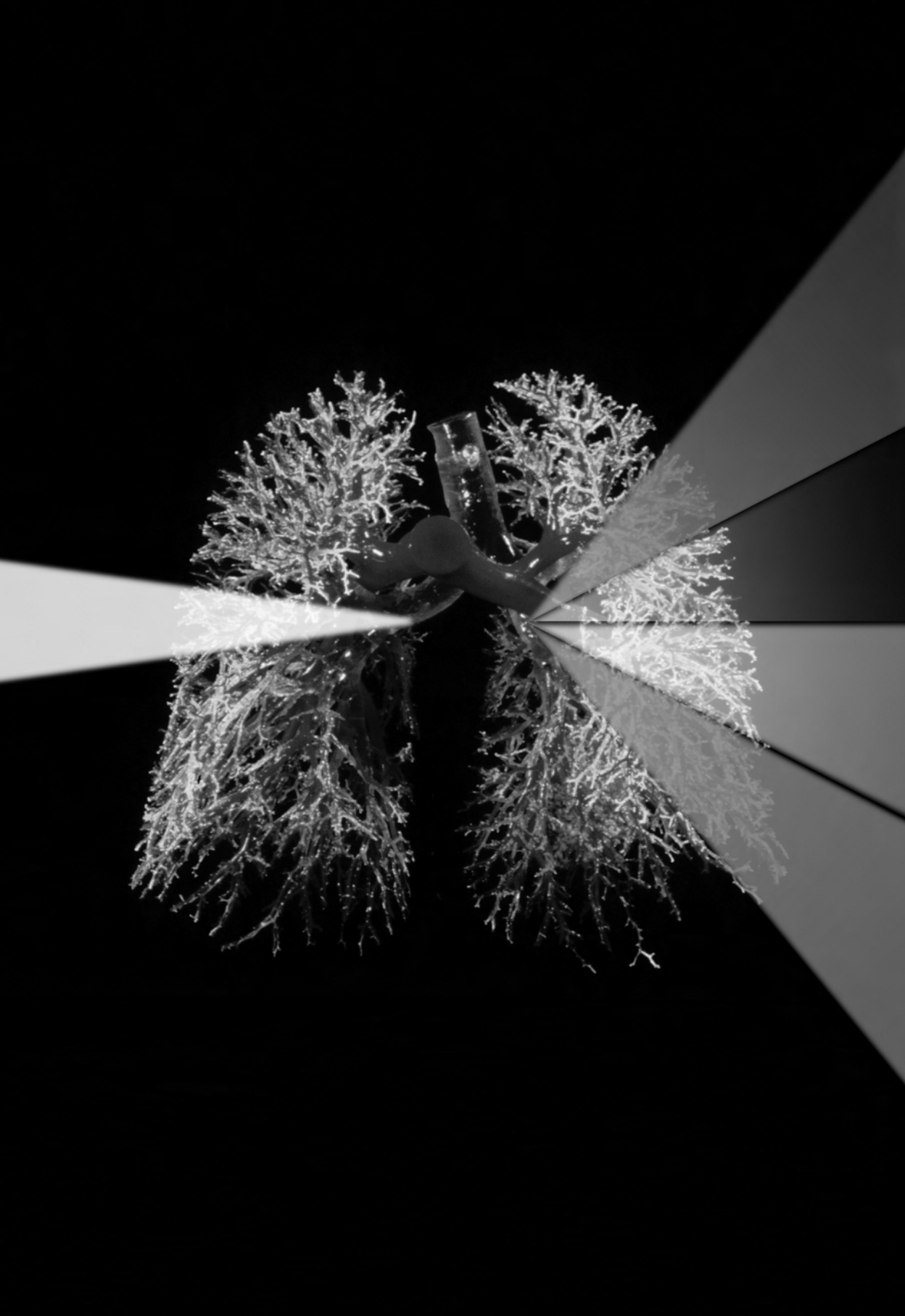
References

1. Janssen-Heijnen ML, Coebergh JW. The changing epidemiology of lung cancer in Europe. Lung Cancer 2003; 41: 245-258.
2. Serke M, Schonfeld N. [Diagnosis and staging of lung cancer]. Dtsch Med Wochenschr 2007; 132: 1165-1169.
3. Azad A, Chionh F, Scott AM et al. High Impact of (18)F-FDG-PET on Management and Prognostic Stratification of Newly Diagnosed Small Cell Lung Cancer. Mol Imaging Biol 2009 Epub ahead of print.
4. Shepherd FA, Crowley J, Van Houtte P et al. The International Association for the Study of Lung Cancer lung cancer staging project: proposals regarding the clinical staging of small cell lung cancer in the forthcoming (seventh) edition of the tumor, node, metastasis classification for lung cancer. J Thorac Oncol 2007; 2: 1067-1077.
5. Hansen O, Sorensen P, Hansen KH. The occurrence of hyponatremia in SCLC and the influence on prognosis A retrospective study of 453 patients treated in a single institution in a 10-year period. Lung Cancer 2009; 111-114.
6. Tas F, Aydiner A, Demir C, Topuz E. Serum lactate dehydrogenase levels at presentation predict outcome of patients with limited-stage small-cell lung cancer. Am J Clin Oncol 2001; 24: 376-378.
7. Cerfolio RJ, Bryant AS, Ohja B, Bartolucci AA. The maximum standardized uptake values on positron emission tomography of a non-small cell lung cancer predict stage, recurrence, and survival. J Thorac Cardiovasc Surg 2005; 130: 151-159.
8. Borst GR, Belderbos JS, Boellaard R et al. Standardised FDG uptake: a prognostic factor for inoperable non-small cell lung cancer. Eur J Cancer 2005; 41: 1533-1541.
9. Higashi K, Ueda Y, Arisaka Y et al. 18F-FDG uptake as a biologic prognostic factor for recurrence in patients with surgically resected non-small cell lung cancer. J Nucl Med 2002; 43: 39-45.
10. Jeong HJ, Min JJ, Park JM et al. Determination of the prognostic value of [(18)F]fluorodeoxyglucose uptake by using positron emission tomography in patients with non-small cell lung cancer. Nucl Med Commun 2002; 23: 865-870.
11. Eschmann SM, Friedel G, Paulsen F et al. Is standardised (18)F-FDG uptake value an outcome predictor in patients with stage III non-small cell lung cancer? Eur J Nucl Med Mol Imaging 2006; 33: 263-269.
12. Lee YJ, Cho A, Cho BC et al. High tumor metabolic activity as measured by fluorodeoxyglucose positron emission tomography is associated with poor prognosis in limited and extensive stage small-cell lung cancer. Clin Cancer Res 2009; 15: 2426-2432.
13. Blum R, MacManus MP, Rischin D et al. Impact of positron emission tomography on the management of patients with small-cell lung cancer: preliminary experience. Am J Clin Oncol 2004; 27: 164-171.
14. Bradley JD, Dehdashti F, Mintun MA et al. Positron emission tomography in limited-stage small-cell lung cancer: a prospective study. J Clin Oncol 2004; 22: 3248-3254.
15. Brink I, Schumacher T, Mix M et al. Impact of [18F]FDG-PET on the primary staging of small-cell lung cancer. Eur J Nucl Med Mol Imaging 2004; 31: 1614-1620.
16. Kamel EM, Zwahlen D, Wyss MT et al. Whole-body (18)F-FDG PET improves the management of patients with small cell lung cancer. J Nucl Med 2003; 44: 1911-1917.
17. Berghmans T, Dusart M, Paesmans M et al. Primary tumor standardized uptake value (SUVmax) measured on fluorodeoxyglucose positron emission tomography (FDG-PET) is of prognostic value for survival in non-small cell lung cancer (NSCLC): a systematic review and meta-analysis (MA) by the European Lung Cancer Working Party for the IASLC Lung Cancer Staging Project. J Thorac Oncol 2008; 3: 6-12.
18. Chen JC, Huang TW, Cheng YL et al. Prognostic value of 18-FDG uptake in early stage NSCLC. Thorac Cardiovasc Surg 2009; 57: 413-416.
19. Dooms C, van Baardwijk A, Verbeken E et al. Association between 18F-fluoro-2-deoxy-D-glucose uptake values and tumor vitality: prognostic value of positron emission tomography in early-stage non-small cell lung cancer. J Thorac Oncol 2009; 4: 822-828.
20. Um SW, Kim H, Koh WJ et al. Prognostic value of 18F-FDG uptake on positron emission tomography in patients with pathologic stage I non-small cell lung cancer. J Thorac Oncol 2009; 4: 1331-1336.

21.   Lee KH, Lee SH, Kim DW et al. High fluorodeoxyglucose uptake on positron emission tomography in patients with advanced non-small cell lung cancer on platinum-based combination chemotherapy. Clin Cancer Res 2006; 12: 4232-4236.
22.   Bural G, Torigian DA, Houseni M et al. Tumor metabolism measured by partial volume corrected standardized uptake value varies considerably in primary and metastatic sites in patients with lung cancer. A new observation. Hell J Nucl Med 2009; 12: 218-222.

General discussion and summary

Detection of premalignant lesions using optical imaging techniques

Lung cancer is a disease with a poor prognosis [1]. Due to nonspecific symptoms, most of the patients are diagnosed with advanced stage of the disease when therapeutic options are limited. Detection at an earlier stage or in a premalignant phase seems to increase survival [2].

At the moment, premalignant lesions are too small for detection by radiological or nuclear modalities. Only by endoscopic techniques detection is possible. In the last 20 years improved imaging techniques with better diagnostic yield for premalignant lesions have been developed [3, 4], but all these techniques have limitations. Detection of premalignant lesions can be divided into wide-field optic imaging and point (spectroscopic) techniques. In **chapter 2** these different imaging techniques are discussed. Current knowledge of biological changes in premalignant lesions and the advantages and limitations of each imaging technique are described. To improve detection of premalignant lesions it is necessary to combine several techniques. We suggest that the highest potential value will be the combination of autofluorescence bronchoscopy with optical coherence tomography (OCT) and differential path length spectroscopy (DPS). Autofluorescence bronchoscopy is the wide-field optical technique which has been studied most. This technique is able to detect potential suspect lesions, however specificity is limited. OCT and DPS are able to confirm the positive lesions seen by autofluorescence bronchoscopy. OCT is able to measure epithelial thickness. DPS is able to inform about local physiology, such as peripheral microvascular saturation, vessel diameter and blood volume fraction. DPS and OCT can be used separately during bronchoscopy but for clinical practice, to save time, a new probe should be developed. This probe should contain two 440 μm fibers incorporated in the protective tube of the OCT probe. These fibers have to be positioned in such a way that they will not disturb the OCT imaging. This is possible when the DPS fibers are located on the tip of the probe and pass by the OCT prism at the back site. In this way OCT view will not be hampered by the DPS fibers and DPS measurements could be performed by placing the tip of the probe on the area of interest.

Differential path-length spectroscopy (DPS) during bronchoscopy in lung cancer

DPS is a spectroscopic technique, which is able to provide information about local physiology of investigated areas [5, 6]. A DPS measuring system that could determine spectroscopy during bronchoscopy *in vivo* was developed. Microvascular saturation of peripheral tumor tissue is one of the physiology parameters that can be obtained. It is not only interesting to use DPS technique in premalignant lesions but also in malignant lesions. Hypoxia is well known in solid tumors and Bard *et al.* detected a decrease of peripheral microvascular saturation in bronchial carcinomas compared to normal tissue with DPS measurements during bronchoscopy [6].

In **chapter 3** the relation between hypoxia related protein hypoxia-inducible-factor 1a (HIF1a) and microvascular saturation, measured by DPS, is discussed. Elevated HIF1a expression is caused by hypoxia [7-10]. The aim of the study was to correlate the spectroscopic measurements with an independent parameter for hypoxia. DPS measurements were performed in normal and malignant lung lesions. A positive correlation between HIF1a expression and low microvascular

saturation of bronchial tissue measured by DPS was found. This study showed that non-invasive DPS measurements do represent tissue physiology.

Historically, lung cancer is subdivided in Non-Small Cell Lung Cancer (NSCLC) and Small Cell Lung Cancer (SCLC) due to its prognosis and treatment options [11, 12]. Because of recent new therapeutic modalities, there is more emphasis to subdivide lung cancer into the four major subclassifications: adenocarcinomas (ADC), squamous cell carcinomas (SCC), large cell carcinomas (LCC) and SCLC [13-15]. In **chapter 4** the hypoxia related parameter microvascular saturation was studied in subtypes of lung cancer. It was shown that there was no difference in saturation between NSCLC and SCLC, although significant differences between the histological subclassifications were observed. ADC and SCC had a higher microvascular saturation compared to LCC and SCLC. The lower microvascular saturation of LCC and SCLC suggests a poorer vascular network due to the type of tumor. No differences in survival were observed between high and low saturated carcinomas. Therefore, peripheral microvascular saturation, measured with DPS, is not a prognostic parameter. More research has to be performed to determine the impact of differences in peripheral microvascular saturation of histological tumor subtypes. When reflectance spectroscopy would only be performed in stage I or II tumors, microvascular saturation might be a prognostic marker. As these tumors are seldom seen with bronchscopy, these measurements have to be performed during computer tomography guided transthoracic puncture. Additionally, reflectance spectroscopy might also help the physician locating the peripheral tumor during the procedure.

Spectroscopy during endoscopic ultrasound-guided fine needle aspiration

Staging is important in lung cancer for prognosis and treatment [16]. Nowadays, new techniques like endoscopic ultrasound-guided fine needle aspiration (EUS-FNA), have been incorporated in the work-up of staging [17]. This EUS-FNA technique is less invasive compared to mediastinoscopy. Although mediastinoscopy is still gold standard, EUS-FNA is an interesting alternative considering it is less expensive, and less likely to induce complications than surgical staging procedures [18-22]. EUS-FNA shows a high diagnostic yield, however the false negative rate is a problem [19-22]. It is known that the vasculature changes in malignant lymph nodes. Aberrant vessels, displacement of vessels or even avascular areas of the central lymph nodes have been observed [23, 24]. *In vivo* determination of lymph node physiology might improve the diagnostic value. In **chapter 5** the incorporation of single fiber reflectance spectroscopy during EUS-FNA is described. To obtain spectroscopic data from lymph nodes a probe had to be made which was small enough to be guided through the EUS needle. For this study setup, a new mathematical model had to be developed to analyze the reflectance spectroscopy data. Additionally absorber bilirubin was added in order to gain a better fit. Also information about manipulation within the lymph nodes was gained. Pressure of the probe on the tissue or a release afterwards resulted in differences in lymph node physiology. In this chapter the technical feasibility of single fiber reflectance spectroscopy is described.

In **chapter 6** the first clinical pilot study on single fiber reflectance spectroscopy during EUS-FNA is reported. Single fiber reflectance spectroscopy was successfully performed without complications. The technique was performed in small normal lymph nodes and enlarged malignant lymph nodes. Differences in

microvascular saturation and blood volume fractions were observed between malignant and normal lymph nodes. Both microvascular saturation and blood volume fraction were lower in malignant lymph nodes. This pilot study showed that single fiber reflectance spectroscopy measurement is sensitive for vascular changes in lymph nodes.

Functional imaging in Small Cell Lung Cancer (SCLC)
Apart from optical imaging techniques, functional imaging modalities have the ability to provide information about tumor microenvironment as well. Reflectance spectroscopy informs about the microenvironment of a small area, often not more than 160 µm deep. Functional imaging techniques provide information about a larger area and furthermore provide complementary information (e.g. glycolysis). PET scanning has become a standard procedure in staging and tumor work up in NSCLC [25]. In contrast to NSCLC, in SCLC bone scintigraphy is advised instead of PET scanning, because of the high incidence of bone metastases. Although several studies showed a higher sensitivity in the detection of bone metastasis with PET scanning compared to bone scintigraphy [26-28], PET scanning has not yet been accepted as a standard tool in the staging procedure of patients with SCLC.

In **chapter 7** the role of PET scanning in the detection of soft tissue metastases in patients with SCLC has been studied. In this study PET scanning was able to find additional soft tissue lesions that had not been found by the regular work up. The PET scan was also able to refute suspect lesions detected by the CT scan. PET scan was responsible for stage shift in 7.9%. The parameter maximal standard uptake value (SUVmax) has been studied extensively in patients with NSCLC [29-33]. Most of these studies demonstrated a low SUVmax value is correlated with a better prognosis. In **chapter 8** the SUVmax value in patients diagnosed with SCLC has been studied. In this chapter it becomes clear that SUVmax seems to be a predictive marker. Patients diagnosed with extended disease (ED) and a high SUVmax value had longer overall survival and longer progression free survival after chemotherapy treatment. Metabolic activity was higher in ED patients compared to LD.

DPS measurements obtained during bronchoscopy showed low microvascular saturation in the SCLC group. Also mediastinal lymph nodes of patients with SCLC had low microvascular saturation. Therefore, it can be hypothesized that PET scanning with a 18F fluoromisonidazole tracer will be of value in patients diagnosed with SCLC. This tracer, which is sensitive for hypoxia, should be able to distinguish between a reactive lymph node and a malignant lymph node.

Future perspective
As described in the thesis, a study using with OCT and DPS has been proposed to improve the detection of premalignant lesions. This will show the additive value of the combination of the two point imaging techniques. At first, this study should be performed in patients with a high risk for lung cancer. This group includes patients after curative resections of NSCLC, patients with head and neck tumors, or with a smoking history. Preferably a randomized trial with two groups should be performed: single autofluorescence bronchoscopy versus autofluorescence bronchoscopy combined with OCT and DPS. Surveillance autofluorescence bronchoscopy with or without point measurement techniques should be performed

every 3-6 months for patients with severe dysplasia or CIS [34], otherwise every 12 month for screening.

There are still many questions about microenvironmental changes of tumors during treatment of tumors. DPS measurements may be of value for *in vivo* analysis of the microenvironment. Studies in which tumor vascularization is examined by DPS before and after treatment with angiogenesis inhibitors or vascular disrupting agents may provide information about the influence of tumor vascularization on the choice of treatment. Also questions about how angiogenesis inhibitors or vascular disrupting agents change the tumor vascularization after treatment might be answered.

In this thesis, the first study on single fiber reflectance spectroscopy during EUS-FNA was described. Whether single fiber reflectance spectroscopy can reduce the false negative rate of malignancy should be the subject of further studies. All spectroscopically measured lymph nodes which are negative on cytology by EUS-FNA, should be confirmed by mediastinoscopy to establish the value of reflectance spectroscopy in this group. By using spectroscopy during EUS-FNA more basic questions about malignant transformation of lymph nodes may be answered as well.

PET scanning in patients with SCLC is not incorporated in the staging standards but most studies showed additional value of this imaging technique [27, 28, 35-39]. In this thesis it was found to add to staging. Further research should compare standard staging (CT scan and bone-scintigraphy) with PET-CT scan staging. In addition we have found indications that SUV values obtained during PET scan may be predictive. Further studies in larger populations have to be performed to confirm our findings. Whether SUV may add to the choice and duration of treatments should be studied next.

General conclusion

Optical imaging plays an important role in the detection of premalignant lesions. One of these optical imaging techniques is DPS. This technique is able to inform about the microvascular saturation, which is correlated with HIF1a expression. DPS can be used during bronchoscopy to provide information about microvascular saturation in the different histological subclassifications of lung cancer.

Furthermore it was possible to obtain useful spectra of mediastinal lymph nodes during EUS-FNA. These measurements can be done during an EUS-FNA procedure without complications. Differences in spectra and physiological parameters between normal and malignant lymph nodes were seen.

At last the value of PET scanning in SCLC was examined. We showed that PET scanning provided additional information in the staging of patients diagnosed with SCLC. With PET scanning SUVmax value can be obtained, which seemed to be a predictive marker. Patients with ED SCLC and a high SUVmax had better overall survival and progression free survival after chemotherapy treatment.

References

1. Jemal A, Siegel R, Ward E, Murray T, Xu J, Thun MJ. Cancer statistics, 2007. CA Cancer J Clin 2007;57:43-66.
2. Mountain CF. Revisions in the International System for Staging Lung Cancer. Chest 1997;111:1710-7.
3. Hung J, Lam S, LeRiche JC, Palcic B. Autofluorescence of normal and malignant bronchial tissue. Lasers Surg Med 1991;11:99-105.
4. Lam S, MacAulay C, Hung J, LeRiche J, Profio AE, Palcic B. Detection of dysplasia and carcinoma in situ with a lung imaging fluorescence endoscope device. J Thorac Cardiovasc Surg 1993;105:1035-40.
5. Amelink A, Sterenborg HJ, Bard MP, Burgers SA. In vivo measurement of the local optical properties of tissue by use of differential path-length spectroscopy. Opt Lett 2004;29:1087-9.
6. Bard MP, Amelink A, Hegt VN, et al. Measurement of hypoxia-related parameters in bronchial mucosa by use of optical spectroscopy. Am J Respir Crit Care Med 2005;171:1178-84.
7. Denko NC. Hypoxia, HIF1 and glucose metabolism in the solid tumour. Nat Rev Cancer 2008;8:705-13.
8. Enatsu S, Iwasaki A, Shirakusa T, et al. Expression of hypoxia-inducible factor-1 alpha and its prognostic significance in small-sized adenocarcinomas of the lung. Eur J Cardiothorac Surg 2006;29:891-5.
9. Hung JJ, Yang MH, Hsu HS, Hsu WH, Liu JS, Wu KJ. Prognostic significance of hypoxia-inducible factor-1alpha, TWIST1 and Snail expression in resectable non-small cell lung cancer. Thorax 2009;64:1082-9.
10. Ryan HE, Lo J, Johnson RS. HIF-1 alpha is required for solid tumor formation and embryonic vascularization. Embo J 1998;17:3005-15.
11. Hirsch FR, Spreafico A, Novello S, Wood MD, Simms L, Papotti M. The prognostic and predictive role of histology in advanced non-small cell lung cancer: a literature review. J Thorac Oncol 2008;3:1468-81.
12. Selvaggi G, Scagliotti GV. Histologic subtype in NSCLC: does it matter? Oncology (Williston Park) 2009;23:1133-40.
13. Scagliotti GV, Parikh P, von Pawel J, et al. Phase III study comparing cisplatin plus gemcitabine with cisplatin plus pemetrexed in chemotherapy-naive patients with advanced-stage non-small-cell lung cancer. J Clin Oncol 2008;26:3543-51.
14. Tiseo M, Bartolotti M, Gelsomino F, Ardizzoni A. First-line treatment in advanced non-small-cell lung cancer: the emerging role of the histologic subtype. Expert Rev Anticancer Ther 2009;9:425-35.
15. Kubota K, Niho S, Enatsu S, et al. Efficacy differences of pemetrexed by histology in pretreated patients with stage IIIB/IV non-small cell lung cancer: review of results from an open-label randomized phase II study. J Thorac Oncol 2009;4:1530-6.
16. Groome PA, Bolejack V, Crowley JJ, et al. The IASLC Lung Cancer Staging Project: validation of the proposals for revision of the T, N, and M descriptors and consequent stage groupings in the forthcoming (seventh) edition of the TNM classification of malignant tumours. J Thorac Oncol 2007;2:694-705.
17. van Beek FT, Maas KW, Timmer R, Seldenrijk CA, de Bruin PC, Schramel FM. [Oesophageal endoscopic ultrasound with fine-needle aspiration biopsy in the staging of non-small-cell lung carcinoma; results from 43 patients]. Ned Tijdschr Geneeskd 2006;150:144-50.
18. Annema JT, Rabe KF. State of the art lecture: EUS and EBUS in pulmonary medicine. Endoscopy 2006;38 Suppl 1:S118-22.
19. Caddy G, Conron M, Wright G, Desmond P, Hart D, Chen RY. The accuracy of EUS-FNA in assessing mediastinal lymphadenopathy and staging patients with NSCLC. Eur Respir J 2005;25:410-5.
20. Tournoy KG, De Ryck F, Vanwalleghem LR, et al. Endoscopic ultrasound reduces surgical mediastinal staging in lung cancer: a randomized trial. Am J Respir Crit Care Med 2008;177:531-5.
21. Talebian M, von Bartheld MB, Braun J, et al. EUS-FNA in the preoperative staging of non-small cell lung cancer. Lung Cancer 2009:Epub ahead of print.

22.   Detterbeck FC, Jantz MA, Wallace M, Vansteenkiste J, Silvestri GA. Invasive mediastinal staging of lung cancer: ACCP evidence-based clinical practice guidelines (2nd edition). Chest 2007;132:202S-20S.
23.   Chikui T, Yuasa K, Maemura S, Kanda S. Change of angiostructure and hemodynamics in lymph node metastases in rabbits. Oral Surg Oral Med Oral Pathol Oral Radiol Endod 2002;93:350-7.
24.   Ahuja AT, Ying M. Sonographic evaluation of cervical lymph nodes. AJR Am J Roentgenol 2005;184:1691-9.
25.   Toloza EM, Harpole L, McCrory DC. Noninvasive staging of non-small cell lung cancer: a review of the current evidence. Chest 2003;123:137S-46S.
26.   Fischer BM, Mortensen J, Langer SW, et al. A prospective study of PET/CT in initial staging of small-cell lung cancer: comparison with CT, bone scintigraphy and bone marrow analysis. Ann Oncol 2007;18:338-45.
27.   Kut V, Spies W, Spies S, Gooding W, Argiris A. Staging and monitoring of small cell lung cancer using [18F]fluoro-2-deoxy-D-glucose-positron emission tomography (FDG-PET). Am J Clin Oncol 2007;30:45-50.
28.   Chin R, Jr., McCain TW, Miller AA, et al. Whole body FDG-PET for the evaluation and staging of small cell lung cancer: a preliminary study. Lung Cancer 2002;37:1-6.
29.   Higashi K, Ueda Y, Arisaka Y, et al. 18F-FDG uptake as a biologic prognostic factor for recurrence in patients with surgically resected non-small cell lung cancer. J Nucl Med 2002;43:39-45.
30.   Jeong HJ, Min JJ, Park JM, et al. Determination of the prognostic value of [(18)F]fluorodeoxyglucose uptake by using positron emission tomography in patients with non-small cell lung cancer. Nucl Med Commun 2002;23:865-70.
31.   Chen JC, Huang TW, Cheng YL, et al. Prognostic value of 18-FDG uptake in early stage NSCLC. Thorac Cardiovasc Surg 2009;57:413-6.
32.   Dooms C, van Baardwijk A, Verbeken E, et al. Association between 18F-fluoro-2-deoxy-D-glucose uptake values and tumor vitality: prognostic value of positron emission tomography in early-stage non-small cell lung cancer. J Thorac Oncol 2009;4:822-8.
33.   Um SW, Kim H, Koh WJ, et al. Prognostic value of 18F-FDG uptake on positron emission tomography in patients with pathologic stage I non-small cell lung cancer. J Thorac Oncol 2009;4:1331-6.
34.   Kennedy TC, McWilliams A, Edell E, et al. Bronchial intraepithelial neoplasia/early central airways lung cancer: ACCP evidence-based clinical practice guidelines (2nd edition). Chest 2007;132:221S-33S.
35.   Azad A, Chionh F, Scott AM, et al. High Impact of (18)F-FDG-PET on Management and Prognostic Stratification of Newly Diagnosed Small Cell Lung Cancer. Mol Imaging Biol 2009.
36.   Blum R, MacManus MP, Rischin D, Michael M, Ball D, Hicks RJ. Impact of positron emission tomography on the management of patients with small-cell lung cancer: preliminary experience. Am J Clin Oncol 2004;27:164-71.
37.   Bradley JD, Dehdashti F, Mintun MA, Govindan R, Trinkaus K, Siegel BA. Positron emission tomography in limited-stage small-cell lung cancer: a prospective study. J Clin Oncol 2004;22:3248-54.
38.   Brink I, Schumacher T, Mix M, et al. Impact of [18F]FDG-PET on the primary staging of small-cell lung cancer. Eur J Nucl Med Mol Imaging 2004;31:1614-20.
39.   Kamel EM, Zwahlen D, Wyss MT, Stumpe KD, von Schulthess GK, Steinert HC. Whole-body (18)F-FDG PET improves the management of patients with small cell lung cancer. J Nucl Med 2003;44:1911-7.

Algemene discussie en samenvatting

Opsporing van premaligne laesies door optische beeldvorming

De longkanker is een ziekte met een slechte prognose [1]. Vanwege niet-specifieke symptomen worden de meeste patiënten gediagnosticeerd wanneer er sprake is van een vergevorderd stadium van de ziekte. Op dat moment zijn er beperkte therapeutische opties beschikbaar. Detectie van de ziekte in een eerder stadium of in de premaligne fase lijkt tot langere overleving te leiden [2].

Op dit ogenblik zijn de premaligne laesies te klein voor opsporing met radiologische of nucleaire beeldvorming. Slechts met endoscopische technieken is opsporing mogelijk. De laatste 20 jaar zijn de beeldvormingstechnieken verbeterd wat geresulteerd heeft in betere detectie van premaligne afwijkingen [3, 4], desondanks hebben alle ontwikkelde technieken beperkingen. Detectie van premaligne laesies kan worden verdeeld in "*wide-field optic imaging*" en in "*point (spectroscopic) techniques*". In **hoofdstuk 2** worden de verschillende beeldvormingstechnieken besproken. De huidige kennis van de biologische veranderingen in premaligne laesies wordt beschreven. Vervolgens wordt aangegeven wat de voordelen en beperkingen zijn van elke techniek. Op dit moment is het nog noodzakelijk om verscheidene technieken te combineren om opsporing van premaligne laesies te verbeteren. Wij zijn van mening dat de combinatie van technieken met de grootste potentie is: autofluorescentie bronchoscopie gecombineerd met optical coherence tomography (OCT) en differential path length spectroscopy (DPS). Autofluorescentie bronchoscopie is de meest bestudeerde "*wide-field optic imaging*" techniek. Deze techniek kan verdachte laesies detecteren, nochtans is de specificiteit beperkt. OCT en DPS kunnen worden gebruikt om te bevestigen of laesies, gedetecteerd met autofluorescentie bronchoscopie, daadwerkelijk premaligne zijn. Middels OCT wordt de epitheliale dikte gemeten, DPS geeft informatie over de lokale fysiologie, zoals perifere microvasculaire saturatie, vaatdiameter en bloedvolume fractie. DPS en OCT kunnen los van elkaar worden gebruikt tijdens een bronchoscopie. Om tijdwinst te boeken zou een nieuwe probe gemaakt kunnen worden waarbij twee 440 µm fibers worden ingebracht in de bescherm huls van een OCT probe. Deze twee fibers dienen zo te worden bevestigd dat deze niet het beeld van OCT belemmeren. Dit is mogelijk wanneer de fibers worden bevestigd op het uiteinde van de probe en langs de achterzijde van de OCT-prisma lopen. Hiermee wordt het beeld dat middels OCT wordt verkregen niet verstoord door de twee DPS fibers. Vervolgens kunnen DPS data worden verkregen door het plaatsen van de probe op de gewenste locatie.

Differential path length spectroscopie (DPS) gemeten tijdens bronchoscopie bij patiënten met longkanker

DPS is een spectroscopische techniek die informatie verschaft over de lokale fysiologie van het onderzochte weefsel [5, 6]. Een DPS metingssysteem is ontwikkeld dat de spectra *in vivo* kan bepalen tijdens bronchoscopie. Eén van de verkregen fysiologische parameters is de microvasculaire saturatie van perifeer tumorweefsel. DPS is een techniek die niet alleen waardevol is bij premaligne laesies maar ook in maligne laesies. Het is bekend dat er sprake is van hypoxie in maligniteiten, Bard *et al.* toonden aan dat de perifere microvasculaire saturatie, gemeten met DPS tijdens bronchoscopie, lager is in bronchiale carcinomen in vergelijking met normaal weefsel [6].

In **hoofdstuk 3** word de relatie van hypoxie gerelateerd eiwit hypoxia-inducible-factor 1a (HIF1a) en de microvasculaire saturatie, gemeten met DPS, besproken.

Verhoogde HIF1a expressie wordt veroorzaakt door hypoxie [7-10]. Het doel van de studie was om reflectie spectroscopische metingen te correleren met een onafhankelijke parameter voor hypoxie. DPS metingen zijn gedaan in normaal longweefsel en in maligne longweefsel. Er bleek een correlatie te zijn tussen HIF1a expressie en lage microvasculaire saturatie van het bronchiale weefsel gemeten met DPS. Deze studie toonde aan dat deze niet-invasieve techniek informatie geeft over weefselfysiologie.

In het verleden werd longkanker op basis van prognose en behandelingsopties onderverdeeld in niet-kleincellig longkanker (NSCLC) en kleincellig longkanker (SCLC) [11, 12]. Tegenwoordig zijn er meer therapeutische mogelijkheden en is het beter om longkanker onder te verdelen in vier subklassen op basis van histologie: adenocarcinoom (ADC), plaveiselcel carcinoom (SCC), onge-differentieerde grootcellig longcarcinoom (LCC) en SCLC [13-15]. In **hoofdstuk 4** is de hypoxie parameter microvasculaire saturatie in de verschillende histologische subklassen van longkanker bestudeerd. Er bleek geen verschil te zijn in microvasculaire saturatie van NSCLC en SCLC. Wel werden er significante verschillen waargenomen tussen de histologische subklassen. ADC en SCC hadden een hogere microvasculaire saturatie in vergelijking met LCC en SCLC. De verlaagde microvasculaire saturatie in LCC en SCLC kan veroorzaakt zijn door een slecht vasculair netwerk dat samenhangt met de histologie van de tumor. Er werd geen verschil in overleving aangetoond tussen carcinomen met een hoge en lage saturatie. Perifere microvasculaire saturatie, gemeten met DPS, is daarom geen voorspellende parameter. Meer onderzoek is nodig om aan te tonen wat de klinische toepasbaarheid is van de verschillen in perifere microvasculaire saturatie tussen de histologische subtypen. Wanneer reflectie spectroscopie verricht zou worden in stadium I en II tumoren zou microvasculaire saturatie mogelijk een prognostisch marker zijn. Deze metingen zouden CT geleid trans-thoracaal kunnen worden verricht. De reflectie spectra zouden dan ook de onderzoeker kunnen helpen bij het bepalen van de positie van de perifere tumor.

Spectroscopie tijdens endoscopische echografie met dunne naald aspiratie
Stadiëring is van belang bij de diagnose longkanker, zowel voor prognose als de keus van behandeling [16]. Tegenwoordig zijn nieuwe technieken opgenomen in de stadiërings onderzoeken, zoals endoscopische echografie met dunne naald aspiratie (EUS-FNA) [17]. EUS-FNA is minder invasief dan de gouden standaard mediastinoscopie. EUS-FNA is een interessant alternatief omdat het goedkoper is en waarschijnlijk minder kans op complicaties geeft [18-21]. EUS-FNA heeft een hoge diagnostische opbrengst, hoewel de fout negatieve bevindingen nog een probleem zijn [19-22]. Het is bekend dat vaatopbouw verandert in maligne lymfeklieren. Afwijkende vaten, foutieve aanleg van vaten of zelfs avasculaire gebieden van centrale lymfeklieren zijn waargenomen [23, 24]. *In vivo* determinatie van lymfeklier fysiologie zou de diagnostische waarde kunnen verbeteren. In **hoofdstuk 5** wordt de integratie van single fiber reflectie spectroscopie tijdens EUS-FNA beschreven. Om spectroscopische gegevens van lymfeklieren te verkrijgen moest een probe worden gemaakt, die klein genoeg was om door de EUS naald te worden geleid. Voor deze studieopstelling moest een nieuw wiskundig model worden ontwikkeld om de reflectie spectroscopische data te analyseren. Licht absorberend bilirubine werd toegevoegd om beter passende spectra te verkrijgen. Ook werd bestudeerd wat manipulatie binnen in de lymfeklieren voor effect heeft op de spectra. De druk van de probe op het weefsel

of het terug trekken van de probe na meting resulteerde in verschillen in lymfeklier fysiologie. In dit hoofdstuk is technische haalbaarheid aan van single fiber reflectie spectroscopie beschreven.

In **hoofdstuk 6** wordt de eerste klinische studie van single fiber reflectie spectroscopie tijdens EUS-FNA beschreven. De single fiber reflectie spectroscopie werd met succes uitgevoerd zonder complicaties. De techniek werd uitgevoerd in kleine normale lymfeklieren en vergrootte maligne lymfeklieren. Er werden verschillen waargenomen in microvasculaire saturatie en bloedvolume fracties tussen maligne en normale lymfeklieren. Zowel microvasculaire saturatie als bloedvolume fractie was lager in maligne lymfeklieren. Dit onderzoek toonde aan dat single fiber reflectie spectroscopie gevoelig is voor vasculaire veranderingen in lymfeklieren.

Functionele beeldvorming in kleincellig long carcinoom (SCLC)

Naast optische technieken kunnen ook functionele beeldvormingstechnieken informatie verschaffen over het tumormilieu. Reflectie spectroscopie geeft alleen informatie over een klein gebied, vaak niet dieper dan 160 µm. Functionele technieken kunnen informatie geven over grotere gebieden en daarbij aanvullende informatie geven (bijvoorbeeld over glycolyse). Het verrichten van een PET scan is onderdeel van de standaardprocedure in de stadiëring van NSCLC [25]. In SCLC wordt de skeletscan, in plaats van de PET scan, geadviseerd vanwege de hoge incidentie van botmetastasen. Hoewel verschillende studies een hogere gevoeligheid in het opsporen van botmetastasen toonden bij gebruik van een PET scan in vergelijking met een skeletscan [26-28], is het verrichten van een PET scan nog niet ingevoerd als standaard beeldvorming bij de stadiërings procedure van patiënten met SCLC. In **hoofdstuk 7** is de rol van de PET scan in de opsporing van weke delen metastasen in patiënten met SCLC bestudeerd. In deze studie kon de PET scan weke delen laesies aantonen die niet bij de standaard beeldvormende technieken werden gevonden. De PET scan kon ook verdachte laesies weerleggen die door de CT scan als maligne beschouwd waren. Door de PET scan was er in 7,9% van de patiënten een verandering van stadium.

De parameter maximale gestandaardiseerde opname waarde (SUVmax) is uitvoerig bestudeerd in patiënten met NSCLC [29-33]. Het merendeel van deze studies toonde aan dat een lage SUVmax waarde gerelateerd is met een betere prognose. In **hoofdstuk 8** is de SUVmax waarde in patiënten met SCLC bestudeerd. SUVmax blijkt een predictieve marker te zijn. Patiënten met uitgebreide ziekte en een hoge SUVmax waarde hadden een langere overleving en een langere ziekte-vrije overleving wanneer zij behandeld werden met chemotherapie. Metabole activiteit was hoger in patiënten met uitgebreide ziekte dan patiënten zonder uitgebreide ziekte.

Toekomst perspectief

Zoals beschreven in dit proefschrift kan de opsporing van premaligne laesies worden verbeterd door een studie te starten waarin autofluorescentie bronchoscopie gecombineerd wordt met OCT en DPS. Deze studie moet de toegevoegde waarde van de combinatie van deze twee "*point (spectroscopic) techniques*" aantonen. Deze studie zou aanvankelijk in hoog risico patiënten met longkanker moeten worden uitgevoerd. Deze groep omvat: NSCLC patiënten waarbij een curatieve resectie heeft plaatsgevonden, patiënten met hoofd-hals tumoren, of patiënten die veel gerookt hebben. Het zou bij voorkeur een

gerandomiseerde studie moeten zijn met twee groepen: autofluorescentie bronchoscopie versus autofluorescentie bronchoscopie gecombineerd met OCT en DPS. Controle autofluorescentie bronchoscopie, met of zonder "*point (spectroscopic) techniques*", dient in patiënten met ernstige dysplasie of carcinoma in situ om de 3-6 maanden uitgevoerd te worden [34]. Bij de overige patiënten dient controle autofluorescentie bronchoscopie, met of zonder "*point (spectroscopic) techniques*", om de 12 maanden plaats te vinden.

Er is nog veel onduidelijkheid over de veranderingen van het tumor micromilieu tijdens behandeling. DPS metingen kunnen van betekenis zijn voor *in vivo* analyse van het tumor micromilieu. DPS metingen, voor en na behandeling met angiogeneseremmers of vascular disrupting agents, kunnen informatie geven over werking van deze medicatie. Andersom zou onderzocht kunnen worden wat het effect is van angiogeneseremmers of vascular disrupting agents op tumor vascularisatie.

In dit proefschrift wordt de eerste studie over single fiber reflectie spectroscopie tijdens EUS-FNA beschreven. Of single fiber reflectie spectroscopie het aantal fout negatieve bevindingen van EUS-FNA in maligne lymfeklieren kan verlagen moet bekeken worden in een volgende studie. Patiënten die lymfeklieren hebben die tijdens EUS-FNA meting met reflectie spectroscopie cytologisch negatief blijken te zijn, zouden vervolgens een mediastinoscopie moeten ondergaan om de waarde van reflectie spectroscopie te bepalen. Door spectroscopie tijdens EUS-FNA te gebruiken, kunnen meer onderzoeksvragen over maligne transformatie van lymfeklieren worden beantwoord.

Vooralsnog is een PET scan bij patiënten met SCLC nog niet opgenomen in de standaard stadiërings onderzoeken, maar meerdere studies toonden de additieve waarde van deze functionele beeldvormende techniek [27, 28, 35-39]. In dit proefschrift werd de toegevoegde waarde van de PET scan bij stadiering beschreven. Verder onderzoek zou moeten plaatsvinden waarbij de standaard stadiërings onderzoeken, bestaande uit CT-scan en skeletscan, vergeleken moeten worden met PET-CT-scan. Daarnaast blijkt dat de SUVmax waarden die tijdens PET scan worden verkregen een predictieve waarde hebben. Verdere studies met een grotere groep patiënten moet worden uitgevoerd om onze bevindingen te bevestigen. Of SUVmax waarden kunnen bijdragen aan de keus en de duur van behandeling zou moeten worden uitgezocht.

Algemene conclusie

Optische weergave speelt een belangrijke rol bij de opsporing van premaligne laesies. Één van deze optische technieken is DPS. Deze techniek geeft informatie over de microvasculaire saturatie en is gerelateerd aan HIF1a expressie. DPS kan worden gebruikt tijdens bronchoscopie en kan informatie geven over de microvasculaire saturatie in de verschillende histologische subklassen. Daarnaast was het mogelijk om spectra van mediastinale lymfeklieren tijdens EUS-FNA te verkrijgen. Deze metingen kunnen worden verricht zonder complicaties. Er waren verschillen meetbaar in spectra en fysiologische parameters tussen normale en maligne lymfeklieren. Tot slot is de waarde van PET scanning in SCLC onderzocht. Aangetoond werd dat PET scanning extra informatie geeft wat leidt tot beter stadiëren van patiënten met SCLC. Met de PET scan kan een SUVmax waarde worden verkregen, dit lijkt een predictieve marker te zijn. SCLC patiënten met uitgebreide ziekte en een hoge SUVmax waarde hebben een betere overleving en ziekte-vrije overleving na behandeling met chemotherapie.

Referenties

1. Jemal A, Siegel R, Ward E et al. Cancer statistics, 2007. CA Cancer J Clin 2007; 57: 43-66.
2. Mountain CF. Revisions in the International System for Staging Lung Cancer. Chest 1997; 111: 1710-1717.
3. Hung J, Lam S, LeRiche JC, Palcic B. Autofluorescence of normal and malignant bronchial tissue. Lasers Surg Med 1991; 11: 99-105.
4. Lam S, MacAulay C, Hung J et al. Detection of dysplasia and carcinoma in situ with a lung imaging fluorescence endoscope device. J Thorac Cardiovasc Surg 1993; 105: 1035-1040.
5. Amelink A, Sterenborg HJ, Bard MP, Burgers SA. In vivo measurement of the local optical properties of tissue by use of differential path-length spectroscopy. Opt Lett 2004; 29: 1087-1089.
6. Bard MP, Amelink A, Hegt VN et al. Measurement of hypoxia-related parameters in bronchial mucosa by use of optical spectroscopy. Am J Respir Crit Care Med 2005; 171: 1178-1184.
7. Denko NC. Hypoxia, HIF1 and glucose metabolism in the solid tumour. Nat Rev Cancer 2008; 8: 705-713.
8. Enatsu S, Iwasaki A, Shirakusa T et al. Expression of hypoxia-inducible factor-1 alpha and its prognostic significance in small-sized adenocarcinomas of the lung. Eur J Cardiothorac Surg 2006; 29: 891-895.
9. Hung JJ, Yang MH, Hsu HS et al. Prognostic significance of hypoxia-inducible factor-1alpha, TWIST1 and Snail expression in resectable non-small cell lung cancer. Thorax 2009; 64: 1082-1089.
10. Ryan HE, Lo J, Johnson RS. HIF-1 alpha is required for solid tumor formation and embryonic vascularization. Embo J 1998; 17: 3005-3015.
11. Hirsch FR, Spreafico A, Novello S et al. The prognostic and predictive role of histology in advanced non-small cell lung cancer: a literature review. J Thorac Oncol 2008; 3: 1468-1481.
12. Selvaggi G, Scagliotti GV. Histologic subtype in NSCLC: does it matter? Oncology (Williston Park) 2009; 23: 1133-1140.
13. Scagliotti GV, Parikh P, von Pawel J et al. Phase III study comparing cisplatin plus gemcitabine with cisplatin plus pemetrexed in chemotherapy-naive patients with advanced-stage non-small-cell lung cancer. J Clin Oncol 2008; 26: 3543-3551.
14. Tiseo M, Bartolotti M, Gelsomino F, Ardizzoni A. First-line treatment in advanced non-small-cell lung cancer: the emerging role of the histologic subtype. Expert Rev Anticancer Ther 2009; 9: 425-435.
15. Kubota K, Niho S, Enatsu S et al. Efficacy differences of pemetrexed by histology in pretreated patients with stage IIIB/IV non-small cell lung cancer: review of results from an open-label randomized phase II study. J Thorac Oncol 2009; 4: 1530-1536.
16. Groome PA, Bolejack V, Crowley JJ et al. The IASLC Lung Cancer Staging Project: validation of the proposals for revision of the T, N, and M descriptors and consequent stage groupings in the forthcoming (seventh) edition of the TNM classification of malignant tumours. J Thorac Oncol 2007; 2: 694-705.
17. van Beek FT, Maas KW, Timmer R et al. [Oesophageal endoscopic ultrasound with fine-needle aspiration biopsy in the staging of non-small-cell lung carcinoma; results from 43 patients]. Ned Tijdschr Geneeskd 2006; 150: 144-150.
18. Annema JT, Rabe KF. State of the art lecture: EUS and EBUS in pulmonary medicine. Endoscopy 2006; 38 Suppl 1: S118-122.
19. Caddy G, Conron M, Wright G et al. The accuracy of EUS-FNA in assessing mediastinal lymphadenopathy and staging patients with NSCLC. Eur Respir J 2005; 25: 410-415.
20. Tournoy KG, De Ryck F, Vanwalleghem LR et al. Endoscopic ultrasound reduces surgical mediastinal staging in lung cancer: a randomized trial. Am J Respir Crit Care Med 2008; 177: 531-535.
21. Talebian M, von Bartheld MB, Braun J et al. EUS-FNA in the preoperative staging of non-small cell lung cancer. Lung Cancer 2009; Epub ahead of print.
22. Detterbeck FC, Jantz MA, Wallace M et al. Invasive mediastinal staging of lung cancer: ACCP evidence-based clinical practice guidelines (2nd edition). Chest 2007; 132: 202S-220S.

23. Chikui T, Yuasa K, Maemura S, Kanda S. Change of angiostructure and hemodynamics in lymph node metastases in rabbits. Oral Surg Oral Med Oral Pathol Oral Radiol Endod 2002; 93: 350-357.

24. Ahuja AT, Ying M. Sonographic evaluation of cervical lymph nodes. AJR Am J Roentgenol 2005; 184: 1691-1699.

25. Toloza EM, Harpole L, McCrory DC. Noninvasive staging of non-small cell lung cancer: a review of the current evidence. Chest 2003; 123: 137S-146S.

26. Fischer BM, Mortensen J, Langer SW et al. A prospective study of PET/CT in initial staging of small-cell lung cancer: comparison with CT, bone scintigraphy and bone marrow analysis. Ann Oncol 2007; 18: 338-345.

27. Kut V, Spies W, Spies S et al. Staging and monitoring of small cell lung cancer using [18F]fluoro-2-deoxy-D-glucose-positron emission tomography (FDG-PET). Am J Clin Oncol 2007; 30: 45-50.

28. Chin R, Jr., McCain TW, Miller AA et al. Whole body FDG-PET for the evaluation and staging of small cell lung cancer: a preliminary study. Lung Cancer 2002; 37: 1-6.

29. Higashi K, Ueda Y, Arisaka Y et al. 18F-FDG uptake as a biologic prognostic factor for recurrence in patients with surgically resected non-small cell lung cancer. J Nucl Med 2002; 43: 39-45.

30. Jeong HJ, Min JJ, Park JM et al. Determination of the prognostic value of [(18)F]fluorodeoxyglucose uptake by using positron emission tomography in patients with non-small cell lung cancer. Nucl Med Commun 2002; 23: 865-870.

31. Chen JC, Huang TW, Cheng YL et al. Prognostic value of 18-FDG uptake in early stage NSCLC. Thorac Cardiovasc Surg 2009; 57: 413-416.

32. Dooms C, van Baardwijk A, Verbeken E et al. Association between 18F-fluoro-2-deoxy-D-glucose uptake values and tumor vitality: prognostic value of positron emission tomography in early-stage non-small cell lung cancer. J Thorac Oncol 2009; 4: 822-828.

33. Um SW, Kim H, Koh WJ et al. Prognostic value of 18F-FDG uptake on positron emission tomography in patients with pathologic stage I non-small cell lung cancer. J Thorac Oncol 2009; 4: 1331-1336.

34. Kennedy TC, McWilliams A, Edell E et al. Bronchial intraepithelial neoplasia/early central airways lung cancer: ACCP evidence-based clinical practice guidelines (2nd edition). Chest 2007; 132: 221S-233S.

35. Azad A, Chionh F, Scott AM et al. High Impact of (18)F-FDG-PET on Management and Prognostic Stratification of Newly Diagnosed Small Cell Lung Cancer. Mol Imaging Biol 2009.

36. Blum R, MacManus MP, Rischin D et al. Impact of positron emission tomography on the management of patients with small-cell lung cancer: preliminary experience. Am J Clin Oncol 2004; 27: 164-171.

37. Bradley JD, Dehdashti F, Mintun MA et al. Positron emission tomography in limited-stage small-cell lung cancer: a prospective study. J Clin Oncol 2004; 22: 3248-3254.

38. Brink I, Schumacher T, Mix M et al. Impact of [18F]FDG-PET on the primary staging of small-cell lung cancer. Eur J Nucl Med Mol Imaging 2004; 31: 1614-1620.

39. Kamel EM, Zwahlen D, Wyss MT et al. Whole-body (18)F-FDG PET improves the management of patients with small cell lung cancer. J Nucl Med 2003; 44: 1911-1917.

DANKWOORD

Dit boekje was nooit tot stand gekomen zonder de hulp van anderen.
De volgende mensen wil ik daarom graag bedanken:

Prof.dr. H.C. Hoogsteden, beste Henk, hartelijk dank dat je mij de mogelijkheid hebt geboden om dit onderzoek te verrichten. Hoewel op afstand waren onze contacten altijd zinvol en ik wil je dan ook bedanken voor de opbouwende commentaren op de door mij geschreven artikelen. Ook in de toekomst zie ik er naar uit om een deel van mijn opleiding binnen jouw afdeling te kunnen volgen.

Dr. J.G.J.V Aerts, beste Joachim, mijn copromotor, zonder jou was dit proefschrift nooit zo ver gekomen. Jouw inzet, energie, wilskracht en doorzettingsvermogen is onuitputtelijk. Van al je promovendi, ben ik waarschijnlijk degene die jou het meest nodig heeft gehad. Met mijn vele vragen mocht ik je altijd lastig blijven vallen. Alles wat jij doet, doe je met volledige overgave. De manier waarop je onderzoek weet te combineren met je klinische werk in een perifeer ziekenhuis is benijdenswaardig. Ik ken geen arts die zich zo voor zijn patiënten inzet.

Prof.dr.ir. H.J.C.M. Sterenborg, beste Dick, precies een jaar nadat jij als professor je eerste college hebt gegeven, mag ik promoveren. Zonder jou en je groep was dit onderzoek nooit van de grond gekomen. Ik wil je bedanken voor de vele discussies die we hebben gevoerd in dat kleine kamertje op de Westzeedijk. Nu op jullie nieuwe locatie is de werkgroep CODT veel beter op z'n plek.

Dr. A. Amelink, beste Arjen, je zult wel eens moe van me zijn geworden en je hebben afgevraagd waarom studenten geneeskunde niet meer natuurkunde gerelateerde studiestof krijgen. Dank voor alle uitleg over reflectie spectroscopie en differential path length spectroscopie. Dank voor de vele analyses die je hebt verricht op de metingen die ik naar je opstuurde. Ook dank voor alle hulp en inzet bij het schrijven van de artikelen en het aanleveren van nieuwe probes als er weer eens eentje sneuvelde.

Dr. S.C. Kanick, dear Chad, thanks for all your support especially with writing. Without your input the papers would have been published much later. You were able to combine the request from the doctors and the physics in such a way that everybody was satisfied.

Beste paranimfen, lieve broertjes, dank dat jullie mij willen bijstaan op deze bijzondere dag. Samen met zuslief Dian zijn jullie één van mijn meest dierbaren. Met z'n viertjes hebben we een onbezorgde jeugd gehad. Nu zijn we allemaal uitgevlogen en iedereen zoekt zijn plek in de wijde wereld. Ik wil jullie bedanken voor alle mooie herinneringen. Ik hoop dat ik in de toekomst ook jullie mag bijstaan bij bijzondere gebeurtenissen.

Beste Maatschap Longziekten, wat een geweldige groep longartsen zijn jullie! Een grote diversiteit aan persoonlijkheden die de maatschap dynamisch maakt, vol met daadkracht en een flinke dosis humor. Ik had zo mijn twijfels toen ik voor het eerst naar het Amphia vertrok, maar heb er geen spijt van gekregen.

Beste collega's van de longziekten (Merijn, Barbara, Tamara, Marjolein, Sevim, Edith, Koen en Nienke), hartelijk dank voor jullie interesse, medeleven en support. Het was erg fijn dat ik op een gegeven moment door jullie flexibiliteit overdag aan mijn proefschrift kon werken. Tijdens de vooropleiding bij de interne mis ik zo nu en dan die chaotische arts-assistenten kamer vol chips, cola en M&M's. In januari 2012 ben ik weer terug.

Dames van het scopieprogramma. Jullie zullen vaak hebben gedacht: "daar heb je hem weer met zijn stellage en zijn fibertjes". Toch heb ik maar weinig tegenspraak gehoord. Hartelijk dank dat jullie mij de tijd en ruimte hebben gegeven om mijn metingen te kunnen verrichten. Tot de volgende bronchoscopie of pleuradrainage!

Lieve vrienden (Niels en Chiara, Ron en Hien, Marieke en Harm-Jan en Akkie en Florien). Met de meesten zijn we al vanaf het eerste jaar geneeskunde samen. We hebben het allemaal druk, maar zo nu en dan zien we elkaar weer eens even. De laatste jaren zijn al onze levens in een versnelling geraakt, en er komen vast nog vele mooie momenten bij. Ik kijk uit naar ons volgende avontuur: de Zeeuwse wateren onveilig maken en daarna... het ruime sop?

Beste Pierre en Joke, ook jullie wil ik bedanken voor alle steun en inzet die jullie hebben gegeven. Heel fijn dat ik zo nu en dan een Engels stuk onder jullie ogen mocht schuiven zodat jullie kromme zinnen en gekke constructies konden bijschaven. Dank voor jullie interesse en voor de zorg om onze kleintjes.

Lieve pap en mam, aan jullie heb ik veel te danken. Jullie hebben altijd in dat kleine mannetje en zijn droomwereld geloofd en nooit zijn dromen belachelijk gemaakt. Het motto was, als je iets wilt dan kom je er ook, al moet het met de nodige omwegen. De weg was langer dan gemiddeld, maar we zitten nu op een mooi spoor. Ik hou van jullie.

Tot slot ben ik de meeste dank verschuldigd aan mijn lief, Eva. Dankzij jou heb ik deze klus uiteindelijk kunnen klaren. Jouw onverlaten steun en doorzettingsvermogen hebben enorm bijgedragen. Op een gegeven moment leek het een co-productie te worden. Ik hoop dat jij net zo trots bent op het eindproduct als ik. De laatste maanden waren dubbel zo hectisch met de komst van onze zoon Wietse. Ons leven heeft een andere dimensie gekregen nu we met z'n viertjes zijn. Ik kijk uit naar de rust die we gaan krijgen, genietend van onze twee hummel de bummels: Fien en Wietse, een mooier span is er simpelweg niet.

LIST OF PUBLICATIONS

Boudesteyn J, **Van der Leest KH**, van der Lelij AJ. [Ghrelin, an important hormone produced by the stomach]. *Ned Tijdschr Geneeskd*. 2002; **146**: 1929-33.

Van der Leest KH, Van der Linde NAJ, Van Hest NAH, Veerhoek MJ, Tan KY, Rudolphus A, Aerts JG. Pericarditis tuberculosa, *Tegen de Tuberculose*. 2007 jaargang 103, nr. 3

Aerts JG, Amelink A, **Van der Leest C**, Hegmans JP, Hemmes A, Den Hamer B, Sterenborg HC, Hoogsteden HC, Lambrecht BN. HIF1a expression in bronchial biopsies correlates with tumor microvascular saturation determined using optical spectroscopy. *Lung Cancer*. 2007; **57**: 317-21.

Van der Leest K, Bogaard J, Rudolphus A, Tan K, van Tilburg A, Mannaerts G, Aerts J. Paraesophageal hiatal hernia-induced dyspnea. *Respiration*. 2009; **78**

Sterenborg HJ, **Van der Leest C**, Kanick SC, Aerts JG, Amelink A. Differential Pathlength Spectroscopy. In: Wax A, Backman V, *Biomedical Applications of Light Scattering,* 2009, 293-312; ISBN 10: 0071598804

Kanick SC, **Van der Leest C**, Aerts JG, Hoogsteden HC, Kascakova S, Sterenborg HJ, Amelink A. Integration of single-fiber reflectance spectroscopy into ultrasound-guided endoscopic lung cancer staging of mediastinal lymph nodes. *J Biomed Opt*. 2010; **15**

Van der Leest C, Kanick SC, Djamin RS, Janssens AM, Hoogsteden HC, Sterenborg HJ, Amelink A, Aerts JG. Characterization of mediastinal lymph node physiology In vivo by optical spectroscopy during endoscopic ultrasound-guided fine-needle aspiration. *JTO*, in press

CURRICULUM VITAE

Cor van der Leest is op 10 augustus 1977 geboren te Brunssum. Hij volgde het middelbaar onderwijs aan de Hooghbeemt in Eindhoven en het Baudartius College in Zutphen. In 1998 begon hij zijn studie Geneeskunde aan de Erasmus Universiteit in Rotterdam, waarna hij in 2005 het artsenexamen haalde. Daarna ging hij als arts assistent werken in het Sint Franciscus Gasthuis te Rotterdam. Sinds 2009 is hij in opleiding tot longarts in het Amphia ziekenhuis te Breda (opleiders Drs. R.S. Djamin en Dr. J.G.J.V. Aerts). Momenteel is hij bezig met de interne vooropleiding in het Amphia ziekenhuis te Breda (opleider Dr. C. van Guldener). Hij is gehuwd met Eva de Wee en zij hebben twee kinderen: Fien en Wietse.

LIST OF ABBREVIATIONS

18F-FDG	18F-Fluorodeoxyglucose
ADC	Adenocarcinoma
ASD	Angiogenetic squamous dysplasia
CIS	Carcinoma in situ
CT	Computer Tomography
DPS	Differential pathlength spectroscopy
ED	Extended disease
EUS-FNA	Endoscopic ultrasound fine needle aspiration
HIF1a	Hypoxic inducible factor 1 alpha
LCC	Large cell carcinoma
LD	Limited disease
NSCLC	Non small cell lung carcinoma
OS	Overall survival
PET	Positron emission tomography
PFS	Progression free survival
SCC	Squamous cell carcinoma
SCLC	Small cell lung carcinoma
SF	Single fiber
SUVmax	Maximum standard uptake value
VEGF	Vascular endothelial growth factor

Abbreviations of the used mathematical equations

DPS (λ)	Reflectance Spectra
λ	Wavelength [nm]
λ_0	Wavelength at 800 nm [nm]
μ_s	Coefficient of light scattering [1/cm]
μ_a	Coefficient of light absorption [1/cm]
μ_a'	Corrected coefficient of light absorption [1/cm]
τ	Pathlenght, distance of light traveling trough the tissue [cm]
a	Mie amplitude
b	Mie slope
ρ	Blood volume fraction
$\mu_a^{oxyHemo}$	Absorption of oxygenated hemoglobin [1/cm of 100% volume fraction]

μ_a^{Hemo}	Absorption of deoxygenated hemoglobin [1/cm of 100% volume fraction]
μ_a^{other}	Other vascular absorbers [1/Mol]
μ_a^{hom}	Homogeneously distributed absorber [1/Mol]
StO2	Oxygen saturation of the blood [%]
R	Radius of the blood vessel [cm]